

Harald Philipson

The effect of thickness and compaction on the recovery of aluminium in recycling of foils in salt flux

Master's thesis in Materials Science and Engineering

Supervisor: Gabriella Tranell

August 2020



Norwegian University of
Science and Technology

The effect of thickness and compaction on the recovery of aluminium in recycling of foils in salt flux

Harald Philipson

Materials Science and Engineering (MTMT)

Submission date: August 2020

Supervisor: Gabriella Tranell, IMA

Co-supervisors: Alicia Vallejo-Olivares, Hans Jørgen Roven, Mertol Göknelma,
Trond Furu, IMA
Anne Kvithyld, Sintef

Norwegian University of Science and Technology
Department of Materials Science and Engineering

Acknowledgement

Thank you NTNU, Norsk Hydro and partners in the Alpakka consortium for the opportunity to contribute in research about food packaging recycling. Except for gained knowledge about the aluminum recycling industry I have come to know fantastic people with great enthusiasm and passion in what they do. This has been more than just a thesis for me, it has been a truly inspiring journey that have opened up opportunities for an exciting future. Thank you all involved, I look forward to staying in touch and collaborating in the near future.

The research team I was part of consisted of Prof. Gabriella Tranell (NTNU), Prof. Hans J. Roven (NTNU), Postdoc. Mertol Göknelma (NTNU), Senior Research Scientist Anne Kvithyld (SINTEF), Prof./Research Manager Trond Furu (Hydro/NTNU) and PhD candidate Alicia Vallejo-Olivares (NTNU). You have been great support and guidance throughout the whole thesis by contributing with knowledge from respective area of expertise. Special thanks to my main supervisor Prof. Tranell for showing great leadership, competence and report-feedback and PhD-student Vallejo-Olivares for guidance and valuable discussions concerning both theory and experiments. Thank you Oskar Altzar (Hydro) and Sabine Hofmann (Hydro) with the help of connecting me with NTNU/Hydro.

The practical help with instruments and experiments is much appreciated. Thank you Pål Christian Skaret for the help preparing and giving instructions on pressing machine, HPT and induction; Dmitry Slizovskiy for instructions and input to muffle furnace melting experiments; Berit Vinje Kramer for teaching sample preparations and heat treatment; Andrey Kosinskiy for teaching surface area analysis with Alicona microscope; Elin Harboe Albertsen for teaching the pycnometer and Ole Tore Buset for all x-ray tomography analyzes.

Thank you KTH Royal Institute of Technology for providing the opportunity to finalize my education in Materials Science and Engineering at NTNU in Trondheim, Norway. Thank you Anders Tilliander, Anders Eliasson and Pär Jönsson for your support before and during the spring. I hope the collaboration between KTH and NTNU can continue and that students can exchange to maximize learning outcomes and personal development.

Abstract

In Norway, more than 40.000 tonnes of aluminum (Al) in food packaging goes to incineration annually. Recycling this waste would save more than 1.5 TWh of energy and several hundred thousand tonnes of CO₂ emissions. However, recycling thin aluminum foil in small packaging is more difficult than recycling of larger and cleaner scrap. In this thesis, properties of compacted coating-free Al foil with five different thicknesses (15, 30, 100, 200, 300 μm) were investigated and related to percentage Al recovery during remelting in salt flux.

This thesis consists of five main parts. Two initial studies involved shredding of the foil into a controlled chip size and compaction of these chips to briquettes of a wide range of bulk densities using three types of compaction techniques. In the following two studies, relevant briquette properties and oxidation behavior were determined. Finally, chips and briquettes were melted in salt flux and the percentage Al recovery was calculated.

The bulk density, porosity and surface areas of the briquettes were significantly influenced by the type of compaction technique. Applied torque and heat in addition to uniaxial pressing were found to be effective measures to increase bulk density. Oxidation was higher for thin Al foil due to higher specific surface area and micro roughness. However, the oxidation of briquettes significantly decreased as the bulk density exceeded 2.4 g/cm³. Briquetting led to significantly increased recovery of the two thinnest foils. For the three thickest foils the effect of briquetting was smaller. For the thinnest foil, recovery increased with compaction. For this foil, even significantly oxidized chips compacted to bulk density 2.6 g/cm³ resulted in 99-100 % recovery. The specific surface area of the aluminum was the most important material property influencing recovery. It is expected that an optimum amount of salt flux and fluoride content related to specific surface area of the scrap can be developed.

Sammanfattning

I Norge förbränns mer än 40 000 ton aluminiumförpackningar årligen. Återvinning av denna mängd aluminiumförpackningar skulle spara 1,5 TWh energi och hundratusentals ton av koldioxidutsläpp. Det mycket svårare att återvinna tunn aluminiumfolie i förpackningar än större och renare aluminiumskrot. I denna uppsats har egenskaper hos komprimerad beläggingsfri aluminiumfolie med fem olika tjocklekar (15, 30, 100, 200, 300 μm) bestämts. Dessa egenskaper är sedan tillkopplade till återvinningsgraden efter smältning i saltfluss.

Uppsatsen består av fem huvuddelar. I de två inledande delarna strimlas foliet till en bestämd spånstorlekt varpå dessa komprimeras med tre olika presstekniker till briketter av olika bulkdensiteter. I de nästa två delarna bestäms relevanta brikettegenskaper och oxidationsbeteendet. I den sista delen bestäms återvinningsgraden av spån och briketter som smälts i saltfluss.

Briketternas bulkdensitet, porositet och ytarea varierade beroende på pressningsteknik. Högtrycksvridning under tillförd värme var ett effektivt sätt att öka bulkdensiteten. Tunnare folie oxiderade mera på grund av stor specifik ytarea och hög mikrosträvhet. Oxidationsgraden för briketter med bulkdensitet över 2.4 g/cm^3 var betydligt lägre än briketter med lägre bulkdensitet. Briketter av de två tunnaste folierna ledde till högre återvinningsgrad jämfört med motsvarande spån. Effekten av kompression på återvinningsgraden var mindre för de tre tjockaste folierna. Återvinningsgraden ökade med ökad kompression för det tunnaste foliet. Trots att denna folie oxiderades relativt mycket var återvinningsgraden 99-100 % efter kompression till 2.6 g/cm^3 . Resultatet indikerar på att främst specifika ytarean påverkar återvinningsgraden av aluminiumet. Baserat på den föreslagna teorin borde ett optimum av saltmängd, fluorinnehåll och ytarea skrot kunna utvecklas för att maximera återvinningsgraden.

Contents

Acknowledgement.....	i
Abstract.....	iii
Sammanfattning	v
1. Introduction.....	1
1.1. Aim of work	2
1.2. Aluminum and the future of recycling.....	2
2. Theory and Literature Survey of Al recycling.....	6
2.1. Short environmental comparison between primary and secondary production of Al.....	7
2.2. Short economical comparison between primary and secondary production of Al.....	8
2.3. Scrap and sources of Al for recycling.....	9
2.3.1. <i>Old scrap</i>	10
2.3.2. <i>Discarded old scrap</i>	11
2.3.3. <i>New scrap</i>	11
2.4. Characterization of Al scrap by series, alloy, cleanliness and size	12
2.4.1. <i>Wrought alloys</i>	13
2.4.2. <i>Aluminum in packaging</i>	14
2.4.3. <i>Cleanliness and size of scraps</i>	15
2.5. Shredding/comminution Al scrap	16
2.6. Sorting of scrap	17
2.6.1. <i>Hand sorting</i>	18
2.6.2. <i>General sorting with automatic sorting techniques</i>	18
2.6.3. <i>Sorting by grade</i>	19
2.6.4. <i>Foil sorting</i>	21
2.7. De-coating scrap.....	21
2.7.1. <i>Thermal and chemical treatment of foil</i>	23
2.7.2. <i>Turnings in centrifuge</i>	24
2.8. Compaction of Al scrap	24
2.8.1. <i>Balers</i>	24
2.8.2. <i>Briquetting</i>	25
2.8.3. <i>High Pressure Torsion (HPT) and Screw Extrusion</i>	27
2.9. Melting to recover scrap	29

2.9.1. Oxidation of Al scrap during heating and melting	29
2.9.2. Alloying elements effect on oxide film growth	33
2.9.3. Reverberatory furnace	34
2.9.4. Sidewell melting furnace.....	34
2.9.5. Rotary furnaces.....	36
2.9.6. Salt flux.....	37
2.9.7. Recovery of thin scrap.....	38
2.9.8. Recovery from melting of chips and briquettes.....	41
2.10. Coalescence of liquid metal in salt flux.....	43
2.10.1. Surface tension	43
2.10.2. Fundamentals of collision and coalescence of droplets.....	43
2.10.3. Coalescence of Al droplets in liquid salt flux	45
2.10.4. Displacement reactions at salt-metal interface	49
2.10.5. CaF ₂ addition in NaCl-KCl salt for recovery of Al scrap	52
2.10.6. Al loss in salt flux.....	54
3. Experimental materials and methods	56
3.1. Materials.....	56
3.2. Overview of experimental steps in the current investigation: from foil to recovered aluminum	56
3.3. Shredding and sieving of foil to produce chips.....	57
3.3.1. Pre-study	58
3.4. Characterization of chips	59
3.4.1. Image analysis using ImageJ - procedure.....	60
3.5. Controlling chip size before pressing – sieving.....	61
3.6. Compression of chips to briquettes.....	63
3.7. Automatic uniaxial pressing	64
3.8. High Pressure Torsion (HPT)	65
3.9. HPT with heat	66
3.10. Oxidizing briquettes by heat treatment	67
3.11. Characterization of briquettes.....	69
3.11.1. Quantifying the briquette surface from optical 3D-microscope	69
3.11.2. Porosity of briquettes determined by X-ray tomography.....	73
3.12. Metal recovery from melting briquettes in salt flux	74
3.13. Melting without salt flux	78

4. Results.....	81
4.1. Shredding behavior of different foil thicknesses.....	81
4.1.1. <i>Initial study of different shred groups</i>	81
4.1.2. <i>Study on sieved 15-300 μm chips</i>	84
4.1.3. <i>The effect of sieving</i>	87
4.1.4. <i>Settling volume and mass of chips</i>	90
4.2. Compaction of chips to briquettes.....	92
4.2.1. <i>Shred group comparison and the relationship between bulk density and applied stress for manually compressed samples</i>	93
4.2.2. <i>Compaction results for automatically compacted sieved chips</i>	98
4.3. Briquettes properties.....	100
4.3.1. <i>Briquette surface area analysis</i>	100
4.3.2. <i>Porosity of briquettes determined by X-ray tomography</i>	104
4.4. Oxidation due to heat treatment.....	106
4.4.1. <i>Oxidation of briquettes</i>	106
4.4.2. <i>Oxidation of sheets</i>	107
4.4.3. <i>Oxide thickness measurement with SEM</i>	108
4.5. Al recovery of melted chips and briquettes.....	109
4.5.1. <i>Recovery of non-heat treated briquettes</i>	110
4.5.2. <i>Pre-study on recovery of heat-treated chips and briquettes</i>	110
4.5.3. <i>Recovery in salt flux with final experimental setup</i>	115
4.5.4. <i>Recovery of briquettes without the use of salt flux</i>	119
5. Discussion.....	124
5.1. Shredding behavior of different foil thicknesses.....	124
5.2. Compaction of chips to briquettes.....	125
5.2.1. <i>Uniaxial pressing</i>	125
5.2.2. <i>High Pressure Torsion (HPT) and with heat</i>	126
5.2.3. <i>Compaction of oxidized chips</i>	126
5.3. Briquette properties.....	127
5.3.1. <i>Porosity and surface area</i>	127
5.4. Oxidation due to heat treatment.....	129
5.5. Al recovery of melted chips and briquettes.....	131
5.5.1. <i>Effect of surface area on recovery</i>	136

5.5.2. <i>Partial solid-state coalescence and the condition of oxide layer</i>	141
5.5.3. <i>Fluoride addition and oxide rupture</i>	143
5.5.4. <i>Coalescence dependency on state of the salt flux</i>	145
5.5.5. <i>Recovery and coalescence – the pre-study</i>	145
5.5.6. <i>Other parameters that may influence recovery</i>	146
5.5.7. <i>Melting without salt</i>	146
5.5.8. <i>Implication of the thesis results for the recovery of thin foil in the recycling industry</i>	148
6. Conclusion	149
6.1. Shredding behavior of different foil thicknesses.....	149
6.2. Compaction of chips to briquettes	149
6.3. Briquette properties.....	150
6.4. Oxidation of chips and briquettes due to heat treatment	150
6.5. Al recovery of melted chips and briquettes	151
6.5.1. <i>The effect of thickness on recovery of heat-treated briquettes and chips in salt flux</i>	151
6.5.2. <i>Melting behavior without salt flux</i>	152
6.6. Additional conclusions	152
7. Bibliography	153
8. Appendices	158

List of Figures

Figure 1.1: Sankey diagram of mass flow of aluminum in the world [2].....	3
Figure 2.1. Life cycle of aluminum [9].	6
Figure 2.2. Typical recycling production routes of Al production adapted from [10].	10
Figure 2.3. Average life, recycle rate and metal recovery of different aluminum scrap [10]....	11
Figure 2.4. Progression of alloys in recycling [8].....	13
Figure 2.5. The recyclability of scrap types with respect to size and cleanliness [8].....	16
Figure 2.6. Double-rotor rotary shear [10].	17
Figure 2.7. Conveyor-type eddy-current separator.....	19
Figure 2.8. Example of a LIBS system for sorting of scrap [24].....	21
Figure 2.9. Examples of baler machines [10]	25
Figure 2.10. Typical briquetting methods: punch-and-die machine (left) and roller press (right) [10].	26
Figure 2.11. Illustration of two modifications of (HPT), (a) unconstrained HPT and (b,c) constrained HPT [39].	27
Figure 2.12. Two different studies showing the relationship between bulk density and compressive stress for Al chips [44, 45].	29
Figure 2.13. Ellingham diagram [54].	30
Figure 2.14. Phases formed during oxidation of pure Al [56].....	31
Figure 2.15. Typical oxidation kinetics of Al [60].	32
Figure 2.16. Cross section of reverberatory melting furnace [63].	34
Figure 2.17. Cross-section of simple sidewell furnace [10].	35
Figure 2.18. LOTUSS scrap submergence system [10].....	36
Figure 2.19. Tilted rotary melting furnace [65].....	37
Figure 2.20. The relationship between metal loss and scrap thickness [58].	38
Figure 2.21. Example of dross skimming operation.....	39
Figure 2.22. Melt loss (%) varies with melting temperature and thickness of scrap [58, 77]. ..	40
Figure 2.23. Schematic sequence of collision of two droplets and subsequent coalescence, agglomeration or repulsion according to Gäbler and adapted by [82].	44
Figure 2.24. Properties of continuous phase, interface and disperse phase that influence coalescence [82].	45

Figure 2.25. Schematic representation of oxide removal and coalescence proposed by Jordan and Milner [85].	46
Figure 2.26. Coalescence behavior of Al UBC droplets in salt flux containing 5 mass% CaF ₂ .	47
Figure 2.27. The reduction in number of Al droplets (coalescence) with time for different fluoride additions [85].	48
Figure 2.28. Quasi-binary section of CaF ₂ -(70:30 NaCl-KCl) of the ternary phase system [98].	52
Figure 2.29. The relationship between metal loss and CaF ₂ addition for different salt/Al ratios [98].	53
Figure 2.30. Change in CaF ₂ content with time [98].	54
Figure 3.1. Schematic illustration of experimental steps.	57
Figure 3.2. The interior of Getecha RS 1600 shredding machine showing the three rotary steel blades and shredded pieces too large to pass the screen.	58
Figure 3.3. Differently prepared foil pieces resulting in the referred shred groups. Flat, much deformed and gently deformed foil pieces prepared for shredding.	59
Figure 3.4. Chips that passed and were collected by the screen, deformed chips and undeformed chips.	59
Figure 3.5. Photo analysis of chips.	60
Figure 3.6. Sieving of chips.	61
Figure 3.7. Settling volume of chips in 175 ml cup (left). An image that demonstrate the deformation degree of shredded chips (100 μm) (right).	62
Figure 3.8. Compaction of chips to briquettes.	64
Figure 3.9. Briquettes produced by HPT.	66
Figure 3.10. The equipment for pressing with induction and the briquette produced.	67
Figure 3.11. Oxidized chips (furthest inside furnace in left figure) and oxidized sheets (middle and right figure).	68
Figure 3.12. Images showing the surface irregularities of briquette compressed uniaxially (left) and HPT (right).	70
Figure 3.13. An example of how 4x4 images are merged into one single image field.	71
Figure 3.14. Briquette of 30 μm foil with a bulk density of 1.38 g/cm ³ . Illustration of the measured surface (left) and the vector with 4 turnings across the projected surface.	72

Figure 3.15. Examples of porosity images obtained from X-ray tomography. From left to right: 15, 30 and 300 μm all in the bulk density range 2.0-2.1 g/cm^3 .	73
Figure 3.16. Crucible with solid and molten briquette, salt flux after operation and coalesced aluminum.	76
Figure 3.17. Chips, crucible with 150 g salt flux, 4 crucibles charged and recovered aluminum.	78
Figure 3.18. Dried crucible (left), charged crucible with briquettes inside (middle) and finished heated briquettes (right).	79
Figure 3.19. Successfully recovered Al (left), visible chips (middle) and fragile Al piece disintegrating (right).	79
Figure 4.1. Size distribution of chip groups A-D of foil thickness 15 μm (non-sieved).	81
Figure 4.2. Size distribution of chip groups A-B of foil thickness 30 μm (non-sieved).	82
Figure 4.3. Shape distribution of 15 μm chips of shred groups A-D.	83
Figure 4.4. Shape distribution of 30 μm chips of shred groups A-B.	84
Figure 4.5. Size distribution of sieved chips of all foil thicknesses.	85
Figure 4.6. Shape distribution of sieved chips of all foil thicknesses.	86
Figure 4.7. Median size of chips plotted against median shape of chips displaying all thicknesses.	87
Figure 4.8. Size and shape characteristics of shred groups (non-sieved) and sieved chips.	88
Figure 4.9. Comparison between size and shape of sieved and non-sieved chips for the two thinnest foil materials.	89
Figure 4.10. Comparison between distribution and median sieved and non-sieved chips of thickness 15 and 30 μm .	90
Figure 4.11. Estimation of settling volume of 20 g chips of 15 and 300 μm thickness. The right image exemplifies the effect of deformation degree on the surface exposed to the camera.	91
Figure 4.12. Average mass per chip with weighted STD (vertical) versus average area of chip with STD (horizontal) for sieved chips of all foil thicknesses.	92
Figure 4.13. Average bulk density of compacted 15 μm foil chips from different shred groups.	94
Figure 4.14. Average bulk density of compacted 30 μm foil chips from different shred groups.	95

Figure 4.15. Bar graph showing average bulk density for 15 and 30 μm foil thickness and the shred groups.	96
Figure 4.16. Bulk density from shred group A and B averaged for 15 and 30 μm with error bars with min-max. interval.....	97
Figure 4.17. Bulk density from shred group A and B averaged for 15 and 30 μm with error bars with min-max. interval.....	97
Figure 4.18. Bulk density of briquettes obtained by automatic compaction of sieved chips....	98
Figure 4.19. Mean bulk density comparison of the three compaction methods.	100
Figure 4.20. True-to-projected area ratio for different bulk density of briquette.....	101
Figure 4.21. Surface height profiles of briquettes of 15 and 300 μm of similar bulk density with the mean height (zero) as reference.....	102
Figure 4.22. The surface height profiles of the same briquettes but at a micro level.....	103
Figure 4.23. Mean porosity measured by x-ray tomography of briquettes with different bulk densities.	105
Figure 4.24. Varying porosity at different layers after HPT.	106
Figure 4.25. Mass increase of chips and briquettes with different bulk densities as a result of oxidation at 650 °C for 1 h.....	107
Figure 4.26. The household foil of thickness 15 μm observed in SEM.	109
Figure 4.27. Attempt to identify the oxide layer by point-analysis in EDS.....	109
Figure 4.28. The recovered Al of briquettes corresponding to column 1, 2 and 4 in Table 4.5 above.	111
Figure 4.29. Recovered briquette of 300 μm , heat treated above melting point prior to melting.	112
Figure 4.30. Recovery of chips and briquettes of 15 μm in salt flux with varying experimental setup.	113
Figure 4.31. Recovery of chips and briquettes of 30 μm in salt flux with varying experimental setup.	114
Figure 4.32. Example of coalesced aluminum and smaller aluminum particles obtained from melting a briquette in salt flux.	114
Figure 4.33. Recovery of heat treated (650°C 1 h) briquettes of 15 μm in the last experimental setup.	116

Figure 4.34. Recovery of heat-treated briquettes of 30-300 μm in the last experimental setup.	117
Figure 4.35. Illustration of briquette floating (left) and sinking (right).	119
Figure 4.36. Unsuccessful coalescence of briquettes with approximate bulk density 2.1 g/cm^3 . 15 and 30 μm , from left to right.	120
Figure 4.37. Unsuccessful coalescence of briquettes with approximate bulk density 2.1 g/cm^3 . 100, 200 and 300 μm , from left to right.	121
Figure 4.38. Briquettes of 15, 100 and 200 μm , with bulk density 2.6, 2.5 and 2.5 g/cm^3 , respectively.....	121
Figure 4.39. Density of melted briquette compared between briquettes of different thickness and compaction.	122
Figure 5.1. Briquettes of 15 μm foil (left) and 100 μm foil (right), both with bulk density 2.09 g/cm^3	128
Figure 5.2. Briquettes of 100 μm foil with bulk density 2.48 (left) and 2.09 g/cm^3 (right).	130
Figure 5.3. Coalescence mechanism of thin and thick chips illustrated.....	134
Figure 5.4. Coalescence mechanism of compacted thin and thick chips.....	136
Figure 5.5. Coalesced Al and spherical “pearls” recovered.....	137
Figure 5.6. Metal loss compared to Rossel’s metal loss showing the thickness of low-alloy scrap/foil melted at 800 °C adapted from [58].....	141
Figure 5.7. Recovered briquette of 300 μm heat treated at 800 °C 3.5 hours (left) and arbitrary briquette recovered after heat treatment at 650 °C 1 hour (right).	143
Figure 8.1. Plotted data on size and shape of chips of 15 and 30 μm for shred groups A-D. .	158
Figure 8.2. Plotted data on size and shape of sieved chips of 15-300 μm (only chips from shred group A).	159
Figure 8.3. Bulk density comparison between chips of different shred groups of the 15 μm foil.	159
Figure 8.4. Average bulk density vs. Compressive force, all shred groups averaged for the two thinnest foil thicknesses.	160
Figure 8.5. Vertical displacement due to applied compressive force on Al chips resulting in briquettes of bulk density 2.06-2.12 g/cm^3	160

Figure 8.6. Vertical displacement due to applied compressive force on Al chips resulting in briquettes of bulk density 1.35-1.4 g/cm³.161

Figure 8.7. Vertical displacement due to 2 kN applied compressive force during heating from room temp. to 450 °C on non-oxidized and oxidized Al chips, displaying the briquettes of bulk densities.161

Figure 8.8. Vertical displacement due to applied compressive force from 2 to 70 kN at 450 °C on non-oxidized and oxidized Al chips, displaying the briquettes of bulk densities.162

List of Tables

Table 2.1. Average lifetimes of aluminum products in years adapted from [20].15

Table 2.2. Data from [90] on metal loss restructured. Pure Al pellet with different mass melted in 66 g equimolar (NaCl-KCl)+10%NaF at 740 °C for 1 hour.....54

Table 3.1. Composition of the household foils (15 and 30 μm) and 8006 alloy (100, 200 and 300 μm).....56

Table 3.2. Distribution of chips after sieving (sieve mesh in mm).....62

Table 3.3. Compaction table showing the bulk density ranges and number of parallel pressings.65

Table 3.4. Number of heat-treated chips and briquettes used for final melting experiments. 68

Table 3.5. The scheme for projected surface area analysis.....73

Table 3.6. Scheme for briquettes analyzed in X-ray tomography.74

Table 3.7. Briquettes melted in final experiments.....75

Table 3.8. The briquettes melted without salt flux.....80

Table 4.1. Settling volume of 20 g chips in a 175 ml cup and average mass per sieved chip for all foil thicknesses.91

Table 4.2. The effect of torque (revolutions) in addition to uniaxial pressing of 300 μm foil. ...99

Table 4.3. Sdq and Sdr values for briquettes of different bulk density and foil thickness.....104

Table 4.4. The mean mass increase per surface area of foil (mg/cm²) for the three thickest foils.108

Table 4.5. Mass increase after heat treatment at 600 °C for 3.5 h plus 800 °C for 1.5 h, and subsequent recovery of 15 μm briquettes.111

1. Introduction

Aluminum (Al) and Al alloys can be produced either by primary production or secondary production. In primary production the source is mainly bauxite ore extracted by mining and in secondary production the source is scrap. The main benefit of the latter production route is large energy savings and less hazardous by-products. Also relative to other material industries, the energy-intensive primary production can partly be replaced by secondary production working towards more resource-efficient material cycles. In addition, in the coming decades the supply of Al scrap and demand for Al products is expected to increase in Europe.

Recycling of Al means recycling of scrap material and by-products containing pure aluminum or aluminum alloys containing other elements. Al objects or pieces of Al are collected and processed (e.g. cleaned, cut into pieces and compacted) before it is refined, melted and solidified into desired alloy and form. The recovered Al is either ready to be used for a certain application or it is further processed by the manufacturing industry.

Aluminum is common in packaging materials, usually in the form of rigid containers or foil products such as food containers, beverage cans aerosols and tubes. Aluminum is the lightest material to offer a complete protection from moisture, gases and light. Aluminum packaging contain high-purity aluminum, which makes it particularly sought-after for recycling. However, Al in packaging is very thin and often attached to plastics or paper. As a result, Al in packaging is difficult to recycle and often lead to relatively large recycling losses. The consumption and hence the scrap of packaging containing Al is increasing, and consequently better recycling methods are needed.

1.1. Aim of work

The recycling industry strives for better understanding of factors that influence recovery yield of input materials. One of these input materials are thin scrap such as foil and sheet aluminum used in packaging. To increase understanding of foil recovery, the characteristics of the input material must be known. In this thesis, differently compacted foil pieces are characterized by their bulk density, surface area, porosity and oxidation. The relationship between these and the recovery is then determined.

As this research is part of a larger recycling project (Alpakka, funded by RCN, Hydro, Metallco, Infinitum, Kavli, SINTEF and NTNU), the main purpose is to provide deeper understanding of the mechanisms associated with the process of compaction, oxidation and remelting of foils. Experiments are small-scale experiments and simplifications of recovery processes found in the recycling industry. However, on the basis of the results, future research is expected to include parameters such as alloying elements, coatings and other industrial remelting methods, with additional focus on quality in terms of pores and inclusions of the recovered Al.

1.2. Aluminum and the future of recycling

Aluminum is used in a wide range of applications due to its advantageous properties such as lightness, conductivity, formability, durability, impermeability and multiple recyclability. Because of its sustainable properties and recyclability, aluminum materials play a significant role in the work towards climate neutral and circular economy for a greener future. By 2050, the demand for aluminum is projected to have increased by 40 % in key sectors such as transport, construction, packaging and renewable energy technologies. Some of this growth expects to be generated by aluminum replacing other materials such as steel, copper, plastics and wood, depending on the markets [1].

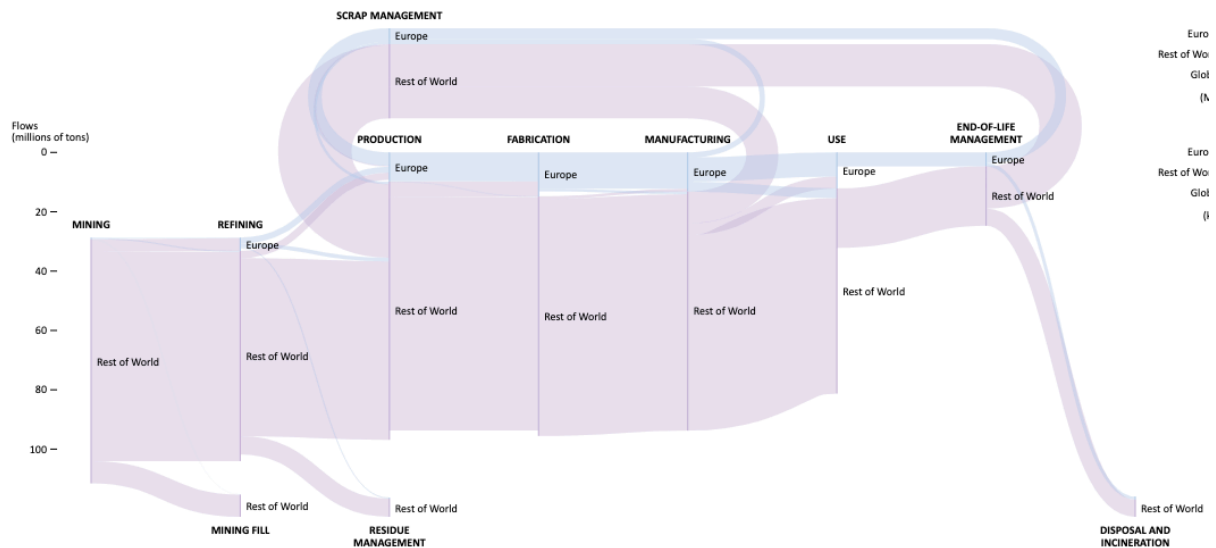


Figure 1.1: Sankey diagram of mass flow of aluminum in the world [2].

In Figure 1.1 above, the mass flow of Al in the world is shown. In Europe, there are several indications of increased usage of scrap in production of aluminum products. Between 2000 and 2017, the scrap supply in Europe has steadily increased. Specifically, it has increased by 105 %, from 2.2 million tons to 4.5 million tons. The amount of old scrap has contributed the most to that increase. For the same time span, scrap as resource in production have increased from 30 % to 50 %, replacing more of primary aluminum extracted by mining [2].

The amount of post-consumer aluminum scrap that can be recycled is expected to double by 2050 (to 8.6 million tons 2050) in Europe. Increased recycling leads to less dependency on carbon-intensive primary imports from other parts of the world, and also generate €6 billion per year for the European economy [1].

The widespread use of aluminum foil in packaging started with Robert Victor Neher in Switzerland who took out a patent 1910 for the continuous rolling process. A year later, Bern-based Tobler started wrapping its Toblerone chocolate in aluminum foil. Since then, the use of aluminum in packaging has continued to rise [1].

Aluminum is the lightest material to offer a complete protection from moisture, gases and light [3]. Aluminum packaging applications range from food containers, beverage cans aerosols and tubes, [1] with beverage cans the most common example. Compared to traditional packaging,

twice as much drinks volume can be transported per truck load. In fact, the weight of the packaging material is less than 10 % of the total weight of the load [3].

Packaging adsorbs 17 % of industry output in Europe, making it the third largest sector. Aluminum packaging contain high-purity aluminum, which makes it particularly sought-after for recycling [1]. Aluminum materials for instance used in the transport sector are alloyed to a greater extent with other elements, which generally is more difficult to recycle into new materials.

Production of thinner and lighter packaging material would not only lead to less materials used for the same performance, but also contribute to less fuel consumption from transport and easier handling at the retail level. In addition, an increased recycling rate of aluminum foil would increase the environmental benefits even further, proceeding environmental goals such as EU's Circular Aluminium Action Plan for 2030 [1, 3].

Other important facts about Al recycling and Al in packaging include [3]:

- 75 % of all aluminum ever produced is still in use
- Recycling saves over 90 million tonnes of CO₂ emission annually
- Aluminum can be recycled infinite amount of times. On average 170 GJ of primary energy (mostly in the form of electricity) is required to produce a tonne of primary aluminum, compared to only 10 GJ in re-melting energy for recycled aluminum.
- According to World Health Organisation (WHO), 30 % of the food in developing countries decompose owing to absence of packaging. In fact, improper packaging result in 10 times more waste than the waste generated during production of the packaging [3].

In the future Europe will need to assume a larger responsibility for Al scrap recycling mainly because of China's reduced demand on scrap and increased investments in recycling, aligned with EU's environmental goals. China has a dominant role in the primary and secondary aluminum market. China has drastically increased the primary production of aluminum, from approximately a tenth of the world production by 2004 to over half of the world production by

2019 [4, 5]. Simultaneously, since 2002 EU has been a continuous net exporter of aluminium scrap and in particular to China. However, in the last years, China is increasingly restraining the import of aluminium scrap [6, 7].

2. Theory and Literature Survey of Al recycling

Aluminum (Al) recycling is recycling of scrap material and by-products containing pure aluminum or aluminum alloys containing other elements. Generally, to recycle Al, objects or pieces of Al are collected and processed before it is melted and solidified into desired form. The recovered Al is either ready to be used for a certain application or it is further processed by the manufacturing industry [8]. In Figure 2.1, the life cycle of Al is illustrated.

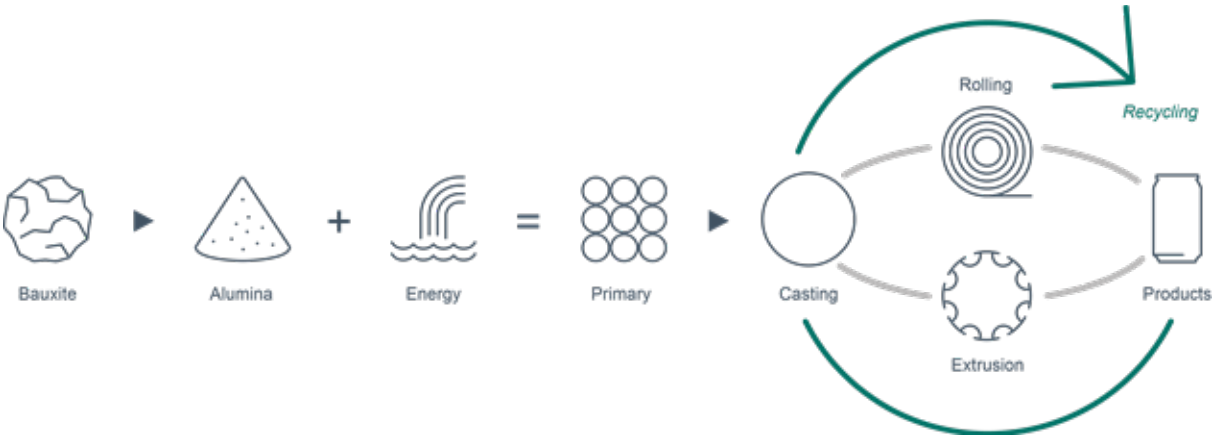


Figure 2.1. Life cycle of aluminum [9].

After collection of scrap, the first step is to identify the scrap. Often, shredding the material to smaller pieces facilitate separation between glass, metal, paper, plastics and dirt. Then, they can be distinguished and separated due to their different material properties with relatively old recycling processes. For instance, the most common materials differ in terms of density, color and magnetic properties. Collection of various Al materials must in turn be separated. Historically, this has been a concern for the industry, as developed technology has proven to be insufficient or too expensive. However, in recent years, new technologies are on the upturn. The scrap can be scanned with information about the composition, and by that is separated alloy by alloy.

After the Al scrap is categorized, the scrap is deoiled by thermal and/or chemical treatment. Scrap is usually contaminated with organic (mainly containing carbon) compounds such as grease, oil, organic resins and lacquers. In a large furnace, the shredded scrap is heated to temperatures below the melting point of Al. For the industry, it has been a challenge to decoat

the scrap completely without also oxidizing it, leading to less recycled Al. This is particularly a common issue for recycling of thin Al scrap.

In the final step, the actual recovery of Al occurs. Most of the scrap is charged in already melted Al pool of desired content, usually pure Al. Dirty scrap or dross is melted with salt flux, which protects the Al from air and promote fusion of the Al pieces. In some cases, small and clean Al particles, usually turnings, can be compressed into a solid Al product, excluding the energy-intensive melting process.

The recovery of dirty and thin scrap is lower than large and clean scrap. Salt flux improve recovery of dirty, thin and small Al scrap. However, the use of salt flux increase costs and generate a residue called salt cake, which is an environmental hazard. Compaction of small and thin Al scrap before charging in either molten Al pool or salt flux is another method. However, the mechanisms involved of recovery of compacted scrap are not yet well described.

2.1. Short environmental comparison between primary and secondary production of Al

The energy required to produce Al from scrap is significantly lower than primary production of Al, especially when considering the energy requirements for extraction of bauxite ore. Al recycling has the widest energy difference between primary and secondary routes, in comparison to the other large base metals and ferrous materials industries such as Cu, Zn and steel [8]. The amount of UBCs recycled in 2005 corresponded to energy savings equal to electricity for 22.7 million US homes for a year [10].

A general approximation is that recycled Al requires only 5 % of the energy used in the primary process. However, this ratio is dependent on the primary production technique as well as the recycling technique used and its Al recovery yield. Comparisons are usually only taking into account energy consumptions for remelting, excluding e.g. energy consumption from mechanical and thermal pre-processing.

For primary production, most of the energy consumption is for molten salt electrolysis of Al_2O_3 . Firstly, substantial amount of energy in terms of electricity is needed to overcome resistance in the electrolyte and to dissolve Al_2O_3 in the molten salt bath. Secondly, large carbon electrodes are used as anode material and the potlining in the electrolysis cell acting as cathode also partly consist of carbon. About half a kg of carbon is consumed per kg Al metal produced, which represents the major part of the carbon consumption in the process. Thirdly, energy is needed to remelt the produced Al ingot for refining into desired alloy [10, 11]. Both the total air emissions (such as fluorides and sulfur dioxide) and CO_2 -emission from primary production is tenfold the amount emitted from secondary production according to Martchek [12].

The main hazardous by-product from secondary production is salt slag. The amount of salt slag produced generally increases as the recycling difficulty of the scrap increases (e.g. thin scrap). For instance, scrap that is coated with organics contain carbon. Upon melting this increase carbide formation and hence more methane generation, which have negative impact on the environment. Another environmental concern is the gaseous emission from salt slag (slurry) as a result of reaction with water. In the leaching process this leads to the formation of products that are explosive, poisonous and odorous gases. Salt slag processing instead of landfilling is nowadays a common procedure in Europe. Al and other metals can somewhat be recovered and the oxide residue can be used in the cement industry e.g. for refractory bricks [13].

2.2. Short economical comparison between primary and secondary production of Al

According to Ayres [14], the economies of scale for primary production is the main reason for its definite economic advantage over smaller and decentralized secondary production. One distinct difference regarding costs in each industry is that secondary production is labor intensive while primary is capital- and resource-intensive. With respect to current tax distribution, given equal output, labor is more expensive than the cost of mining, energy and landfill associated with primary production [10].

Primary production requires fixed assets of higher costs. From ore to pure aluminum, it requires a mining operation, a Bayer process plant and electrolytic pot line plant (electrolytic cells).

Secondary Al production requires fewer processes and lower investment and production costs [15].

The price of Al is the single most important cause of declined recycling rate in history. This is coupled to the fact that marginal cost is higher for the secondary industry than for primary. Primary production is favorable because (1) Al in ore is abundant and by mass the third most abundant element in earth's crust, (2) Extracting technology is powerful, (3) Social costs of mining is not included.

Garbage occupy land. More scrap and garbage generated means that more land is required. To avoid an increased need of land there is an incentive for recycling. The cost of landfilling can be lower than anticipated. At the same time, if the cost of melting operations are increased, the incentives to collect scrap are reduced.

It is expected that the total Al produced will originate from recycled Al in larger proportions with time. This is because the forecast of demand of Al is expected to grow, increased recycling yield with advancement in technology and policies promoting environmental-friendly secondary production prior to primary production. Improved recycling technology can be divided into three main areas. This includes improved (1) collection infrastructure, (2) sorting of alloys and (3) recovery yield of input scrap. The advancement in technology will contribute to decreased costs in the whole production chain.

There is already mined and deposited bauxite enough to provide hundreds of years of primary production at present consumption levels. However, the production of primary Al is more sensitive to changed energy costs, environmental policies, recycling technology development and change in consumption behavior [10].

2.3. Scrap and sources of Al for recycling

Al scrap can be characterized as being old, new or dross. Old Al scrap is post-consumer scrap. These are difficult to identify and sort because knowledge about the manufacturer and composition is usually unknown. In addition, in many products, Al is coated or attached to

plastic or paper, which is challenging in many recycling processes. An exception is used beverage cans (UBCs), which has well established recycling routines [8].

New scrap is produced as a by-product in the manufacturing industry. In the manufacturing industry, Al products are often cut into desired shape, which results in so-called Al turnings or trimmings as a residue. New scrap can also be incorrectly produced pieces and stamping skeletons. Most of the new scrap can be successfully recovered today because the content is often known [8].

Dross is generated as a by-product from primary or secondary re-melting operations. Relative to old and new scrap, dross contains less amount of Al. Many process steps are required to recover Al from dross and in some circumstances, the costs are higher than the profits. However, the incitement to recover dross increases as more countries set up regulations due to environmental concerns with dross [8]. In Figure 2.2 a schematic illustration of recycling routes is shown.

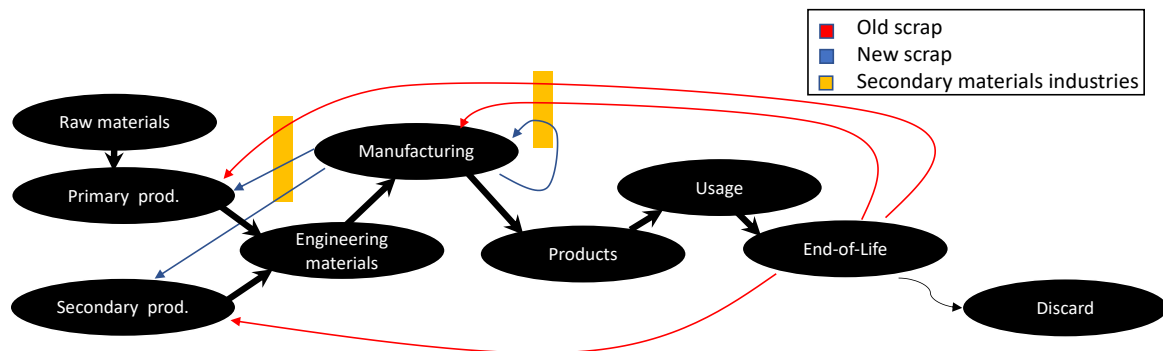


Figure 2.2. Typical recycling production routes of Al production adapted from [10].

2.3.1. Old scrap

The availability of old scrap depends on the amount concentrated geographically, type of scrap, amount of actual Al in the product, legislation and the commitment from the industry. Concentration of scrap in an area have to be large enough to be economically justifiable. Type of scrap that is large and bulky e.g. extrusions and castings are more easily recycled than thin and mixed scrap e.g. foil and wiring. Because of this, large bulky scrap is recycled to a greater

extent. This average product life, recycling rate and estimated metal recovery was compiled by Bruggink in [10], presented Figure 2.3 below.

Market	Average Product Life (years)	Estimated Recycle Rate (%)	Estimated Metal Recovery (%)
Building and construction	40	15	85
Transportation: aerospace	30	30	90
Transportation: auto and light truck	13	80	90
Transportation: trucks, buses, and trailers	20	70	90
Transportation: rail	30	70	90
Transportation: other	20	70	90
Consumer durables	15	20	90
Electrical	35	10	90
Machinery and equipment	25	15	90
Containers and packaging: foil	1	2	80
Containers and packaging: other	1	25–60	90
Other	15	20	90

Figure 2.3. Average life, recycle rate and metal recovery of different aluminum scrap [10].

The amount of actual Al in the alloy is an important factor for the secondary industry. Although products can be thin and contaminated, sufficiently high content of Al in the scrap can make it reasonable to recycle. Finally, legislation have historically affected the recycling rate but also the degree of commitment from industry sectors have had a great influence on the amount that is recycled [10].

2.3.2. Discarded old scrap

Unfortunately, all old scrap produced is not recycled. Scrap that is not recycled back into the loop is either lost, landfilled or used in another purpose and becomes dissipated. An example of the latter is the use as deoxidant in molten steel refining processes. Al as deoxidant removes the undesired oxygen in the steel melt and becomes Al_2O_3 and the value of the Al is lost. [10].

2.3.3. New scrap

A common type of new scrap are turnings/chips from machining operations. In the manufacturing industry, cast Al products are machined into desired shape or form to meet customer needs. Chips are created in rolling mills through the milling off of the casting surface. So-called edge trimming shavings are also created during the machining of sheets, coils or foils.

Pressing plants are producing chips primarily through reprofiling and sawing of cast round bolts as well as finished extruded sections [16].

2.4. Characterization of Al scrap by series, alloy, cleanliness and size

Although some materials contain pure Al such as foils and electric conductor, Al is usually alloyed with other elements to enhance properties, for instance ductility, strength and formability. Pure Al by itself is a weak material. However, only small amounts of alloying of other elements such as Si, Cu, Zn, Fe, Pb and Ni significantly increases its strength and hardness [8, 10].

It is not uncommon that a large fraction of metallic alloying elements are added. Typical alloying amounts are 0.3-12 wt%, primarily with Si, Mg, Cu, Mg and Zn. Different amounts of alloying elements together form different types of Al materials or alloy families. In order for the scrap industry to successfully recycle Al it is important to be aware of the type of Al material, its alloying elements and the amount of these [8].

Al alloys are divided into two major categories – wrought alloys and casting alloys. The primary difference between wrought and casting alloys is the amount of silicon (Si) it contains. Wrought alloys are in turn divided into six subcategories and casting alloys into four subcategories. However, the distinction between categories are not always clear, owing to continual development of new compositions [8].

Preferably, scrap with known composition is recycled into the same alloy category. This is usually the case for new scrap generated by the manufacturing industry. There is an incitement to separate Al alloys into categories. The more knowledge about the composition, the higher it is valued in the scrap processing business. In addition, mass balance calculations are in that case straightforward, which facilitate control of the composition of the alloy to be produced from recycled Al scrap [8].

The composition of postconsumer or old scrap, which is most often a mix of many alloys, is more challenging to identify. Sampling methods used to identify mixed scrap are not accurate.

Small samples often risk of not representing the total scrap chemistry while large scale sampling is costly. Consequently, it is a challenge to utilize the postconsumer scrap for production of standard alloys. However, postconsumer scrap such as UBCs is most easily sorted. Additionally, wrought and cast alloys can be sorted, illustrated in Figure 2.4 below [8].

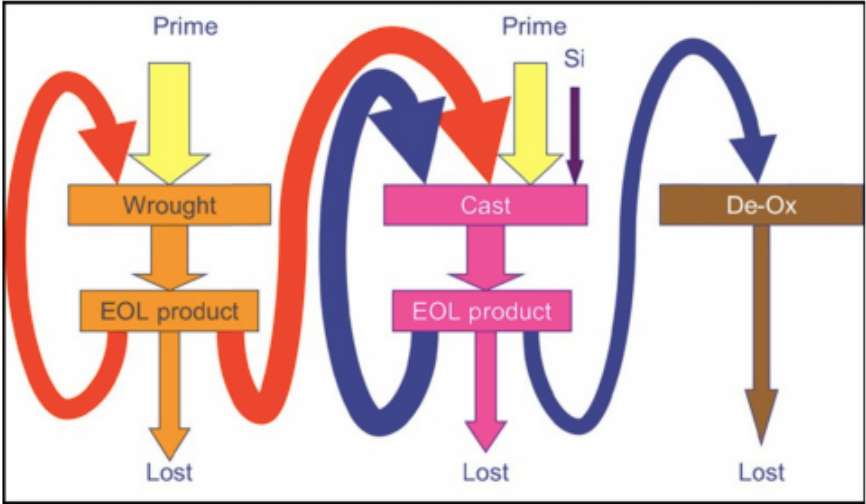


Figure 2.4. Progression of alloys in recycling [8].

In Figure 2.4 a schematic overview of the recycling paths of wrought and casting alloys is shown. Both end-of-life (EOL) wrought and casting products are effectively recycled to their respective category, given enough information about the composition. Furthermore, Al from primary production is utilized in both categories. As illustrated, EOL wrought alloys can be used in the processing of cast alloys, but not the opposite. The recycling scrap for production of wrought alloys have more narrow requirements. Cast alloys i.e. high alloyed scrap is not used to produce wrought alloys i.e. low alloyed scrap. This is a consequence of the thermal properties of Al relative to other alloying elements. Because Al is more reactive with oxygen than most alloying elements, traditional refining techniques in molten state where alloying elements are removed is difficult. Too contaminated EOL cast products can be utilized in the steel refining process. The Al function as a deoxidant with the purpose to remove dissolved oxygen in the steel melt [8].

2.4.1. Wrought alloys

Wrought alloys have been extruded, forged or rolled and contain at least 90 % Al, but most often above 95 % Al. Because of its high Al content, it is possible to recycle wrought alloys for

production of both wrought or cast alloys. The wrought alloys, like cast alloys, are divided into alloy series from 1xxx to 8xxx, each with certain characteristics. As this thesis focus on Al material used for packaging and foil, only the series 1xxx and 8xxx is described. The 1xxx alloy is produced for packaging. This series has the highest percentage of Al and is therefore particularly suitable to remelt into any other series. 8xxx alloys is a general series and is the class that include all other types of alloys. Usually, the Al is alloyed with elements not used in the other series such as Fe, B, Li, V, Sn.

The main issue of recycling wrought alloys is due to the strict limits of composition for fitting into a specific series. Mixing of different series/classes may lead to element contents below or above the requirements to suite a class, hence become undesired on the market. Because mixing is difficult and removing elements with refining is often thermodynamically challenging, scrap is preferably diluted with pure Al from primary production [10].

2.4.2. Aluminum in packaging

The category aluminum packaging refer to either rigid containers or foil products [17]. Extensive consumption of beverage cans started in the late 1950's in the Unites States as the competitiveness of aluminum can exceeded the ones of steel. Until today, Al as a material choice for beverage cans competes with plastics and glass. One of the important contributors to its competitiveness is because it is recyclable. The value of recycling Al is higher than for plastics and glass [10].

A beverage can is typically produced from 3xxx and 5xxx alloy series. The body (75wt%) consist of the 3xxx series, usually 3004 but sometimes also 3104. The rest i.e. the lid and the tab may consist of a variety of 5xxx alloy series. Unfortunately, the mixture of Al alloys used in typical beverage cans contain high Mg and Mn content, which is difficult from a recycling perspective. Consequently, a remelted beverage can as-is cannot qualify into either a 3xxx or 5xxx series alloy, hence have to be diluted with primary produced Al or low-alloy scrap [18].

Aluminum foil or strip is used in packaging such as food trays, pouches and single-serve beverage containers. Common alloys for these containers are rolled 1xxx alloy series or alloy

8011. Although these materials are low-alloyed, which is favorable in recycling, products of foils and strips are often composites with other materials. These are mainly larger quantities of paper and plastic such organic coatings and paint, but steel and lead can also enter in scrap dealing and sorting processes. Paper and plastic attached are difficult to separate and expensive in terms of per unit weight of Al recovered. For this reason, consumed Al packaging have lower recycling yield than other scrap categories [19].

In foil production, relatively low percentage of input Al turn into (new) scrap. Foil production in average generate about 10 % scrap and other container and packaging about 25 %. This can be seen in relation to Al scrap from manufacturing of airplanes which generate 60 % scrap. Although many manufacturing industries utilize so-called closed-loop recycling, scrap can be mixed up, hence the content is unknown. These are most often processed by secondary industries but in recent decades also been recycled in greater amounts by primary industries. This is called open-loop recycling [10]. In Table 2.1, the average lifetimes of different Al products is shown.

Table 2.1. Average lifetimes of aluminum products in years adapted from [20].

Product	Years
Transport	12
General Engineering	15
Electrical Engineering	20
Building and construction	30
Packaging	<1
Home and office	10
Others	10

2.4.3. Cleanliness and size of scraps

High recycling yield of scrap is in general increased when the level of contamination is low, the size of the scrap is large and the Mg content is low. A schematic comparison of various scrap types is illustrated in the Figure 2.5 [8].

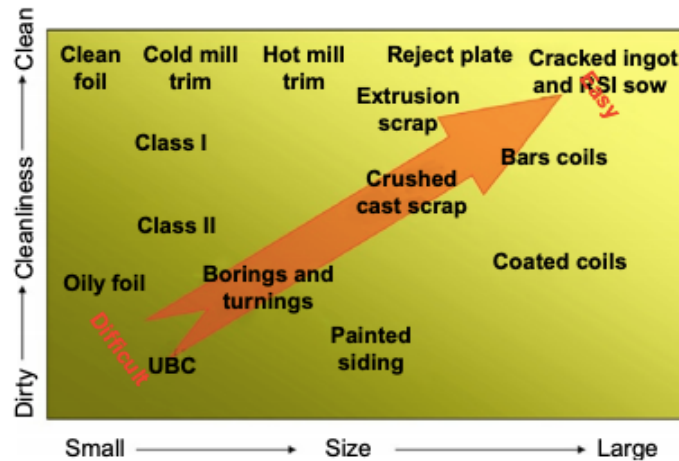


Figure 2.5. The recyclability of scrap types with respect to size and cleanliness [8].

Because it is more difficult to gain high recycling yield from small scrap pieces, these are in many cases preferably compressed into more dense bales [8].

2.5. Shredding/comminution Al scrap

An essential processes of scrap recycling is shredding (or comminution) i.e. transformation of the scrap into smaller pieces. The two main reasons for shredding is reducing the size of the scrap and removing parts that may worsen the recycling process. Shredding enable separation of dirt and materials attached to the Al product, facilitate transportation and promote further processing [10].

Mixed materials attached to the Al is most effectively removed by shredding, followed by magnetic separation. In addition, shredding and mechanical separation of metallic elements is superior to melt-refining owing to thermodynamic barriers i.e. metallic alloying elements are difficult to remove from an Al melt. Another benefit of shredding is shortened melting time of small Al pieces than larger ones [8].

Shredding of UBCs result in uniform size of the Al scrap and the inside lacquers of the cans get exposed facilitating de-coating and moisture and contaminants entrapped in the UBC being able to be drained away.

The comminution machines commonly used for shredding foils, UBCs, wire and cable scrap is rotary shredder (or rotary shear). The main benefits, compared to common hammer mill, is its combination of low speed and high torque. This result in a more uniform piece, reduced dust and fines and less noise. In addition, the scrap becomes less crumbled or compressed, which facilitate removal of coating and paint [10].

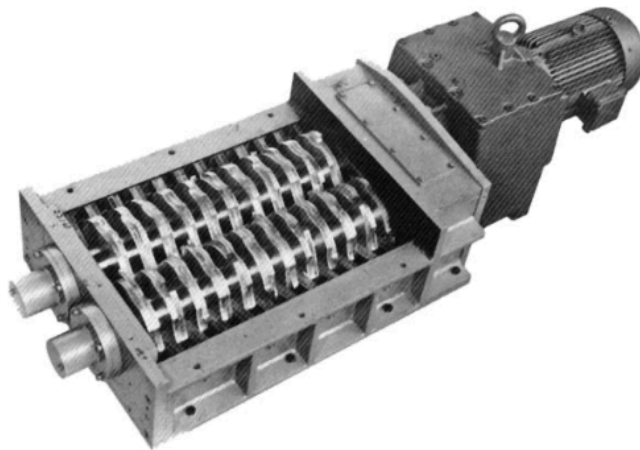


Figure 2.6. Double-rotor rotary shear [10].

Although shredding is typically included in the processing of scrap to reduce large pieces such as stamping skeletons and cable to fit into the furnace, it is also preferred to shred turnings to facilitate compaction into briquettes.

2.6. Sorting of scrap

Municipal recycling facilities (MRFs) collect all sorts of scrap. The scrap can then be hand sorted, sorted semi-automatically, automatically or a combination of these. Labor costs associated with hand sorting have led to incentives for new automatic sorting processes [21, 22].

For beneficiation of scrap, screening can be used to remove small or large items that can contaminate the material. Oversized materials can for instance be paper and cardboard and undersized materials can be glass shards and bottle caps. Trommels is a commonly used device for screening. An air separator can be used to separate heavy materials such as glass and steel from lighter Al. Furthermore, magnetic separator can be used to separate ferrous materials

from non-ferrous. An eddy-current separator (ECS) is a technology used mainly for separating nonmetallic impurities from Al such as plastics and paper [10].

2.6.1. Hand sorting

Hand sorting can in some cases be a suitable option to separate scrap. It helps remove items with similar densities but different alloys e.g. piece of copper wire mixed with Al scrap. Plastics covering the copper wire results in densities approx. the same as Al and because of copper's similar conductivity as Al, it reacts on the eddy-current separation. The advantage of hand sorting is higher in countries with relatively low labor cost. It has been common for US and Europe to ship scrap to China because of lower labor costs [10].

2.6.2. General sorting with automatic sorting techniques

Automated sorting technologies are relatively new. A high rate of development began approximately in the beginning of the 2000s. Automatic sorting techniques include [10]:

- **Air classification.** Removes low-density contaminants - an upward flow of air lift lighter plastic and paper from heavier Al metal.
- **Magnetic separation.** Remove iron, steel and Ni-alloys. Because iron contamination is increasingly undesired, magnetic separation both for upgrading and before charging in remelting furnace.
- **Eddy-current sorting (ECS).** A magnetic field causes different degrees of deflection of scrap depending on its conductivity and density. Because Al (however much similar to Mg) have high conductivity/density ratio, these are deflected (hence separated) from lower ratios of e.g. copper, silver but also other non-metals such as plastic and paper. An issue is however stainless steel, which is significantly affected by the fields similar to Al, and also not removed by hand sorters and magnetic separation. An example of a eddy-current separator is presented in Figure 2.7 below. Other factors that affect the eddy-current sorting is mass and shape of the scrap particles. A larger size and a more non-spherical will deflect more. To reduce the effect size has on sorting outcome, a uniform-sized feed is preferred.

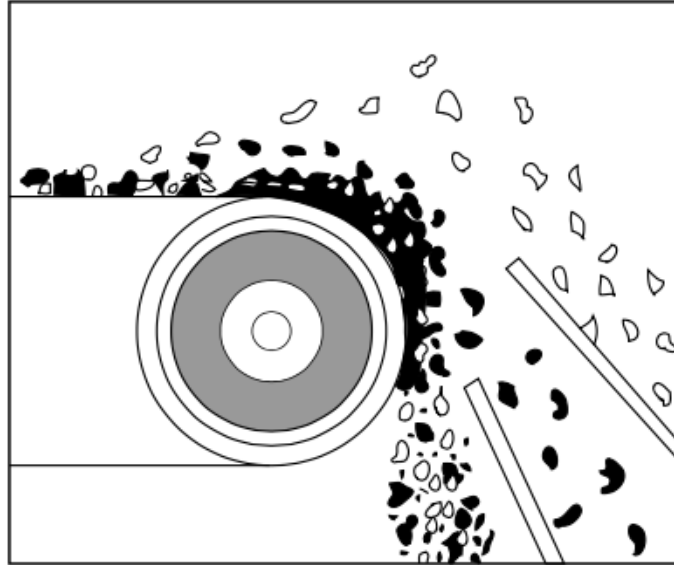


Figure 2.7. Conveyor-type eddy-current separator.

- **Heavy-Media separation (HMS).** The scrap is separated in a fluid with a density between those scrap being separated.
- **Thermal separation.** For some scrap products that contain different alloys or attached with other metals, thermal processing can be used for separation. The difference in melting points between the materials are utilized. Having a process temperature between the melting points of the alloys or metals, the material with lower melting temperature melted before the other material, hence is separated. A common difference between melting points is for wrought and cast alloys as well as between Al and Fe.

2.6.3. Sorting by grade

By tolerance, one refers to the ability to which an alloy can absorb different grades of scrap during manufacturing. The majority of alloys produced from scrap are cast alloys. Cast alloys have high tolerance while the tolerance of most wrought alloys is low. Usually the scrap contains too much silicon, iron, copper or zinc for it to be used for production of wrought alloys. Because of the wide recycling possibilities with wrought alloys, they are particularly valuable. Forecasts claim that the demand on wrought alloys will increase in the transport sector more than for cast alloys. Additionally, other sectors where wrought alloys are currently used are

estimated to experience higher demand. At the same time, the constantly strive for higher quality means that the acceptance of iron content and other contaminants are reduced [10].

To meet the increased demand on wrought alloys and its increased quality without using primary Al as a source in production, there are two main areas that must be developed. The first possibility is to improve the melt refining process of Al alloys. The other method is to improve the separation of alloys during the upgrade process.

There are several techniques to separate wrought from cast alloys:

- **Image-analysis.** Development of image-analysis systems have been made to replace the earlier hand sorting.
- **X-ray scanning.** X-ray scanning can distinguish particles by respective composition. Heavy metals appear darker, and because cast alloys contain more silicon and copper it appears darker than wrought alloys.
- **Acids and bases.** Acids and bases applied on the surface can change the surface color of Al alloys. Etching with sodium hydroxide makes cast alloys black and wrought grey and other colors for different alloy families. It is also discovered that nitric acid can make the discrimination even clearer. However, sodium hydroxide is a potential plant hazard.
- **Laser-induced breakdown spectroscopy (LIBS).** Another method with greater success is laser-induced breakdown spectroscopy (LIBS). A laser beam focused on the scrap makes the surface fluoresce. To this, an optical emission spectroscopy (OES) of fluorescence photons is used for composition analysis. The data is processed by comparing with alloy specifications and subsequently sorted. The composition is well determined, however, surface preparations are required for good results. Paint and coatings need to be removed to allow composition analysis. LIBS is sensitive to alkali and alkaline earth metals and detects silicon to much lower levels than x-ray devices [23]. Good separation of magnesium and wrought and cast alloys can occur with the rate of 5 tonnes per hour. The particles are shredded scrap with a fairly uniform size and mass, 20-50 grams [10, 23].

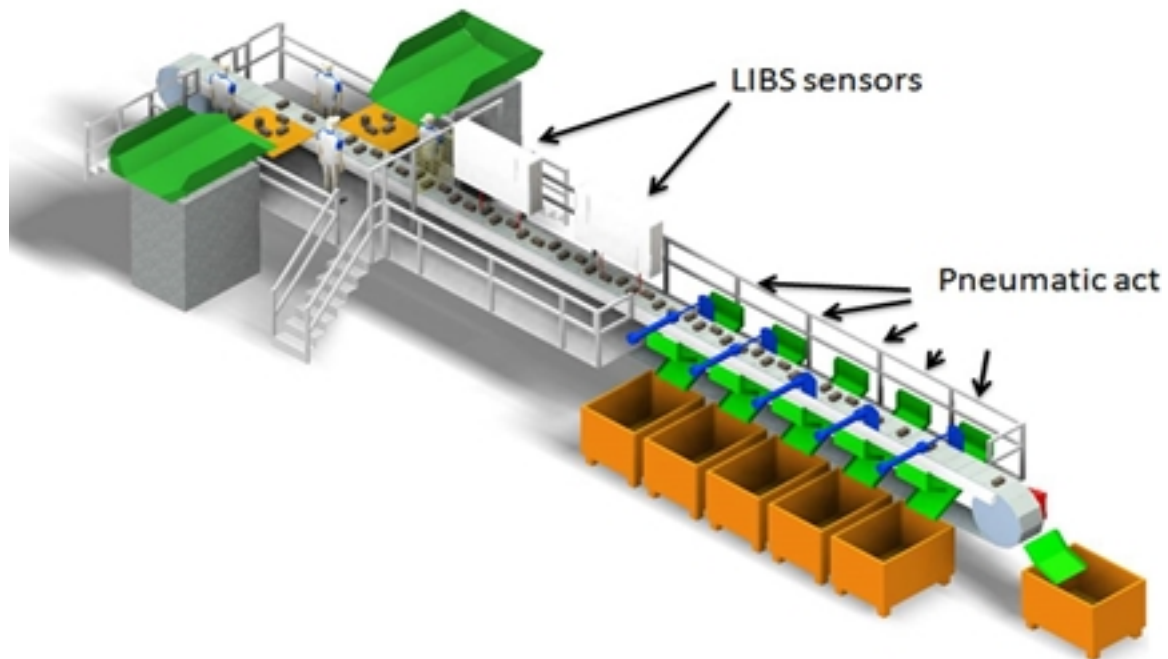


Figure 2.8. Example of a LIBS system for sorting of scrap [24].

2.6.4. Foil sorting

Packaging materials usually contain Al foil and considerable amount of plastic and paper. Both of these scrap properties complicate recycling. Large amount of plastics and paper in combination with thin Al is difficult to separate. Neither density difference nor metallic properties can be utilized for separation [10]. Some shapes such as foil and wires cannot be sorted effectively by ECS, as these do not generate eddy current [17]. As a result, the incentives and commitment to recycle Al foil has historically been low because of its complexity and costs.

2.7. De-coating scrap

A challenge with recycling aluminum products is that they often are coated with an organic material, mostly lacquer or a polymer. Extruded products such as cans and foils are coated; 2xxx and 7xxx alloys are painted; and new scrap, turnings and bearings, are covered with grease and oil [10, 25] UBCs contain 2-3 wt% lacquers and paint. This is relatively low compared to converted foil that contain 7 % lacquers and ink. Mill foil and machine turning contain <10 and <20 wt % oils, respectively.

Negative effects that arise upon melting scrap with organics coatings are (1) emissions of smoke and soot as well as dioxins and furans created from burned organics, which cause a hazardous workplace and are difficult to remove (2) significant increase in oxidation of the scrap with coatings compared to bare scrap, and hence increased metal loss. This effect holds regardless of alloys. McAvoy et al. [26] also found that melting coated scrap under salt flux reduced the melt loss somewhat but in total, lacquered scrap melted in salt flux still had higher metal loss than bare scrap.

Kvithyld et al. [27] reported that thermal de-coating of scrap is dependent on de-coating temperature and type of atmosphere. Furthermore, de-coating occurs in three steps: breaking of polymer chains, formation of VOCs (volatile organic compounds) and oxidation of char (residue on the surface generated from formation of VOCs). The oxidation of char was avoided when an oxygen-free atmosphere was used. The research showed that high temperatures lead to a more uncontrolled process and difficult to operate autothermally (the coating as the heat source in the process). In addition, high temperatures increased surface oxidation of the metal, hence higher metal loss.

Based on these findings, it was realized that recovery yield is dependent on the trade-off between (1) a lower temperature (480-520 °C) to minimize metal oxidation with risk of having coating remaining on the surface and (2) rapid heating and higher temperatures (590-620 °C) below melting point, leading to removal of coating but risk metal oxidation if the heat exposure is too long.

The oxide thickness of coated scrap can be 10 times the thickness of uncoated due to anodization process applied before coating [28]. Melting of aluminum discs that were not de-coated effectively, resulted in lower Al recovery.

There are other advantages of de-coating. Because the scrap is heated during de-coating, the time for remelting the scrap is less. This in turn means that the efficiency is improved i.e. more

scrap per time unit can be melted and recovered. Additionally, the utilization of the organic compounds (VOCs) as fuel saves energy [10].

2.7.1. Thermal and chemical treatment of foil

Products that contain Al foil also contain large proportions of plastics or paper. PET is usually attached to Al foil and upon heating generate much more char compared to pyrolyzed lacquer on Al cans.

Bare foil of wrought alloy is less prone to oxidize than many other Al alloys such as alloys with Mg content. However, foil scrap may still oxidize because it is thin (approx. 7-9 microns) and significant amount of plastics and paper are attached to the Al foil. As a result, too high de-coating temperatures should be avoided. This results in more formation of char (also known as coke) but because paper and plastic are loosely attached to the Al, the char can be knocked loose from the surface and removed by screening.

Two common process techniques to separate foil in packaging are described. Laminated beverage cartons is a common product that is recycled. They consist of paper, Al and polyethene (PE). One method is the hydra pulping process. In the hydropulping tank, the glue holding the laminate together dissolves and the paper is separated. The paper is then sorted by wet screening. Furthermore, the Al and PE is separated by shredding and subsequently eddy-current separator (ECS). Because ECS cannot remove all PE, the material undergoes pyrolysis at approx. 480 °C. For pyrolysis, although rotary-kiln is most common, it is possible to use the moving-bed de-coater [29, 30].

The other process technique to recycle laminated beverage cartons excludes hydra pulping process. Instead, shredded materials is directly inserted in a pyrolysis oven. Consequently, the scrap that has relatively high fraction of organics, a large amount of char is produced. The amount of char is too high to be charged to a furnace, and therefore must be removed by sieving and controlled oxidation [31].

2.7.2. Turnings in centrifuge

New scrap such as machine turnings are covered in moisture, grease and oil. This is removed mechanically, without the need of heat. They are commonly cleaned using a centrifuge. The spinning of the centrifuge allows the liquid to be removed, hence the turnings are safely charged in the furnace [8]. The size and the amount of oil on machine turnings varies greatly. With centrifuging it can be reduced from approx. 20 wt% to approx. 2 wt% [32].

2.8. Compaction of Al scrap

Compaction of scrap, usually denoted bailing or briquetting, is to facilitate transportation, handling and storage in addition to higher recovery upon remelting [10]. Scrap processors usually compact UBCs to bales and new scrap turnings to briquettes. Bales are much larger and have lower density compared to smaller and well compacted briquettes.

2.8.1. Balers

Shredded pieces of scrap can be baled (Figure 2.9) i.e. mechanically compressed into larger structure usually in the form of a cube. Loose pieces from shredding are characterized with low bulk density, compared to more compacted briquettes. Initially, shredded pieces were baled to facilitate transportation (particularly shipping), handling and reduce the amount of moisture pick-up during this transportation.

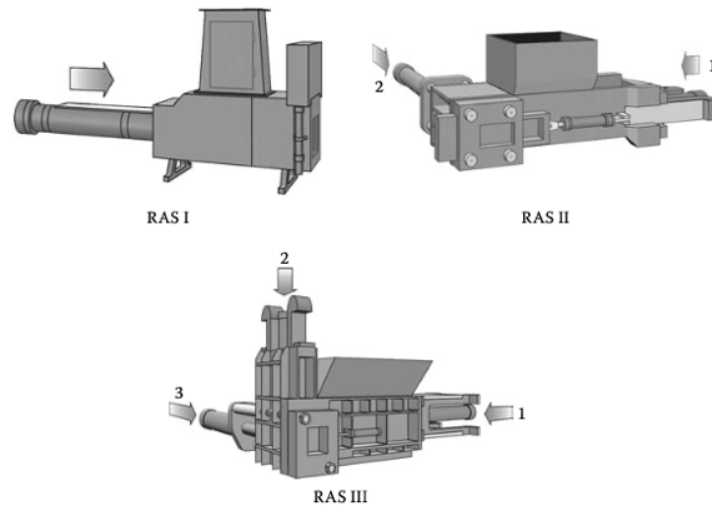


Figure 2.9. Examples of baler machines [10]

Some scrap manufacturers do not prefer scrap in the form of bales. The large size can be too big to be charged in the furnace and contain unexpected moisture, contaminants, grease and oil. Consequently, receiver of bales usually shred and reprocess them.

2.8.2. Briquetting

New scrap such as borings and turnings produced as a by-product from machining operations is widely known as a scrap type that is difficult to recycle [33]. The main reasons for this is because of its large specific surface area and large amount of contaminants. High surface to volume ratio means that the scrap is more prone to oxidation. Large amount of grease and oil from the machining operations end up with the turnings and borings, resulting in lower recovery.

Briquetting of new scrap is a relatively old method used for handling and recycling of scrap. From a recycling perspective, briquetting squeezes the grease and oil out of the feed facilitating processing. Also, incineration and oxidation during the remelting process is reduced [10, 16].

Chips are typically compressed under pressure of 30 MPa resulting in a briquette with significantly smaller in size but higher densities than bales [33]. The briquetting company RUF report that the chips are compacted to a density of 2.2-2.4 g/cm³. Refiners have reported an increase in metal yield between 2-7 % as a consequence of less incineration and oxidation [16].

Also, charging of chips can lead to high content of impurities in the cast material such as non-metallic inclusions [34, 35].

Pietsch [33] report two common briquetting methods. One is a punch-and-die machine that produces cylindrical briquettes, also known as pucks, seen in Figure 2.10 (left).

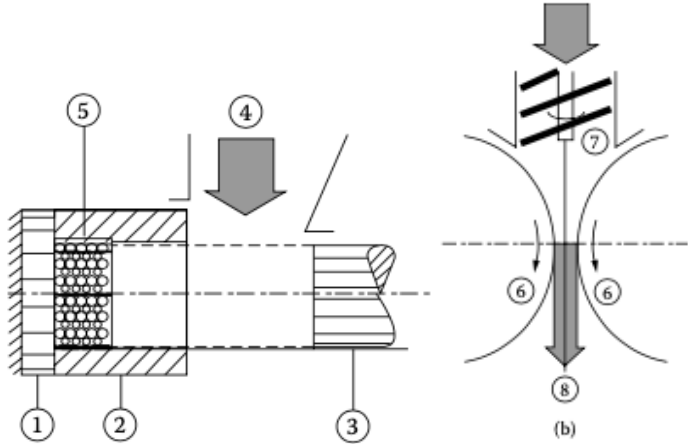


Figure 2.10. Typical briquetting methods: punch-and-die machine (left) and roller press (right) [10].

The diameter of the briquette can be 12-15 cm with a height of approx. 10 cm. The punch-and-die can better compact turnings and boring that are more elastic and it is a cost-effective method. The other briquetting method is the roller presses, seen in Figure 2.10 (right). The chips are fed in continuously operating roller press. It is more efficient and higher densities near the theoretical can be achieved. After briquetting, degreasing by thermal de-coating is necessary if the amount of grease and oil is above 1 %. This is usually the case for turnings and bearings. Were the contents to be lower than this, it can be charged directly in the remelting furnace [33].

Severe plastic deformation (SPD) of chips to produce solid extrusions can be achieved by many different techniques including cold/hot extrusion, high pressure torsion (HPT) and screw extrusion. The main objective of SPD is to produce a metallic body with suitable mechanical properties. Specifically, SPD can lead to grain refinement and minimized cracks and voids between chips. The bonding between chips depend on material properties such as ductility, present oxide layer and crystallographic reorientation (recovery or recrystallization) at the chip-

chip interface [36, 37]. Research show that the oxide layer must be ruptured before contact between metal can occur [38, 39].

2.8.3. High Pressure Torsion (HPT) and Screw Extrusion

The properties of metallic materials can be improved by applying high strain without changing the shape of the material. Recent plastic deformation techniques are accumulative roll bonding (ARB), equal channel angular pressing/extrusion (ECAP/ECAE), high pressure torsion (HPT) and compressive torsion process (CTP). In the two latter techniques, compressive stress and shear are applied simultaneously. However, in HPT high compressive stress is applied on a thin disc as (a) or a bulk sample (b,c) (Figure 2.11). HPT can be used for solid state recycling of chips. Furthermore, HPT is widely considered an effective grain refinement method in addition to consolidating chips or powders. In CTP, lower pressures can be applied (hundreds of MPa) on a bulk cylindrical specimen, powder or chips [40]. Even low compressive pressures result in consolidation and a dense body [39-41].

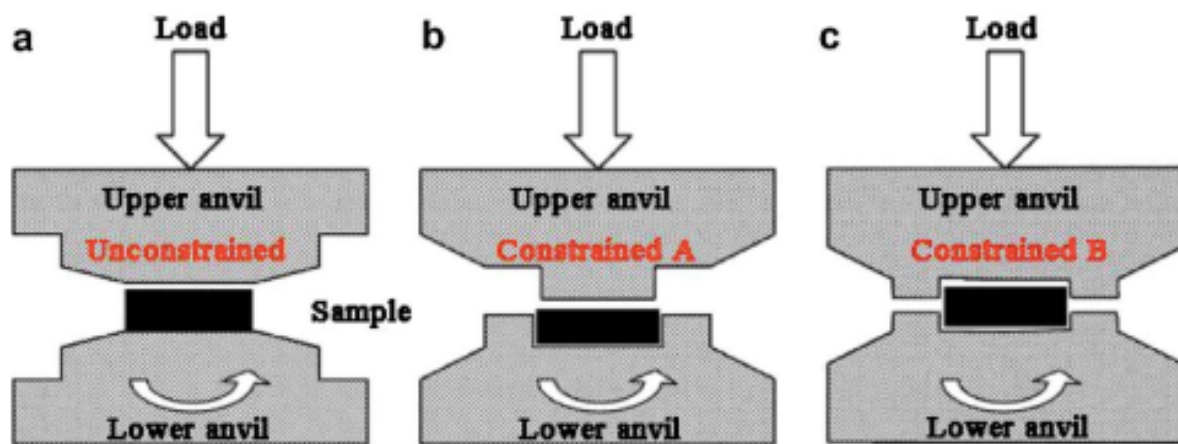


Figure 2.11. Illustration of two modifications of (HPT), (a) unconstrained HPT and (b,c) constrained HPT [39].

By solid state recycling the aluminum scrap particles are compressed to maximum bulk density to real density or slightly below. By that, the material properties are similar to those of a cast product of same composition. In [40] relative density of 98 % was achieved by compaction of 7050 aluminum alloy chips. The chips were uniaxially compressed to 700 MPa prior to applied

torque of 30 revolutions at temperature of 100 to 470 °C. Micro void coalescence was seen as the fracture after tensile testing. It was reported that high temperature pressing prior to CTP resulted in less pores compared to pressings at lower temperature. The compressed chips alloy showed worse elongation but similar strength to the non-recycled alloy.

Screw extrusion is a suitable method to transform granulated Al chips to continuous extrusion material. The screw motion in conjunction with heat deforms the granules through a nozzle producing a consolidated solid product. The advantage of screw extrusion is particularly the phenomenon of combined compression and rotation in a continuous process. The shear force significantly improves the compression effect compared to merely axial compression [39].

The mechanisms of consolidation of Al chips due to compression with shear force is also relevant to describe for this thesis. The consolidation starts with oxide layer rupture caused by the applied shear force. Subsequently, the direct contact between metal can occur and interface bonding of chips is achieved. Research indicates that voids, cracks and pores are distributed around the interface of the chips [42]. Another proposed theory states that metallurgical bonding i.e. atom diffusion bonding between chips occurs due to SPD. Subsequently, as the specimen becomes fully dense, nodular oxides are uniformly dispersed in the Al matrix. In addition, interface and crystal defects caused by shear deformation may act as diffusion paths for atoms. Shear effectively ruptures the oxide layers into oxide particles because of multi-pass shear deformation and reduces the pores between chips [39, 43].

Uniaxial pressing of chips to improve the recycling yield has been studied by Mashhadi et al. and Fogagnolo et al. [44, 45]. In Figure 2.12, below two cold pressing results are shown. In the right image [45], the maximum bulk density of 2.48 g/cm³ was achieved by applying 650 MPa. In the left image [44], a bulk density of 2.5 g/cm³ was achieved by applying 900 MPa. The size and thickness of the chips were not reported.

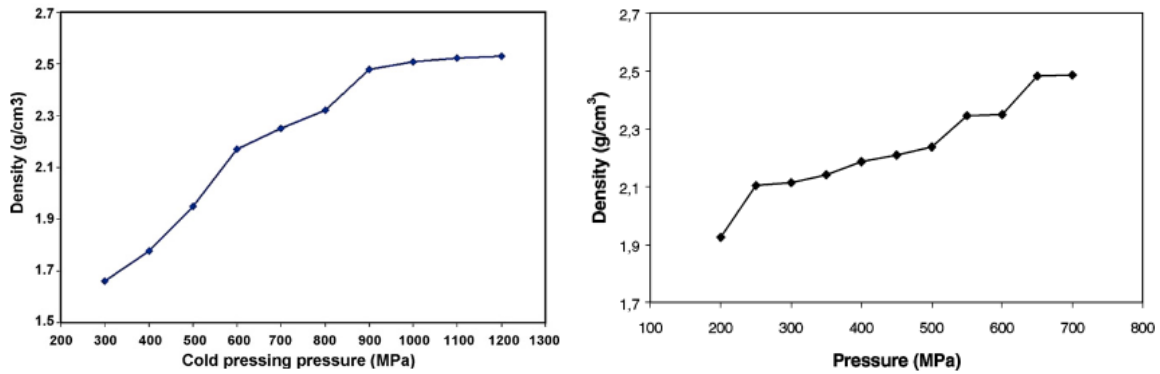


Figure 2.12. Two different studies showing the relationship between bulk density and compressive stress for Al chips [44, 45].

2.9. Melting to recover scrap

Wide variety of furnaces and specific modifications of these are used to melt light, small and contaminated scrap. Light scrap is usually melted by fossil-fuel driven furnaces i.e. burners with high heating efficiency are used. New design such as the geometry, placement of burners, and scrap feeding systems is continuously developed to increase the heat transfer as well as decrease oxidation, refractory wear and inclusions in Al melt. In general, to effectively recover Al from thin scrap, salt fluxes or a submerge system such as vortexing are used.

2.9.1. Oxidation of Al scrap during heating and melting

Material properties that have an impact on oxidation are alloy composition and surface properties. Specific alloying elements and the amount of these, and large surface area lead to more oxidation. Furthermore, parameters associated with melting operation that have an impact on oxidation are temperature, time and atmosphere. High temperature, longer heating or melting times and higher partial pressure of oxygen in the atmosphere promote oxidation. In practice, pouring, stirring and skimming operated in the industry all contribute to increased oxidation. In recycling industry, measures that reduce oxidation lead to less dross formation and increased recovery of Al [46-53].

Like many other metals, metallic Al alone is never found in the earth's crust. Because of high affinity to oxygen (O), there is a high driving force of Al to recombine with oxygen accordingly:



This is physically quantified with “Gibbs free energy of formation” expressed in the unit kJ/mol element (Figure 2.13). A more negative value of the Gibbs free energy corresponds to higher driving force in proceeding the reaction to the right. The Gibbs energy of common industrial oxidation reactions is compiled in the Ellingham Diagram [8].

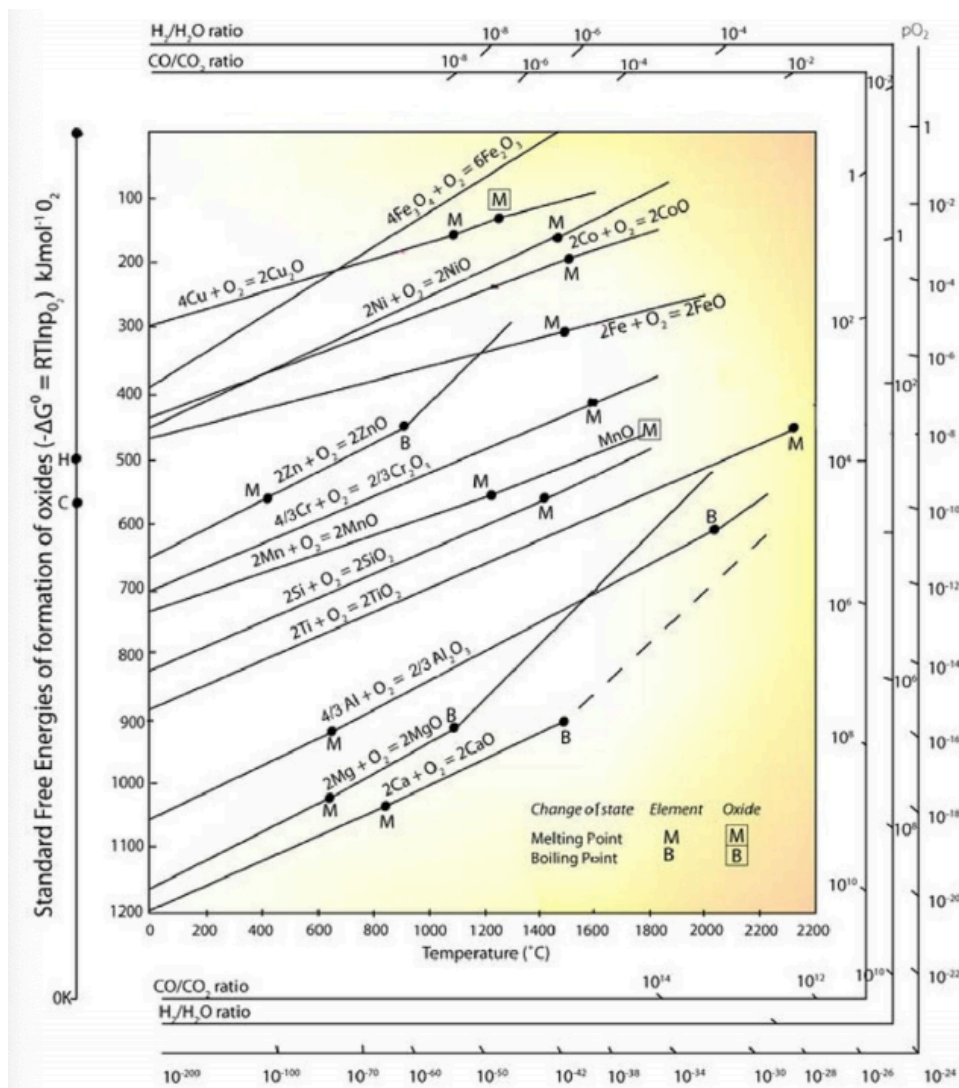
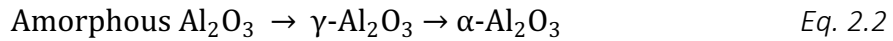


Figure 2.13. Ellingham diagram [54].

Gibbs energy of formation is dependent on given metal oxide, mole oxygen reacted and temperature. The Ellingham show the relative stability of elements and corresponding oxides. Only Mg, the alkalis and alkaline earths are more reactive with O. As Al has higher affinity to O

compared to many other alloying elements, it from a recycling perspective important avoid presence of other metal oxides. For instance, SiO_2 present during melting operation is reduced by Al, leading to dross formation [55].

The growth and ability to protect Al from further oxidation depends on the phase of Al_2O_3 . In general, Al_2O_3 undergo phase transformation accordingly:



The oxide transforms from an initial amorphous compound into the crystallographic γ -phase and ends with the most stable, α -phase. In recycling, $\alpha\text{-Al}_2\text{O}_3$ is undesirable because it is very stable and has very limited solubility. Oxide of α -phase cannot be further processed, and the inherent Al is considered lost. High temperatures above melting point and time are two factors that promote formation of α -phase transformation, as illustrated by Trunov et al. [56] in Figure 2.14 below. Trunov et al. studied the oxide growth on pure liquid Al, however, the phase transformation is similar for solid Al [8].

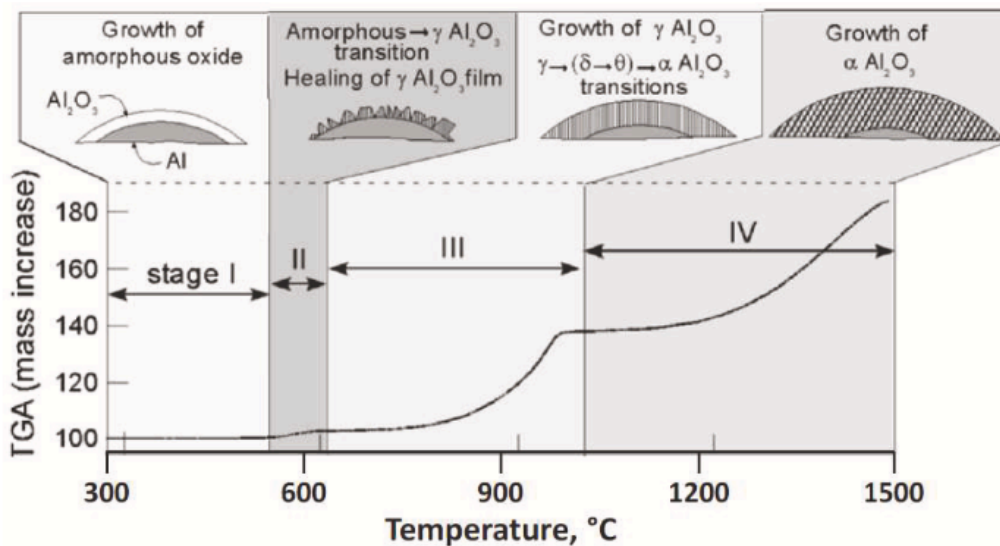


Figure 2.14. Phases formed during oxidation of pure Al [56].

The transition from amorphous phase to crystalline γ -phase is slow as the temperature is below the melting point of Al [51, 53, 57]. The oxidation rate is dependent on the phase transformations. A consequence of transformation from γ to α is volumetric change. This induces stress on the oxide that in turn result in rupture of the oxide, hence new nucleation sites are generated for further oxidation. It is further argued that rupture results in renewed oxidation, known as breakaway oxidation i.e. increased oxidation rate [58]. As the Figure 2.14 above illustrate, the weight increases most as γ -phase is transformed to α -phase [59].

The general oxidation kinetics for Al is shown in Figure 2.15 below. As seen in the graph, oxidation can be separated into the sections: incubation, breakaway and passivation.

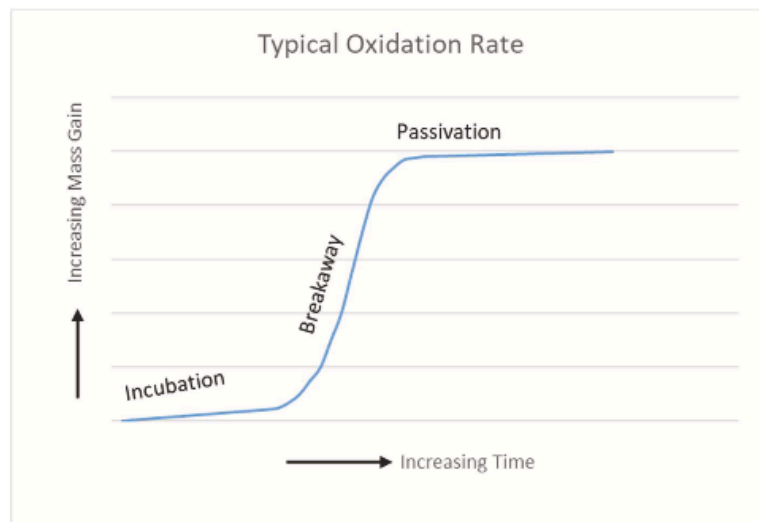


Figure 2.15. Typical oxidation kinetics of Al [60].

An oxide film is always formed and present on the surface regardless of solid or liquid state. In the incubation stage, the oxide growth is linear and rapid until a critical thickness is reached. For given circumstances, breakaway oxidation can occur i.e. the oxide thickness rapidly increases owing to phase transformation of the oxide. Breakaway oxidation depends on circumstances such as composition, temperature and time. Finally, the oxidation rate is significantly reduced as the phase transformation of the oxide is complete i.e. the passivation stage is reached. [48, 60]

The mass increase showed in the Figure 2.14 and Figure 2.15, correspond to increase thickness of the oxide. The thickness of the formed and stable oxide film is limited. In room temperature, the limiting thickness is 1-3 nm, 20 nm at 300 °C and 200 nm at 600 °C [61].

2.9.2. Alloying elements effect on oxide film growth

The oxide film thickness and configuration is dependent on alloying elements. Alkali and alkaline elements that are more reactive to oxygen such as Li, Na and Mg have shown to increase the oxidation of Al alloys. The Pillings-Bedworth (PB) ratio, defined in Eq. 2.3, is the most common measure used to characterize the protective effect of the oxide film:

$$PB = \frac{\text{volume of oxide produced}}{\text{volume of metal consumed}} \quad \text{Eq. 2.3}$$

The value of PB informs about the influence alloying elements have on the protective Al oxide film. A value below one means that the film will shrink and crack, which results in further oxide film growth. The PB ratio of Li, Na and Mg oxides are below one [8].

As Mg is a common alloying element, the impact of Mg additions has been studied by many. The oxidation rate depends on the amount of Mg in the alloy [62]. The MgO film that is created is less protective than Al₂O₃, leading to increased oxidation and hence more dross is formed [8].

With respect to thermodynamic laws, some alloying elements will be distributed to the oxide layer. This in turn has an impact on the morphology and the ability to protect from further oxidation. Volatile elements that vaporize for a given vapor pressure, cause pores in the oxide layer. As a result, the protective nature of the oxide is weakened, and the oxidation is favored. Formation of pores in the oxide facilitate transportation of ions to form more oxide. Thiele showed that this is the case for the elements sodium (Na) and selenium (Se) [49].

Alloying elements have shown to affect the strength of the oxide film. Experiments by Kahl and Fromm indicate that evaporation or incorporation of elements lithium (Li), sodium (Na) and

calcium (Ca) effects the strength of the oxide layer. Moreover, these alloying elements are also known for promoting oxidation of Al [61].

2.9.3. Reverberatory furnace

The dry heart furnace is suitable for melting large and bulky scrap. To maximize recovery of light gauge postconsumer scrap, a modification of the dry heart furnace is made by adding an external box that can contain metal, called side bay. With this modification is often referred to as side bay melter or reverberatory furnace, as seen in Figure 2.16. It is used in the scrap processing industry because of its low costs and high capacity. Unlike dry heart furnace, the fuel is not in direct contact with the scrap. Moreover, the heart of the furnace contains burner-flue configuration that supply heat to the metal. The heart is characterized by always containing molten metal. Molten metal is pumped from the heart to the side bay. Melting of the charged scrap occurs in the side bay owing to conduction from the molten pool and as a result higher recovery is achieved while flame impingement is avoided. To increase the recovery further, salt flux is used in the side bay to protect from oxidation and promote metal coalescence. This furnace is suitable for processing of light scrap with large surface area such as turnings, foil and UBCs. The reverberatory furnace is often coupled with a rotary kiln to process UBCs [8].

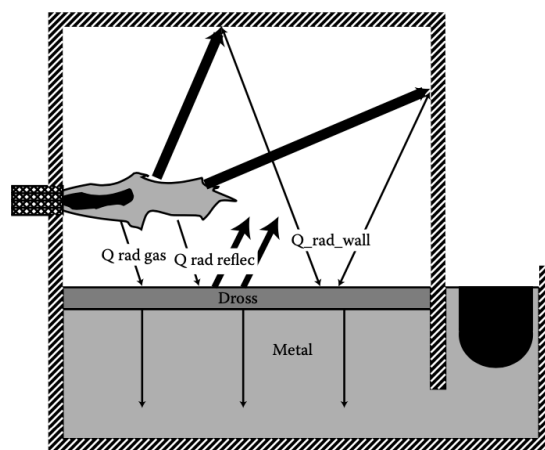


Figure 2.16. Cross section of reverberatory melting furnace [63].

2.9.4. Sidewall melting furnace

The sidewall melting furnace was developed to melt light scrap such as UBCs, as seen in Figure 2.17 [64]. It was designed to eliminate direct contact between combustion gases and solid scrap – to reduce melt loss and dross formation.

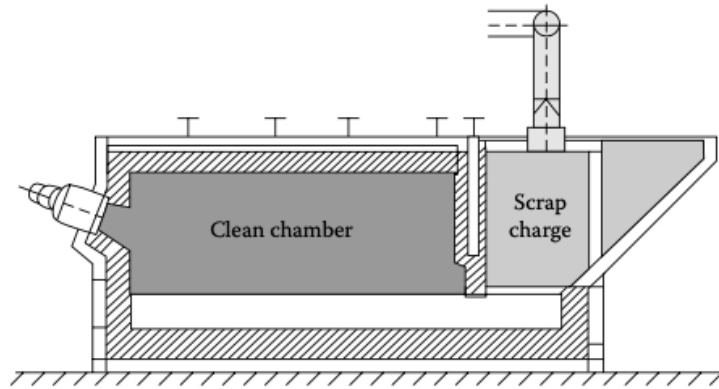


Figure 2.17. Cross-section of simple sidewell furnace [10].

Only the molten metal is heated by the burners i.e. the combustion gases avoid direct contact with the scrap. The molten metal flows under a baffle, heating and subsequently melting the charged scrap. The dross produced lies on the surface and protect from further oxidation. The solid scrap is more prone to oxidize by the local high temperature generated by the burners. Disadvantages such as poor fuel efficiency, slow melting rate and oxidation of finely divided scrap lead to the development of vortex furnaces. With vortex the scrap is quickly submerged in the melt before it can oxidize. In Figure 2.18 below, one of the developed furnaces are shown. It consists of three parts, vortex chamber, intermediate well and main chamber. In the intermediate well, the floating dross can be removed. Superheated molten metal is continuously pumped into vortex chamber. Both coated and de-coated can be charged in this furnace, although metal loss is higher for coated scrap pieces [10].

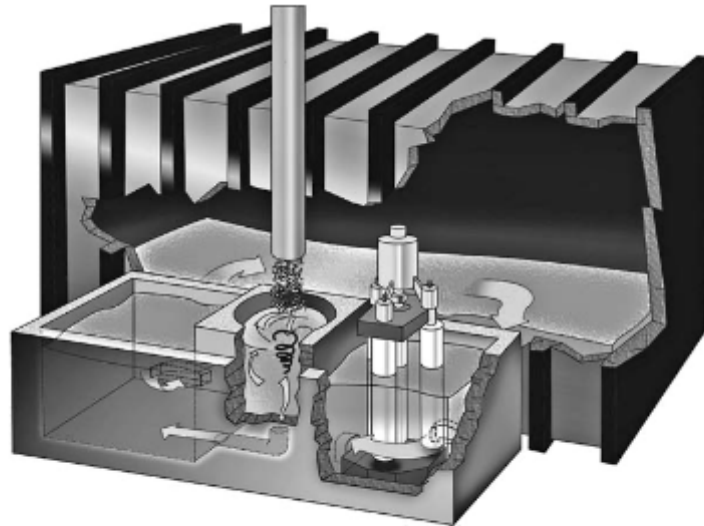


Figure 2.18. LOTUSS scrap submergence system [10].

Stirring such as vortexing facilitate larger inclusions dissolved in the metal melt to be transferred to dross by argon bubbles [10]. Hearth type melting furnaces can be equipped with vortex-installations, which can be operated with electromagnetic or mechanical pumps. This leads to the chips being stirred into the molten mass [16].

2.9.5. Rotary furnaces

Salt flux is often a requirement for scrap with high content of oxide in relation to aluminum such as thin scrap and dross. In a tilted rotary furnace, molten Al is mixed with salt flux. By rotation the molten Al is separated from the produced salt slag. An example of a rotary furnace is shown in Figure 2.19 below.

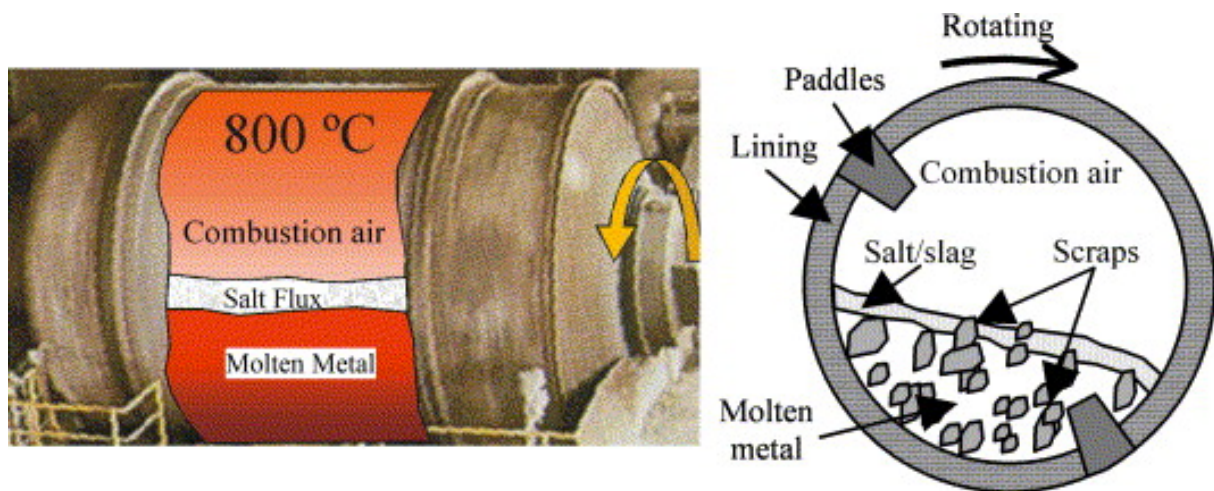


Figure 2.19. Tilted rotary melting furnace [65].

The chamber of a rotary furnace is long sloping tube with burners that combust gas or fuel from the bottom. It is tilted one way for charging and combustion and the other way for tapping of metal and dross. The tube rotates slow as scrap is solid, to prevent wear on refractory walls. With time as scrap becomes liquid the rotating speed is increased. It is most suited for melting oxidized scrap such as dross [66, 67].

2.9.6. Salt flux

Salt fluxes are used in both primary and secondary industries, added to increase the recovery of aluminum scrap and processing of skim. Salt flux is usually added in a rotary melting furnace or similar unit. The salt flux wets the oxide present with the scrap or skim charge, hence separate the aluminum. Aluminum droplets coalesce and a continuous molten pad is produced under the salt. The salt flux also function as protection from further interaction between aluminum and oxygen atmosphere and absorb contaminants [68, 69]. Coalescence is favorable in recycling of aluminum, including recovery of other metals such as magnesium [70].

Other important properties that a salt flux should possess are [71]:

- Not react or contaminate the Al
- Melting point below 660 °C
- Density less than molten Al (2.3-2.4 g/cm³) and low viscosity
- Have low vapor pressure

- Avoid adsorbing water
- Not toxic and recyclable

One of few materials that meet these requirements is chloride and fluoride salts [71]. A 50 wt% NaCl and 50 wt% KCl composition dissolves the oxides but do not effectively cause coalescence. This was solved by adding small amount of fluoride salts, hence the metal recovery yield was also increased. The mechanism of oxide removal and coalescence is further described in section Coalescence of liquid metal in salt flux.

2.9.7. Recovery of thin scrap

The weight of cans has reduced with time. In early 2000's the can weighed only a third of the weight in 1970 [10]. In other words, the thickness of the most common thin Al scrap is continuously reduced. It is expected that the thickness of the Al in other packaging has reduced to similar extent.

The Al loss from remelting of scrap with respect to alloying elements Mg and Mn, scrap thickness and temperature have been investigated [58]. In Figure 2.20, the relationship between thickness and melt loss is presented.

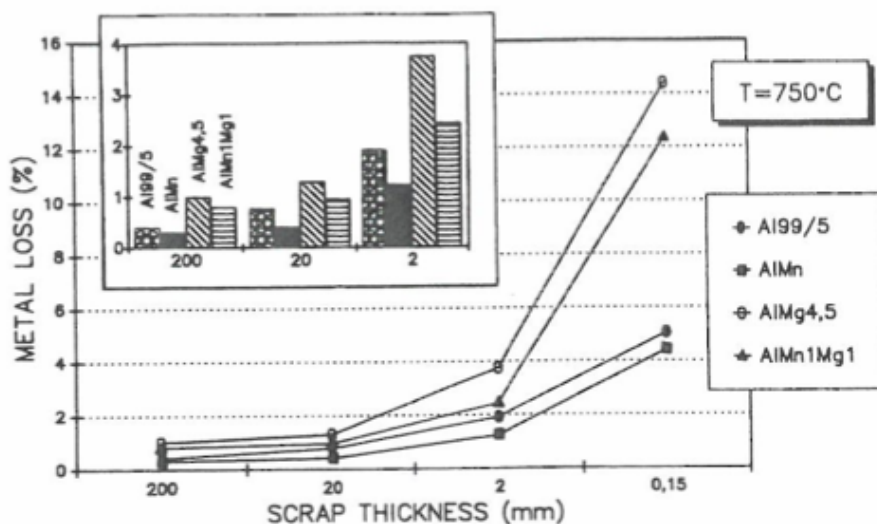


Figure 2.20. The relationship between metal loss and scrap thickness [58].

Many parameters are involved in melting scrap that can influence the recovery outcome, such as:

- Type of furnace
- Type of scrap (size, alloying elements, contamination etc.)
- Melting medium used
- Temperature and kinetics
- Operation practices

Few studies at a larger scale are available. In contrast, Rossel [58] used a fired hearth-type furnace to melt 200 kg bare scrap, having a metal surface of 0.5 m². The melt loss is the sum of the oxides (mostly Al₂O₃) and Al entrapped in the dross generated on the surface (Figure 2.21 below). It was reported that melt loss can occur due to (i) oxidation at the liquid Al surface depending on temperature and atmosphere, (ii) oxidation during scrap melting and superheating (iii) dross formation on the surface.



Figure 2.21. Example of dross skimming operation.

It is evident that there is a relationship between oxidation and metal loss. Thickness of the oxide layer can vary between 2-10 nm and can grow to 200 nm during the heating-up process close to the melting point. Oxidation also depends on composition, atmosphere, time, temperature, moisture, organic contaminants, surface area exposed and surface roughness [72-75].

One relationship found was an exponentially increased melt loss with decreased thickness of scrap, regardless of alloy. The melt loss also increases with increased Mg content. The melt loss

of 150 μm thin scrap was 5-8 %, depending on temperature. Melt loss was seen to increase with melting time and temperature. Furthermore, the melting time increases with decreases thickness of scrap possibly due to lower thermal conductivity (higher porosity and more oxides) [58]. In [34, 35, 76], the melting time was longer for more dense material.

Thinner gauge sheet or finer chips are characterized by its larger surface area per given volume or mass (i.e. specific surface area). Consequently, this can result in a higher specific oxide content upon heat treatment or melting [8]. In Figure 2.22 below, the increased melt loss with decreased thickness is illustrated.

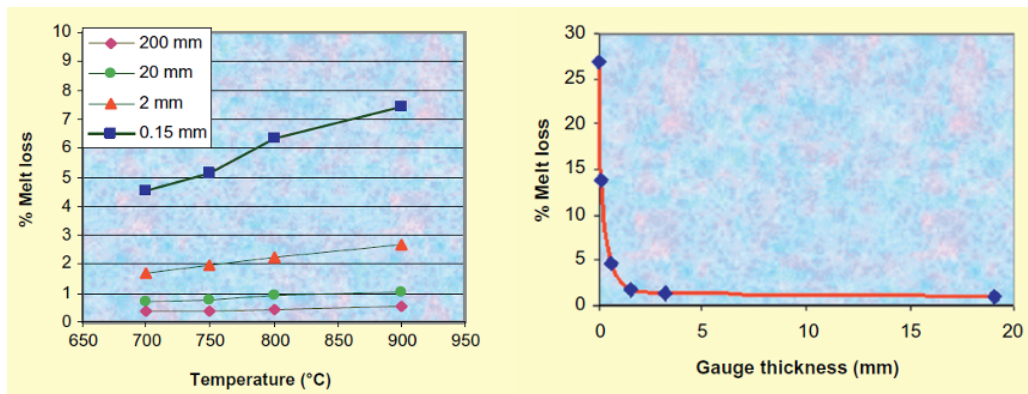


Figure 2.22. Melt loss (%) varies with melting temperature and thickness of scrap [58, 77].

The size of the scrap influences the melting process and recovery in salt flux, as investigated by Yang et al. [76]. The recovery of metal in salt flux is increased with increased coalescence. Coalescence of melted foil in salt flux was shown to be difficult compared to other scrap types such as cast ingots, rolling mill cuttings, printing plates etc. Increasing process time, stirring and temperature indicated an increased coalescence of Al metal in salt flux. The average recovery of melting granules with a size less than 1.4 mm was 68.7 wt% and 92 wt% for granules larger than 6 mm. The fluoride compound added to the NaCl-KCl salt in the research by Yang et al., was Na_3AlF_6 , the salt/Al ratio was 2 and the process time 2 hours. The melting time of smaller scrap was shorter. Melting time was shown to be related to efficiency and energy consumption, which is an important factor at an industrial scale.

2.9.8. Recovery from melting of chips and briquettes

Research on the topic of melting of chips and compacted chips in the form of briquettes in salt flux or liquid Al pool to measure the effect on recovery has been carried out by several researchers [34, 35, 44, 78-80]. Parameters that has been investigated include bulk density, process/holding time, temperature, stirring, protective atmosphere and oxide removal with ultrasonic sound.

Parameters that has been investigated before are bulk density, process/holding time, temperature, stirring, protective atmosphere and oxide removal with ultrasonic sound.

Paulitsch et al. [78] investigated the recycling yield by compacting Al turnings into briquettes that were subsequently charged with salt flux. Turnings charged directly to the surface melt led to metal losses up to 70 %. The results show that the Al content that was lost in the by-product salt cake was larger for melted chips than it was for briquettes.

Puga et al. [34, 35] investigated the recovery of aluminum swarf/turnings compacted to different extent and melted by induction with argon atmosphere. Their studies included investigation of the effect of bulk density, melting time and temperature on the recovery in liquid Al pool without the use of salt flux. It was found that the recovery varies with different compressive stresses applied on the chips. The temperature had relatively low effect on recovery. However, the relationship between compaction and recovery varied between their studies. In their first study, it was argued that recovery increases as the density of the bales decreases. It was also argued that the melting time have an impact on recovery. As melting time also was shorter for briquettes of lower density, it is uncertain to what extent the time and the density impacted recovery. Furthermore, it is uncertain whether it is the thermal conductivity and melting time related to density; or the oxide content related to specific surface area and density that is the determining factor of recovery [35]. In their second study, although the densities were similar, the highest recovery was obtained for the briquette with intermediate density. The explanation proposed was that there is a trade-off between floating time on surface and total melting time of the compressed material. This was confirmed as the recovery significantly increased as a result of argon atmosphere. It was stated that recovery

decreases with shorter melting time because the exchange of Al metal from the dross could not be completed. Moreover, perhaps the recovery could be increased if holding time is increased [34].

The recovery was increased with the use of argon flush as protective atmosphere. By that, it is expected that oxidation at this high temperature is avoided. Argon flushing in conjunction with ultrasonic sound merged in the melt are described as the two most important measures for achieving high recovery [34, 35]. The effect of stirring was also investigated. Stirring was observed to affect oxidation, heat transfer and facilitated rupture and removal of the oxide films. It was argued that applied stirring (with simultaneous argon flushing) resulted in rupture and removal of the oxide films and also reduces melting time due to increased heat transfer [35].

The recycling of Al turnings was also studied by Mashhadi et al. [44]. They studied recovery from chips and briquettes of casting alloy AA336 melted in salt flux, liquid Al and bare scrap i.e. without any melting medium. Melted in salt flux, the bulk density had no or little effect. However, the recovery increased with increased bulk density for the melting trials in liquid Al and of bare chips and briquettes.

Kvithyld [79] investigated the recovery of alloy AA6063 turnings and the compaction of these. The turnings and compacted pieces were melted in liquid Al without added salt flux. Also in this study, higher recovery was obtained as the turnings were compacted and as the compaction increased.

Xiao and Reuter [80] studied the recovery of loose turnings of different alloys melted in salt flux. They found that recovery of turnings depended on the scrap type, contaminant, specific surface area and size distribution. In addition, the recovery increased with coalescence and turnings not completely covered resulted in lower recovery. Larger specific surface area, smaller sizes, wider size distribution and more contaminants correlated to less recovery of the Al turnings. A smaller size results in larger specific surface area and in turn larger surface area covered with oil and grease. A clear distinction between these and the effect on recovery was difficult to determine. Investigating multi co-linearity of these quantities may give indications

on how oxide film, aluminum size and mass or contaminants effect the recovery and coalescence.

With respect to research available, the effect that compaction, melting time and oxidation has on recovery is yet to be determined. In addition, the relationship between the chips properties (such as mass, surface area etc.) and the effect of compaction of these chips have not yet been thoroughly studied.

2.10. Coalescence of liquid metal in salt flux

2.10.1. Surface tension

Surface tension is a characteristic of a liquid that describes the tendency of liquid surfaces to shrink into minimum surface area. This can be explained by cohesive forces and adhesive forces acting in opposite direction, which lead to equilibrium. Considering a liquid in air, higher attraction between liquid atoms (caused by cohesive forces) than attraction between liquid and gas (caused by adhesive forces) result in a surface tension. The relationship between cohesive and adhesive forces can be determined by wetting, the contact angle and the shape of the meniscus. Furthermore, this means that the surface tension determines the shape of liquid droplet. The tension between two liquids is instead denoted interfacial tension i.e. the interfacial tension determines the shape of the Al droplet in molten salt. A spherical shape minimizes the interfacial tension of the surface layer according to Laplace's Law. Surface tension is usually denoted with γ and is measured in force per unit length or energy per area [81].

2.10.2. Fundamentals of collision and coalescence of droplets

Coalescence is important to Al recycling yield and a highly complex phenomenon that has been studied by many researchers since the beginning of 1900's and still is the focus of recent research [82]. Before two droplets coalescence, collision must occur due to relative velocity in different flow regimes. The droplet velocities are different from the surrounding continuous flow field. Many flow regimes can be found stagnant continuous phase to fully turbulent flows. If the velocity gradient of the continuous phase flow is neglected, then the relative velocity only

depends on the drop sizes. In a dense-packed zone the relative velocity is near zero, however, coalescence events induce fluctuations and movement in the dispersion band [82].

Prior to coalescence, three other processes occur described by Vijayan and Ponter [83] and Jeffreys and Davies [84] according to [82]: (i) approach, (ii) contact and deformation and (iii) drainage of continuous film trapped between drop interfaces. The kinetics of these processes vary depending on chemical conditions. In Figure 2.23 below, these process steps are illustrated.

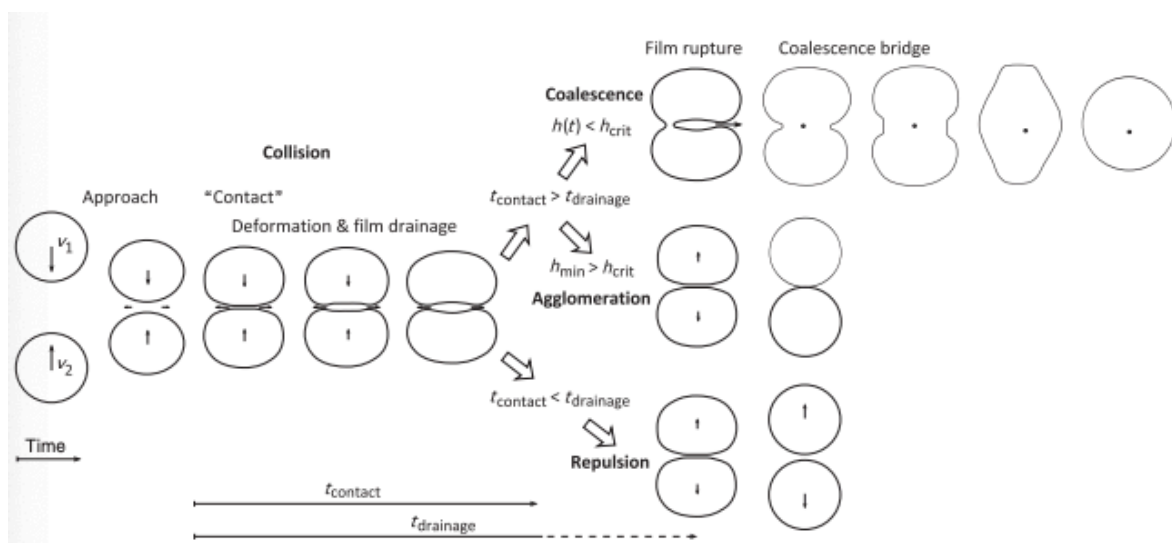


Figure 2.23. Schematic sequence of collision of two droplets and subsequent coalescence, agglomeration or repulsion according to Gäbler and adapted by [82].

Factors that have an impact on the coalescence is complex because several physical aspects are altered simultaneously when one property is changed. Generally, the probability of coalescence is influenced by interfacial properties and surface-active elements. The coalescence is affected by the properties of the continuous phase (here salt), the dispersed phase (here aluminum) and the corresponding interface between them, as summarized in Figure 2.24.

Continuous phase	Interface	Disperse phase
Viscosity Density Energy input/velocity Flow pattern/regime Ionic strength, pH (if aqueous)	Interfacial tension Surface potential Surface active components: surfactants, particles, ions Mass transfer	Viscosity Density Drop diameter Ionic strength, pH (if aqueous)
Ambient and system conditions Temperature, pressure, geometry, surface wetting, electrostatic field, microwaves, ultrasound		

Figure 2.24. Properties of continuous phase, interface and disperse phase that influence coalescence [82].

Because coalescence is an interfacial phenomenon, factors that affects the interface have a significant impact on coalescence. The interfacial phenomenon is driven by minimization of interfacial area/energy. Concerning the dispersed phase, the drop diameter is probably the most important influencing factor on coalescence [82].

2.10.3. Coalescence of Al droplets in liquid salt flux

The oxide film removal and coalescence of Al in salt flux has been the subject of many studies [68, 85-93]. The morphology and thickness of the oxide layer are crucial factors. The tearing strength of aluminum oxide is high enough to withstand expanding liquid of 20 times the weight of the oxide [58]. According to Jordan and Milner and Storchai [94, 95] the mechanism of oxide removal by salt flux is electrochemical; oxide cathode, aluminum anode and electrolyte of salt flux. In this process, salt flux penetrates the oxide and detaches the oxide from the aluminum while Al^{3+} ions weaken the oxide layer.

Many researchers including Roy and Sahai [85, 86, 90] have reported that change in interfacial tension between salt, Al and alumina is the driving force for oxide removal. Furthermore, improved oxide removal is stated to favor coalescence ability. Minimum interfacial tension between two phases is thermodynamically favorable with regards to the principle of minimum

energy (based on second law thermodynamics). The high activity of elements in the salt flux is the main argument of a reduction of interfacial tension between Al and salt. Because of this high activity, displacement reactions occur at the Al-salt interface. Displacement reactions not only lead to removal of the oxide layer, but also adsorption of salt elements in Al and dispersion of Al in the molten salt, the latter leading to metal loss.

In many studies, the interfacial tensions have been measured in a salt-aluminum-oxide system of different fluxes. The results have shown that decreased interfacial tension between molten salt and Al metal promotes the removal of oxide film present on the Al droplet surfaces [85, 86, 90, 92, 93]. The process steps of oxide removal were illustrated by Jordan and Milner accordingly (Figure 2.25):

1. Openings develop in oxide layer
2. Salt penetrates between the oxide and metal
3. Oxide layer is stripped

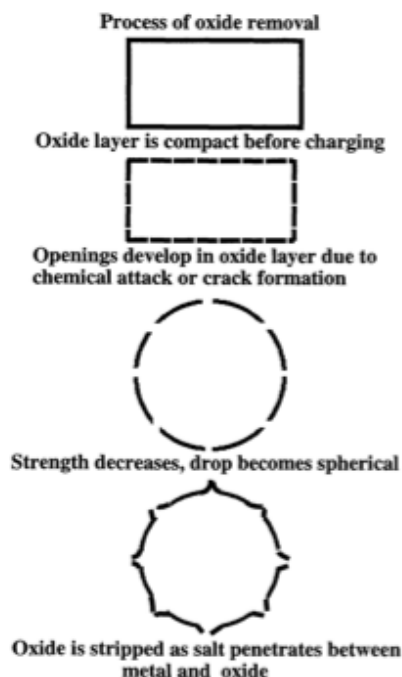


Figure 2.25. Schematic representation of oxide removal and coalescence proposed by Jordan and Milner [85].

In 1., openings develop the oxide ruptures, which according to [85, 86, 96] is caused by a simultaneous process of thermal expansion of Al due to heating and chemical attack of salt elements. The attack by salt elements is stated to undermine the oxide layer.

Furthermore, the shape transformation to spherical takes place i.e. the surface area/energy of Al droplets is reduced. Minimum free energy in the system is at last achieved as Al droplets coalesce i.e. by merging of multiple smaller droplets into one large droplet the surface area is minimized.

Shape change to spherical did not occur before the coalescence phenomenon for all different fluoride additions [85]. This concerned compounds such as NaF, KF and Na_3AlF_6 , all of them which contributed to excellent coalescence ability but also more melt loss. This is caused by relatively higher surface activity of the elements, which lead to more significant reduction in interfacial tension between Al and molten salt. For CaF_2 , spherical shape transformation took place before coalescence, as seen in Figure 2.26 below.

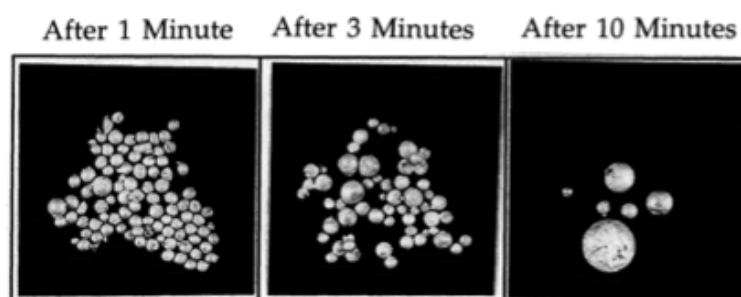


Figure 2.26. Coalescence behavior of Al UBC droplets in salt flux containing 5 mass% CaF_2 .

The condition of the oxide layer was studied by Roy and Sahai [85] and it can be seen that spherical transformation can occur as the oxide layer is ruptured without having to be stripped. Melting of the droplets and hence thermal expansion and spherical transformation to reach minimum free energy cannot alone rupture the oxide layer and promote coalescence. Instead, this indicates that the activity of surface-active elements is a more important factor for the probability of coalescence. In Figure 2.27 below, the coalescence with time can be seen for different fluoride additives.

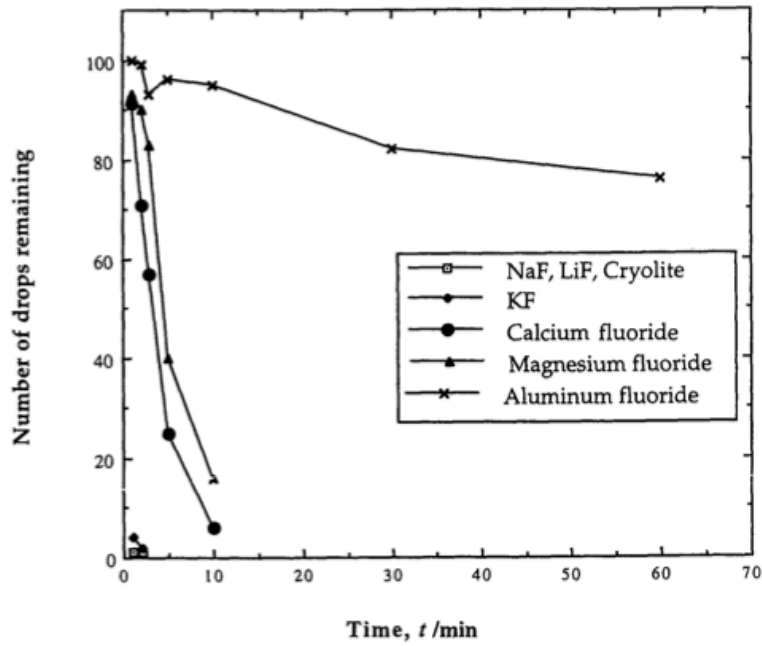


Figure 2.27. The reduction in number of Al droplets (coalescence) with time for different fluoride additions [85].

It is evident that all different addition of fluoride compounds significantly improves coalescence of Al. The metal loss observed as CaF_2 was added in equimolar NaCl-KCl was 0.45 %, i.e. low relative to the other fluoride compounds. The other fluoride compounds with excellent coalescence resulted in more metal loss because metal loss is related to interfacial tension due to displacement reactions, which is further described in section Displacement reactions at salt-metal interface.

According to Sully et al. the following relationship between surface tensions must hold for oxide removal to occur:

$$\gamma_{\text{metal/flux}} + \gamma_{\text{oxide/flux}} < \gamma_{\text{metal/oxide}} \quad \text{Eq. 2.4}$$

i.e. the interfacial tension between metal-flux and oxide-flux must jointly be lower than interfacial tension between metal-oxide in order for oxide removal process to be energetically favorable [96].

Girifalco and Good [97] developed a general expression (Eq. 2.5) used to calculate the interfacial tension in metal-molten salt systems:

$$\gamma_{\text{metal-salt}} = \gamma_{\text{metal-gas}} + \gamma_{\text{salt-gas}} - 2\phi(\gamma_{\text{metal-gas}} \gamma_{\text{salt-gas}})^{0.5} \quad \text{Eq. 2.5}$$

where ϕ is an interaction parameter, dependent on free energy of adhesion between two phases and the geometric mean of free energies for cohesion of separate phases (ΔW_1 and ΔW_2) accordingly:

$$\phi = \frac{-\Delta W^a}{(\Delta W_1 \cdot \Delta W_2)^{0.5}} \quad \text{Eq. 2.6}$$

where

$$\begin{aligned} -\Delta W_1 &= 2\gamma_{\text{metal-gas}} \\ -\Delta W_2 &= 2\gamma_{\text{salt-gas}} \\ -\Delta W_3 &= \gamma_{\text{metal-gas}} + \gamma_{\text{salt-gas}} - \gamma_{\text{metal-salt}} \end{aligned}$$

Where the interaction parameters are closer to zero as the interaction between the phases decreases. Empirical values of interfacial tension matched reasonably well [90]. This can be expressed in terms of free (Gibbs) energy:

$$\Delta G = S(\gamma_{\text{metal/flux}} + \gamma_{\text{oxide/flux}} - \gamma_{\text{metal/oxide}}) \quad \text{Eq. 2.7}$$

Where, ΔG is the change in Gibbs free energy, S is surface area of the oxide and γ 's are interfacial tension between the phases. Accordingly, a negative ΔG means that oxide removal process occurs spontaneous.

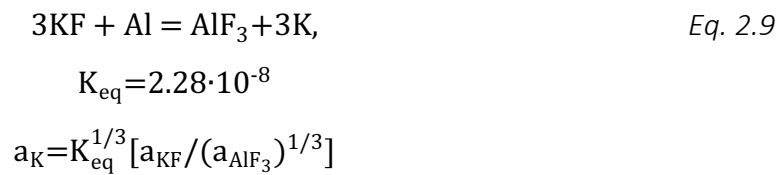
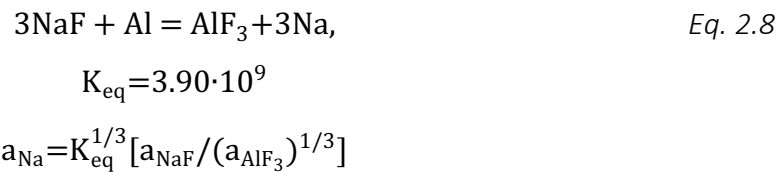
Wetting characteristics and interfacial tension in the Al-salt-oxide system have been measured by several researchers because it was found in early research to relate to coalescence ability [94, 95]. Gibbs free energy have been calculated and was slightly positive regardless of type of salt fluoride compound added i.e. the oxide removal process is not spontaneous [96]. However, only a small amount of energy is required for oxide removal to occur and the influence of the parameter S , surface area of the oxide, was not closely studied.

2.10.4. Displacement reactions at salt-metal interface

The interfacial tension between Al and salt is related to displacement reactions according to Roy and Sahai and Ho and Sahai [86]. Displacement reactions at the aluminum-salt-interface is

in turn related to the activity of surface-active elements originating from the salt. By measuring interfacial tension using the drop detachment method, the activity was observed to differ depending on the type of fluoride compound that was added in equimolar NaCl-KCl.

In addition to interfacial tension measurements, the adsorption of salt elements in liquid Al was measured using EPMA analysis of metal samples. Depending on salt mixture, the activity of the surface-active elements Na and K varied. The interfacial tension depended on the adsorption of these surface-active elements at the salt-metal interface. Results from measuring the adsorption of surface-active elements and measuring the interfacial tension showed that the activity of these elements was the crucial factor. Specifically, the interfacial tension between salt-aluminum decreased as the activity of sodium (Na) and potassium (K) increased. The activity was calculated with respect to displacement reactions accordingly:



The calculation above refers to reactions due to addition of NaF in equimolar NaCl-KCl at 740 °C. However, similar for all different fluoride compounds added, the Al binds with F while Na and K ions become surface active elements. The fluoride compound additions such as NaF and KF increase the activity of Na and K the most. In addition, the adsorption of Na and K increased, which was observed by the EPMA analysis. As a consequence of high activity, the interfacial tension between salt and Al is lowered. Lowered interfacial tension between salt and Al promoted oxide removal, coalescence and melt loss as AlF₃ is dispersed in the molten salt [86].

Other relevant results were the effect of Mg content on coalescence ability. As fluoride compound was added in NaCl-KCl, the activity of surface active elements are expected to increase according to the follow displacement reactions:



$$K_{\text{eq}} = 5.34 \cdot 10^{-11}$$

$$a_{\text{K}} = K_{\text{eq}}^{1/2} [a_{\text{KCl}} \cdot (a_{\text{Mg}})^{1/2} / (a_{\text{MgCl}_2})^{1/2}]$$



$$K_{\text{eq}} = 9.94 \cdot 10^{-9}$$

$$a_{\text{Na}} = K_{\text{eq}}^{1/2} [a_{\text{NaCl}} \cdot (a_{\text{Mg}})^{1/2} / (a_{\text{MgCl}_2})^{1/2}]$$

According to these displacement reactions, the activity of surface active elements Na and K increase as Mg content is increased. As emphasized earlier, this reduces the interfacial tension between salt and Al, hence the driving force of oxide layer removal is larger. However, from experiments in [85] the coalescence ability and coalescence rate were worse for UBC alloy containing 1.9 wt% Mg than for pure Al. The reason is the thicker oxide layer of MgO, which prevent adsorption of Na and K and reduced interfacial tension. Therefore, coalescence is inhibited as the Mg content is increased in Al [86].

Although the interfacial tension between Al and salt is lower when Al contains Mg, addition of NaF in the salt less effectively reduced the interfacial tension. In the case of pure Al, smaller addition of NaF in salt resulted in the same decrease in interfacial tension. In other words, Al containing Mg is more resistant to interfacial change, presumably owing to the thicker oxide layer [85, 86]. Another important finding was that the oxide was stripped only when the salt (containing NaF) was molten.

Roy and Sahai [85] charged 2 g chips in 20 g NaCl-KCl salt with 5 wt% CaF₂. The metal loss reported was 0.009 g, corresponding to a loss of 0.45 %. Of all fluoride compounds, CaF₂ had the lowest metal loss. Addition of 5 wt% NaF resulted in metal loss of 3.55 %, which was the highest. This is related to displacement reactions and change interfacial tension. The activity of surface active elements is higher for NaF, which result in most change in interfacial tension and hence very good coalescence. Addition of CaF₂ does not lead to as large change in interfacial tension i.e. coalescence is worse, but the metal loss is lower.

Racunas [91] developed a relationship for the dependence of aluminum droplet size on velocity gradient, flux viscosity and salt-metal interfacial energy. As the product of velocity gradient and viscosity was minimized, the Al droplet size and hence coalescence was maximized. In other words, stirring influence coalescence of the Al droplets.

2.10.5. CaF_2 addition in NaCl-KCl salt for recovery of Al scrap

Salt flux prevents oxidation with air and adsorption of metal surface contaminants. The properties of the salt flux significantly increase the oxide stripping rate, which improve coalescence. In Europe, the salt flux composition of 70 wt% NaCl and 30 wt% KCl with relatively small additions of CaF_2 is a normal for recovering aluminum scrap. The price of CaF_2 is relatively low and additions of 2-5 wt% is common [98].

Above approximate 2 wt% of CaF_2 in 70:30 NaCl-KCl, the solubility of CaF_2 significantly increases with increasing temperature. At 800 °C, the solubility is below 4 to 6 wt% CaF_2 , depending on study, as seen in Figure 2.28 below.

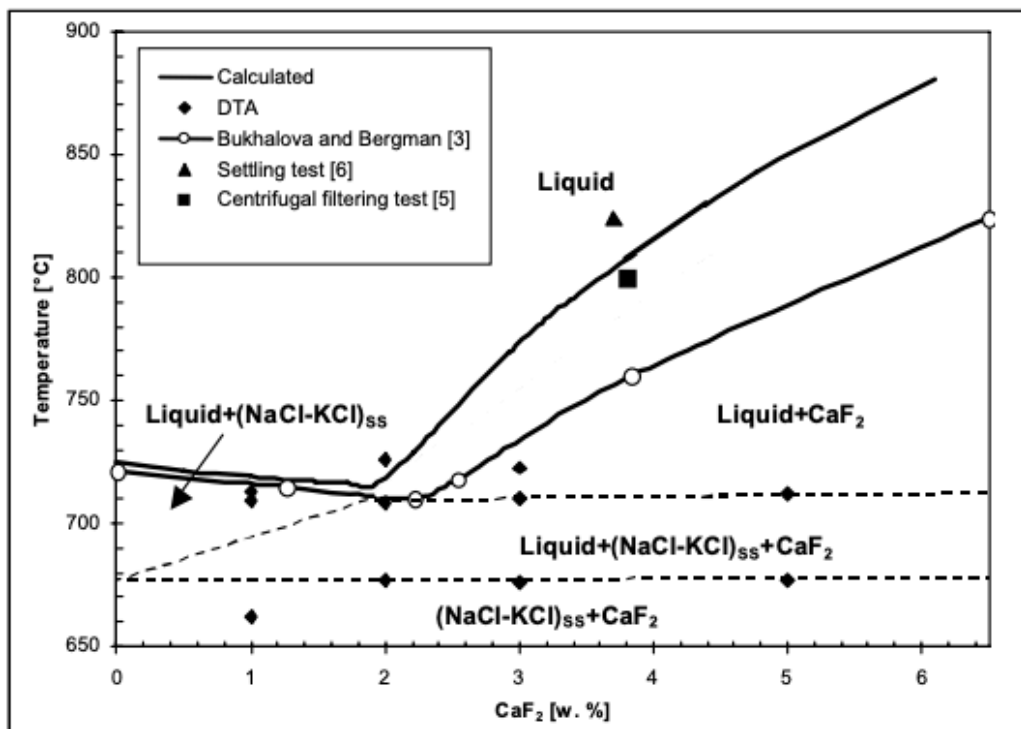


Figure 2.28. Quasi-binary section of CaF_2 -(70:30 NaCl-KCl) of the ternary phase system [98].

Milke et al. [98] reported that only dissolved fluoride ions lead to improved oxide removal. Higher additions than its solubility increase viscosity of the salt flux and also decrease the

interfacial tension, which has seen to increase melt loss. Removed oxide layers that are dispersed in the salt flux also increase the viscosity. Solubility above 730 °C for this salt composition 70:30 wt% NaCl-KCl is significantly lower than the only available phase diagram by Bukhalova and Bergman. In this study, semi-industrial experiments were carried out using a fixed axis drum furnace with volume 25 l, 1 rpm and burner output power of 100 kW. Higher Al/salt ratios lead to more metal loss, as seen in Figure 2.29 below. For maximum recovery it is therefore recommended that minimum amount of salt flux but enough to cover the Al should be added [98].

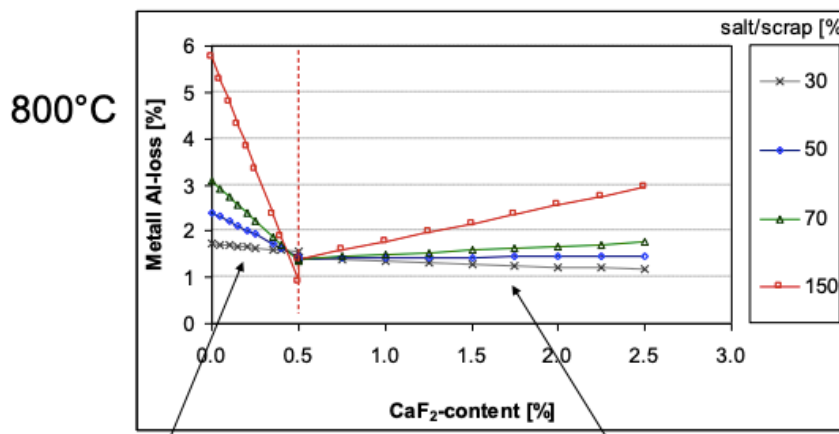


Figure 2.29. The relationship between metal loss and CaF₂ addition for different salt/Al ratios [98].

In Figure 2.30 below, the fluoride loss decreases with time, especially in the period Al is melting (possible due to higher surface area of solid scrap than Al droplets). Measurements of fluoride content without any Al added showed no change in content. This indicate that reaction between Al and salt flux occurs.

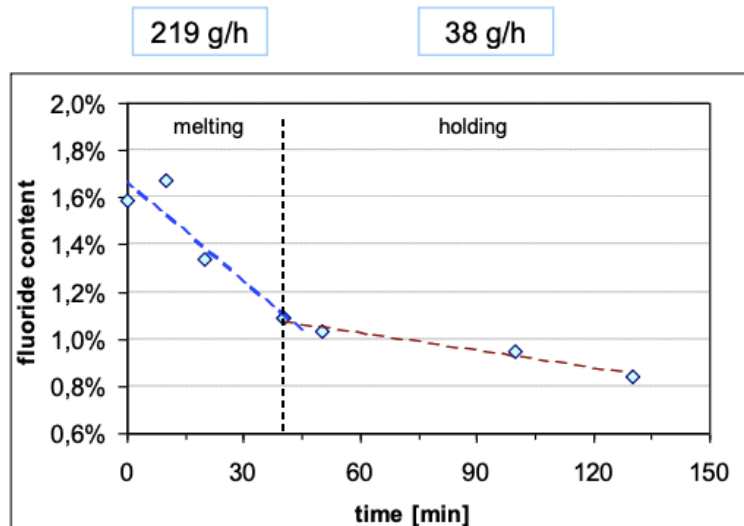


Figure 2.30. Change in CaF₂ content with time [98].

2.10.6. Al loss in salt flux

The effect of initial metal mass on the metal loss have been investigated by Ye and Sahai [90]. In this study, 1, 3 and 6 g of Al was melted in 66 g equimolar NaCl-KCl with 10 mass% NaF at 740 °C and held for 1 h. This corresponds to a salt-Al ratio of 66, 33 and 11. For pure Al, the effect of fluoride content, salt amount, initial mass and time were measured. The metal loss increased linear with increased NaF content, to maximum 1.33 mass% Al loss as the addition reached the maximum of 15 wt%. For the same amount of cryolite the loss was only 0.33 mass%. The metal loss was relatively unchanged with amount of salt added. With fluoride addition of 15 wt% NaF, salt-Al ratio from 10 to 43 had only a very small increased. The metal loss with different initial masses of Al can be summarized with Table 2.2 (approx. values obtained from graphs).

Table 2.2. Data from [90] on metal loss restructured. Pure Al pellet with different mass melted in 66 g equimolar (NaCl-KCl)+10%NaF at 740 °C for 1 hour.

Mass of Al pellet (g)	1	3	6
Al loss [mass%]	2.2	0.93	0.75
Al loss [g/cm ²]	0.08	0.05	0.05

The smallest metal drops had the largest metal loss per unit of area and per gram (mass%) as shown in Table 2.2 above. The metal loss per unit area are more similar than the mass% for the three samples. This indicate that increased specific surface area may contribute to increased metal loss.

3. Experimental materials and methods

The main objective of this study was to understand the relationship between thickness of the compressed material, degree and type of compression, heat treatment and metal yield for re-melting in salt.

3.1. Materials

In total, foils of two different alloy families and with five different thicknesses were investigated. The thicknesses and compositions are summarized in Table 3.1. The two thinnest foils were commercial household foils of thicknesses 15 μm and 30 μm and their compositions were measured by handheld XRF. The three thickest foils were aluminum alloy 8006, received from Norsk Hydro and their composition is shown in Table 3.1 below.

Table 3.1. Composition of the household foils (15 and 30 μm) and 8006 alloy (100, 200 and 300 μm).

Thickness of foil	Al	Fe	Si	Mg	Mn	Cu	Zn	Remain.	Al+Fe+Si
15 μm	98.6 \pm 0.4	0.73	0.53	<0.16				Bal. (<0.05)	99.9
30 μm	98.9 \pm 0.4	0.8	0.11	<0.17				Bal. (<0.05)	99.9
100-300 μm	95.9-98.5	1.2-2	\leq 0.40	\leq 0.10	0.3-1	\leq 0.30	\leq 0.10	Bal. (\leq 0.15)	

3.2. Overview of experimental steps in the current investigation: from foil to recovered aluminum

In general, the study can be summarized into four steps:

1. Shredding of the foil and sieving of chips to obtain a controlled chip size fraction
2. Compacting the foil chips using different pressures and temperatures
3. Heat treating the chips and pressed briquettes
4. Melting the chips and briquettes

A procedure scheme is shown to facilitate understanding of the experimental steps (Figure 3.1). Each step is thoroughly described in the following sections.



Figure 3.1. Schematic illustration of experimental steps.

3.3. Shredding and sieving of foil to produce chips

The size and shape of the particles (and in this thesis called chips) that is compressed could affect all of these parameters. For instance, smaller foil particles could lead relatively less porosity and more oxide in relation to aluminum. In that regard, it was important to quantify the size and shape of the chips before they were compressed or melted as is. This was accomplished by photo analysis and sieving.

Similar to large scale scrap processing and recycling, the foils were shredded into small pieces, and are in this thesis denoted chips (also known as turnings, granules, fragments, trimmings etc.). In order to successfully shred large amount of foil, it was necessary to split the foil into smaller pieces before inserting the pieces into the shredding machine. The most suitable method with regards to the large amount of chips needed was to tear the household foils and cut the thicker 8006 alloy foil. Accordingly, the pieces prepared for shredding were arbitrary teared or cut into similar sizes. The prepared pieces were then inserted at a frequency that minimized the cutting effort of the pieces, which easily could be controlled by listening to the cutting noise during operation. The pieces were shredded by Getecha RS 1600-A1.1.1 as seen

in Figure 3.2. It operated with three rotary blades at a rotor revolution of approx. 240 rpm. The screen size in which the shredded pieces pass to exit the machine 8 mm diameter. Detailed information about the machine is found in [15].

3.3.1. Pre-study

Initially, for the (thinner) and most easily deformed household foils, different shredding methods' effect on size and shape of the chips produced were investigated. Three trivial methods were tested. The term shredding method is determined by the degree in which the teared foil piece was compressed by hand i.e. not compressed, little compressed, or very compressed. Three shredding methods resulted in four shred groups. The last shred group was characterized as the chips that did not pass the screen and exit the machine (as seen in Figure 3.2 below). As a result, in addition to mapping out the overall chip size and shape with regards to thickness of foil, the effect of deformed foil pieces on the size and shape was determined.

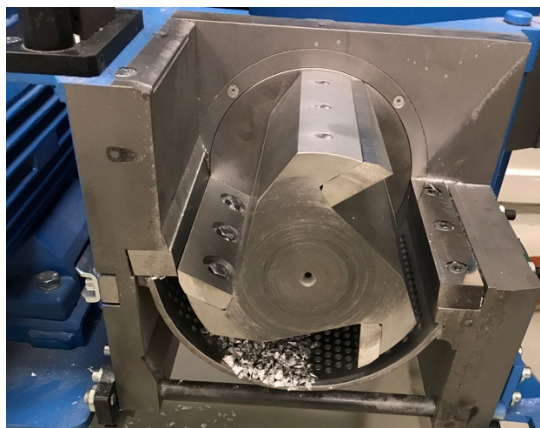


Figure 3.2. The interior of Getecha RS 1600 shredding machine showing the three rotary steel blades and shredded pieces too large to pass the screen.

The size of the ripped and cut pieces was arbitrary. However, the short and long cross section was estimated to 5-13 cm. Three shredding methods resulted in four different groups of chips:

- Shred group A: Ripped pieces that were not deformed (flat).
- Shred group B: Ripped pieces pressed into small balls
- Shred group C: Ripped pieces gently deformed into large balls

- Shred group D: All of the chips that did not pass the screen i.e. separately collected after shredding operation

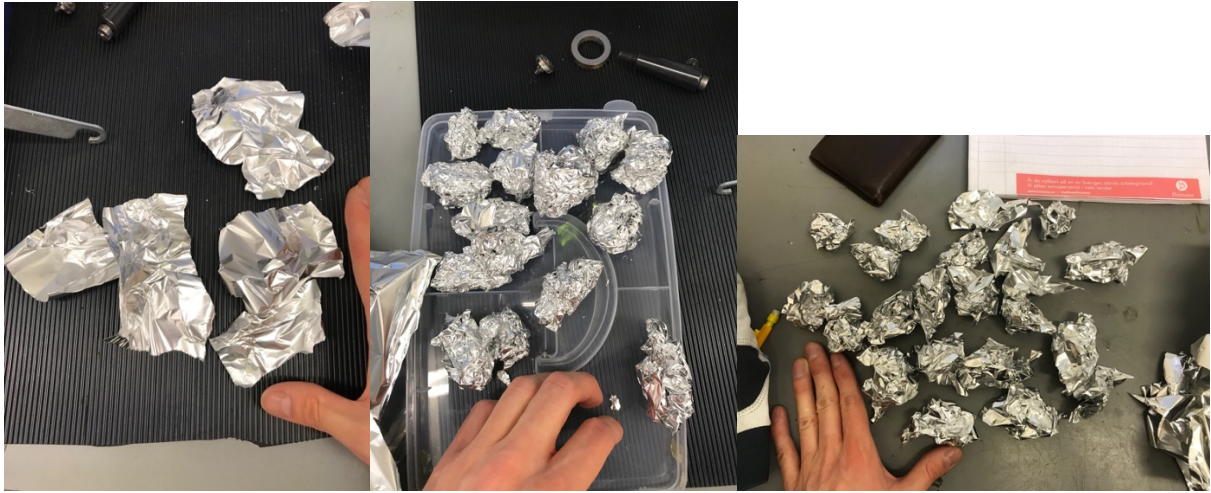


Figure 3.3. Differently prepared foil pieces resulting in the referred shred groups. Flat, much deformed and gently deformed foil pieces prepared for shredding.



Figure 3.4. Chips that passed and were collected by the screen, deformed chips and undeformed chips.

3.4. Characterization of chips

Photo analysis using ImageJ was utilized to determine the size and shape in terms of distribution and median with median absolute deviation. The parameter for size was area.

Shape was quantified using the parameter aspect ratio i.e. the ratio of major and minor axis. In Figure 3.5 below, an example of photo analyzed chips is shown.



Figure 3.5. Photo analysis of chips.

3.4.1. Image analysis using ImageJ - procedure

A sample of chips, approximately 50-100 was spread out (and not touch) on a black piece of paper. Only for the sieved chips, the sample of chips was weighed. A ruler was beside the chips as scale reference. The chips were then photographed with similar contrast for every sample, ensuring shadows were avoided. In ImageJ, the threshold was manually adjusted because a macro lead to unreliable measurements. Finally, the data provided was area, aspect ratio, circularity, round and solidity. However, only area and aspect ratio were further processed.

Characterization is made under the assumption that every particle is exposing its maximum area perpendicular to the ground (and hence the camera). This means that only the longest and medium dimension of the chip is measured, while the shortest dimension i.e. the height of the chip is not included in calculations. The camera used was a mobile phone camera with 12 MP i.e. can produce images with 12 million pixels.

3.5. Controlling chip size before pressing – sieving

To reduce the risk of introducing errors owing to chips size and shape and their oxide amount, the shredded chips were sieved. The chips were sieved using a Retsch AS200Tap. Although sieving is most efficient for more circular particles, the method was seen to effectively remove outliers i.e. dust particles and bulky chips. The intention of sieving was to modify the distribution from wide to narrow, as well as controlling for potential size and shape differences obtained from the five foils with different thicknesses. Given that the mass of a piece of foil is constant, the smaller chips produced from the foil, the larger the specific surface area is. In turn, larger specific surface area means that aluminum oxide covering the aluminum surface is larger in relation to the aluminum. Despite a very thin aluminum oxide layer covering the actual aluminum, the isolation effect of the oxides was considered important to account for. By sieving, the size and size distribution are manipulated to a common distribution between all foil materials. In addition, manipulating the size distribution reduces the risk of irregular porosities and surfaces of the briquette. This could in turn affect the final recovery of the aluminum in the melting operation.

Two sieves were used, a 2 mm and 5 mm (US standard). A sieving batch corresponded to approximately 50 to 100 g. The chips were then vibrated for one minute. The resulting separation of the chips is seen in Figure 3.6 below.



Figure 3.6. Sieving of chips.

The majority of the chips were too large to pass a 2 mm sieve and small enough to pass the 5 mm sieve (Table 3.2). The chips between 2 mm and 5 mm sieves was collected and compressed. The larger and smaller chips was saved for potential compression for further research.

Table 3.2. Distribution of chips after sieving (sieve mesh in mm).

Foil material	< 2 mm	2 to 5 mm	> 5 mm
15 μm chips	7 wt%	82 wt%	11 wt%
30 μm chips	10 wt%	88 wt%	2 wt%
100 μm chips		85 wt%	

After sieving, three samples from all five chips material was separately analyzed in ImageJ and compared with chips that were not sieved. The mass of each sample of chips photographed was noted in order to enable calculation of mean mass per chip. Also, the settling volume of 20 g of each chips material was noted in a 175 ml plastic cup (Figure 3.7).

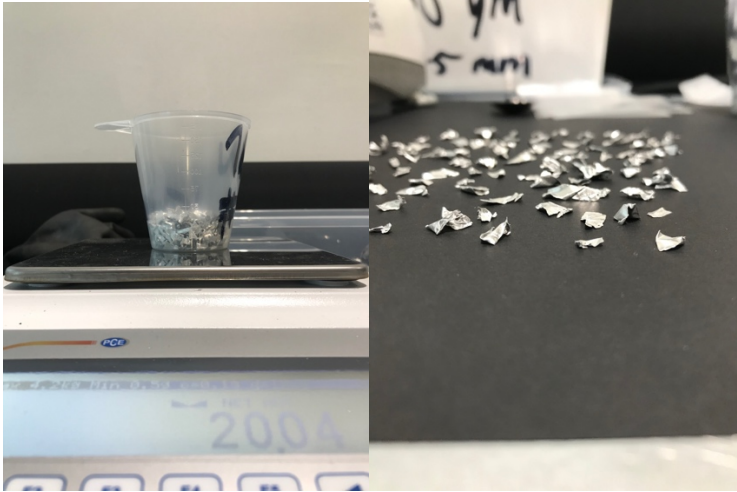


Figure 3.7. Settling volume of chips in 175 ml cup (left). An image that demonstrate the deformation degree of shredded chips (100 μm) (right).

3.6. Compression of chips to briquettes

Chips from each shred group was then compressed to briquettes by uniaxial pressing to varying extent. 20 g of each chips group was poured into the steel crucible with a teflon sheet in the bottom to avoid sticking. In order to fill the crucible with 20 g, the chips were manually slightly compressed by a wooden hammer. On the control panel, the compressive force could be controlled. Stopping the compression resulted in slight fluctuations among the reached force. To control for this and promote consistency, the force of interest was slightly exceeded a number of three times for all pressings. A number of two or three parallel pressings were performed to enable error analysis. The diameter of the crucible was 4 centimeter. Three different overall pressing routines were tested:

- Uniaxial pressing at room temperature with pressures between 0.4 and 121 MPa
- High Pressure Torsion (HPT) (uniaxial pressing and subsequently applied torque)
- HPT during induction heating at 450 °C

After compression (Figure 3.8), the briquettes were removed, and the height was measured with a caliper. Four height measurements were made and all four times ensuring the caliper was completely flat against the briquette surface. The measured height together with known mass and diameter was then used to calculate the bulk density of all briquettes. The stress was calculated with regards to the applied compressive force and was illustrated graphically with bulk density for each shred group.



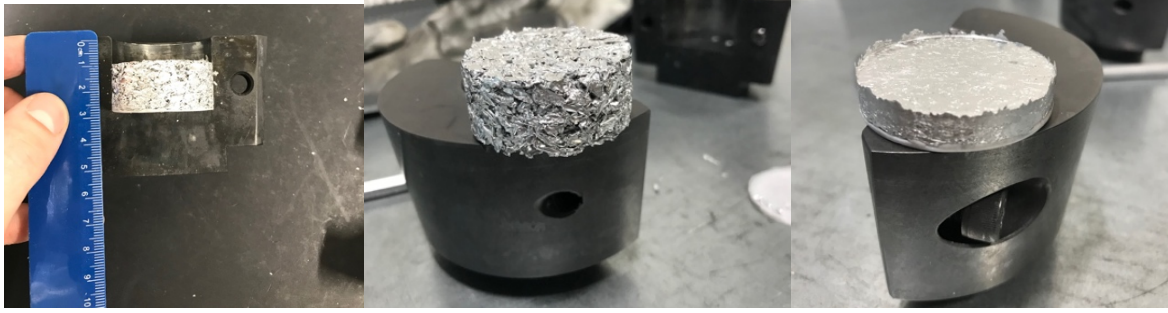


Figure 3.8. Compaction of chips to briquettes.

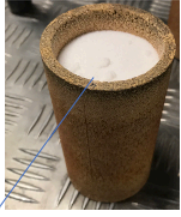
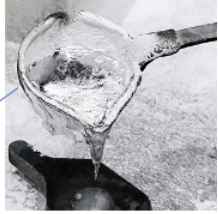

3.7. Automatic uniaxial pressing

Given the results from the initial study of different shred groups, deviations in bulk density could be caused by compaction errors. To reduce the risk of errors from compression and to more accurately reach targeted bulk density for all five foil materials, the chips were compressed by automatic pressing instead of initial manual pressing.

It was determined to only compress shredded chips from shred group A of all foil thicknesses. These chips were subsequently sieved and compressed automatically with pre-set settings. The velocity of the speed press was set to 10 mm/min and the holding time at the force of interest was 5 seconds until it was released and the briquette removed from the crucible. Similar ranges of bulk density seen in the final compression scheme (in Table 3.3 below) was strived for. “xNumber” represents the number of parallel pressings performed. As observed in the two lower rows in the compaction scheme, HPT and HPT at 450 °C was also applied to analyze their effect on compaction parameters which is discussed more thoroughly below.

Table 3.3. Compaction table showing the bulk density ranges and number of parallel pressings.

Bulk density (g/cm ³)	15 μm Household foil	30 μm Al foil	100 μm AA 8006	200 μm AA 8006	300 μm AA 8006
0.86-0.90	x3	x3	_*	_*	_*
1.35-1.40**	x3	x3	x3	x3	x3
1.5	Approx. density of molten salt flux				
2.06-2.12	x3	x3	x3	x3	x3
2.38	Approx. density of liquid Al				
2.41-2.54 (Torsion)	x3	x3	x3	x3	x3
2.62-2.67 (Torsion+450°C)	x4	x1	x2		x1

*Not possible, chips fall apart →

**Lowest possible density for 100-300um

Another benefit of automatic compression is the data acquisition of vertical displacement of the compression tool in relation to the force applied. This data was extracted for analysis of the deformation behavior of the different chips. The automatic pressing procedure is further described:

- A safety limit was set well above the intended compressive force to be reached. Exceeding this limit would stop the compression.
- For the data acquisition the level increment was set to 0.1 seconds
- The velocity of the compression tool was set to 10 mm/min
- The data display was set to Force vs Displacement in order to observe the relationship graphically in real time
- The load limit i.e. the maximum force was set individually for all chips
- The hold time was set to 5 seconds
- The release rate after compression was set to 10 kN/sec with absolute end level of 0

3.8. High Pressure Torsion (HPT)

Torque was applied by 4 revolutions and 1.2 rpm (revolutions per minute) as a step immediately after desired uniaxial pressing was done (Figure 3.9). Torque causes torsion i.e. shear strain from twisting of the compressed material. Once the compressive force of interest was reached,

the corresponding compressive force was held constant as the torsion started. After operation, the briquette was removed and further analyzed. For these compactions, the uniaxial pressing was controlled manually in difference from the uniaxial pressings for the lower bulk densities (Table 3.3). This procedure was repeated for all five foil materials.

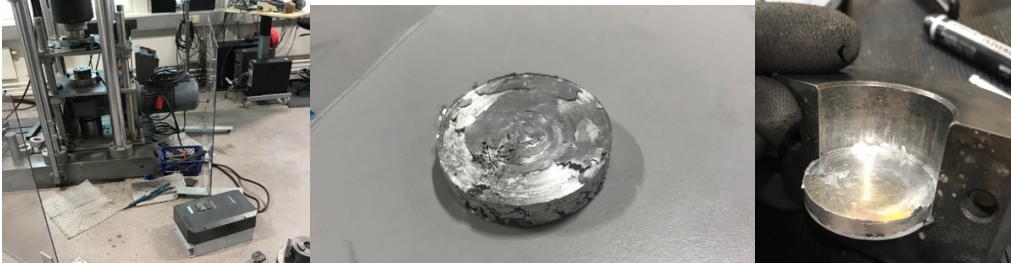


Figure 3.9. Briquettes produced by HPT.

3.9. HPT with heat

In addition to applied torque, heat was applied with EFD induction device (type MINAC 6/10) as seen in right Figure 3.10 below. The copper induction coil was water cooled and mounted as seen in left Figure 3.10 below. The steel tool was lowered until it slightly touched the chips, which could be confirmed by observing the force change. The steel tool was set free to move vertically. Then, the induction was turned on. The crucible began heating up after setting to DC power to 3.9 kW, AC current to 23 A. During operation, the frequency varied between 17.2-17.6 kHz. These settings resulted in a temperature of 440 °C in 20 minutes. The temperature was observed with a K-thermocouple. When the temperature had reached 440 °C the induction was turned off. The temperature would then quickly drop to 420 °C. Simultaneously, the uniaxial pressing began, compressing again at 10 mm/min. As a consequence, the temperature increased, reaching a maximum of 480 °C before slowly decreasing back to 450 °C during uniaxial pressing and torsion. As the force of interest was reached, the pressing tool was held and torsion could start. Again, the torsion in terms of four revolutions was applied. The time needed for one turning was 40-50 seconds. Finally, the crucible was removed and cooled in room temperature before removing the briquette.



Figure 3.10. The equipment for pressing with induction and the briquette produced.

3.10. Oxidizing briquettes by heat treatment

As oxidation behavior is a common phenomenon in recycling of aluminum, the amount of oxidation was determined by measuring the weight gain from heat treatment at high temperatures.

As an unwanted side effect in the recycling industry, thermal treatment of scrap, to e.g. remove coatings, usually lead to oxidation of the aluminum material. To replicate this phenomenon, the foil materials were heat treated and as a consequence oxidized. Briquettes, sieved chips and sheets from the five foil materials entered a Nabertherm furnace featured with air circulation at 650-660 °C (as seen in Figure 3.11). After one hour, the furnace was turned off and allowed to cool down to 500 °C, whereupon the briquettes, chips and sheets were removed. The time required to cool down to 500 °C was approximately 25-30 minutes. Because oxidation is assumed equivalent to mass gain during heat treatment, the mass before and after heat treatment was noted.

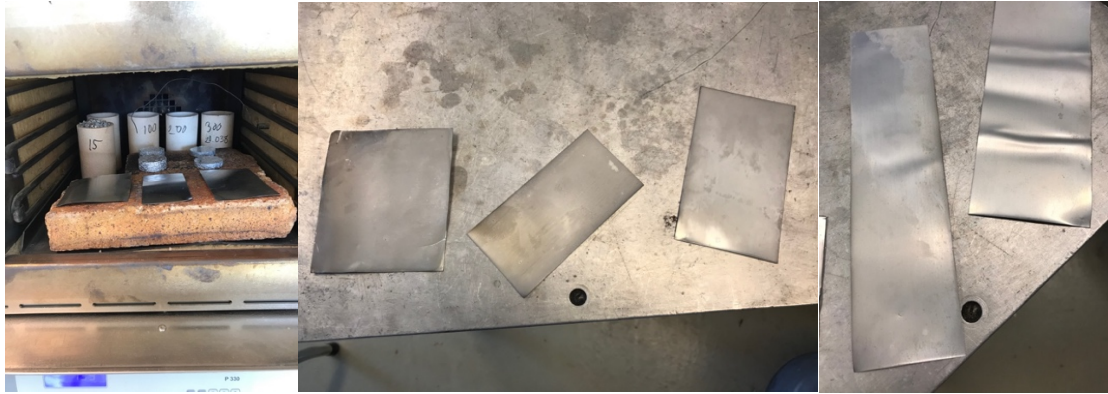


Figure 3.11. Oxidized chips (furthest inside furnace in left figure) and oxidized sheets (middle and right figure).

To understand the impact of a certain temperature and heating time has on the mass increase, temperatures up to 800 °C and heating times up to 3.5 hours was tested. The briquettes used for these tests were briquettes produced from the initial shred group study and briquettes that did not fit into the range specified in Table 3.3. The number of loose chips as well as briquettes compacted from sieved chips using automatic compaction that were heat treated in 650-660 °C for 1 hour is shown Table 3.4 below. In addition, the mass increase of sheets with thicknesses 100, 200 and 300 μm (8006 alloy) with same surface area as well as same mass were compared.

Table 3.4. Number of heat-treated chips and briquettes used for final melting experiments.

Bulk density (g/cm^3)	15 μm Household foil	30 μm Al foil	100 μm AA 8006	200 μm AA 8006	300 μm AA 8006
Loose/free chips	x3	x3	x3	x3	x3
0.86-0.90	x2	x2	-	-	-
1.35-1.40	x2	x2	x2	x2	x2
2.06-2.12	x2	x2	x2	x2	x2
2.41-2.54	x2	x2	x2	x2	x2
(HPT)					

An attempt to measure the oxide thickness with scanning electron microscopy was made without success.

3.11. Characterization of briquettes

The parameters that may influence percentage of recovery of aluminum are bulk density, surface area and porosity of the compressed material. The bulk density was measured simply with a caliper. The surface area of the briquette was projected with optical 3D-microscope and the porosity was determined by x-ray tomography.

3.11.1. Quantifying the briquette surface from optical 3D-microscope

Surface topography is relevant to determine as the area of chips and briquette exposed to the surrounding medium may affect the percentage recovery of Al foil. The relationship between surface topography on oxidation, bulk density, porosity and subsequent recovery is relevant to investigate in order to improve recycling yield.

Roughness of foil

The roughness of Al foils with thickness 6.3 and 9.0 μm have been measured by Larsson [99]. The parameters Sa (Arithmetical mean height) could vary between 200-400 nm depending bright or matt side analyzed and the manufacturer of the foil. The Sdr (developed interfacial area ratio) or surface offset varied between 1 to 5 %. The surfaces clearly varied in both macro roughness (large but less frequent height difference) and micro roughness (small but frequent height difference). It is also reported that foil with higher ductility can result in more distortion of the surface and as a result become coarser.

Roughness of the material have shown to be a factor significantly influencing oxidation. Impey [100] referred to several studies including the earliest one by Lewis, Plumb and Cochran, Sleppy that indicated increased oxidation with increased surface roughness.

Roughness parameters

True-to-projected area ratio indicates the surplus that is generated due to surface irregularities. The true or real area of the measured region is divided by the projected area that is equivalent to measured region in the horizontal plane.

Root mean square gradient (Sdq) is the root mean square of slopes at all points of the measured surface. Steep height variations and flat surface correspond to a high and low value of Sdq , respectively [101].

Developed interfacial area ratio (Sdr) indicates the percentage of additional surface area generated by the texture with respect to the ideal plane of the measured area. Sdr depend on the spatial intricacy of the texture and is both affected by spacing and texture amplitude. The parameter is typically of interest to obtain for coated materials. The obtained values of Sdr is relevant to compare to compacted foils that are coated [102].

As the surface topography of the briquette could influence the final recovery of the briquette, surface parameters were determined with an optical microscope manufactured by Alicona. An example of different briquette surfaces can be seen in Figure 3.12. Images showing the surface irregularities of briquette compressed uniaxially (left) and HPT (right).below.



Figure 3.12. Images showing the surface irregularities of briquette compressed uniaxially (left) and HPT (right).

The non-heat-treated briquette was centered below the 5x AX lens before the software was opened. The following settings were held constant for all surface analysis:

- The brightness and contrast were set to 433 us and 0.83, respectively
- Light source was set to Ring light
- The measurement type and ImageField type was set to 3D Dataset and General ImageField, respectively
- The vertical and horizontal resolution considered appropriate was 1.0 and 8.38 microns, respectively

After the settings above were set, individually for each briquette, the lower and upper limit for the measurement of the image field was adjusted until image was blurry. The approximate vertical depth needed to include all surface irregularities was 1 mm. A 5x AX lens was used, which was the lens with shortest focal length, resulting in the largest possible image for this microscope. However, the image field created for analysis was smaller than the entire surface of the briquette. By recording an array of images which are aligned in a rectangular area and then merged into one image, the final image field was created as seen in Figure 3.13 below.

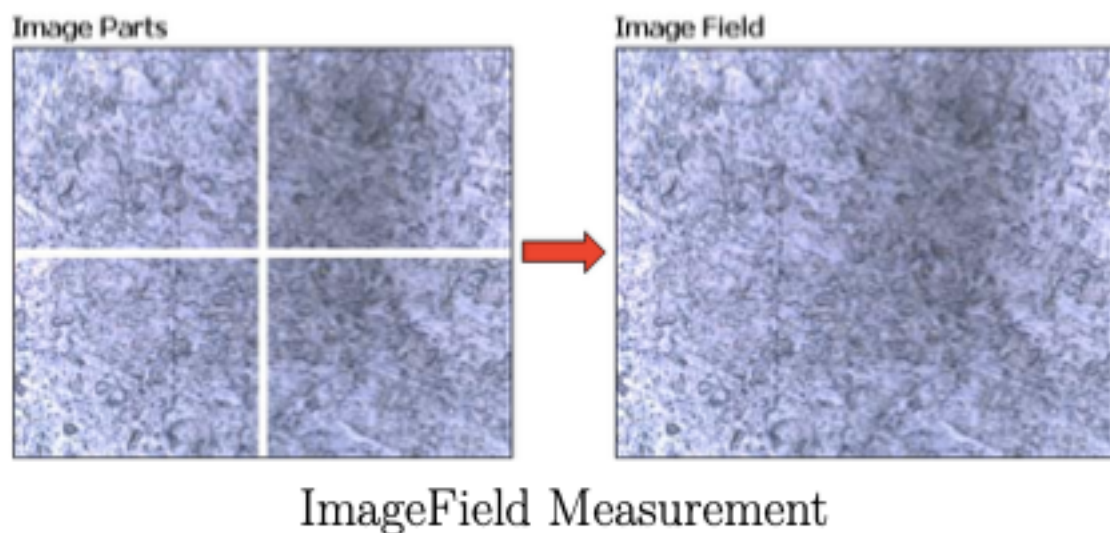


Figure 3.13. An example of how 4x4 images are merged into one single image field.

Specifically, a 4x4 to 6x6 assembly of images was created, having an area between 1.7 and 4 cm², but most of them around 3 cm². The array of images was possible owing to the motorized

stage movement of the lens in x and y direction i.e. horizontal movement. Two types of measurements was performed. Firstly, in ProfileRoughnessMeasurement, a height profile i.e. the variation in depth of the valleys across the surface was generated by a drawn vector with 4 turns across the projected surface (Figure 3.14 below). Secondly, in SurfaceTextureMeasurement, the true and projected surface area was obtained, and the ratio between the two.

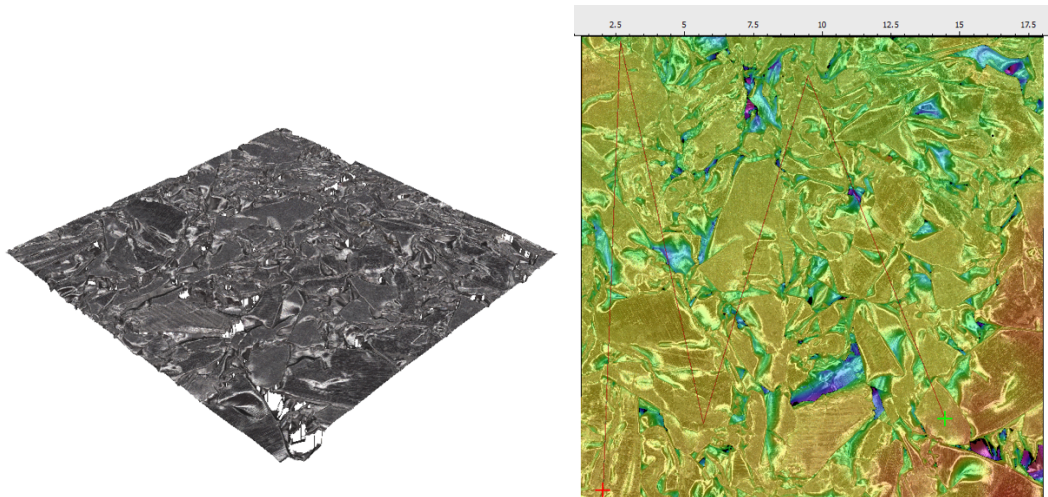


Figure 3.14. Briquette of 30 μm foil with a bulk density of 1.38 g/cm^3 . Illustration of the measured surface (left) and the vector with 4 turnings across the projected surface.

A scheme was made for the surface area analysis. As seen in Table 3.5 below, the briquettes compressed with HPT are here excluded because the majority of their surfaces were smooth or differently cracked. This means that the projected surface area is only analysis between surfaces achieved from uniaxial pressing.

Table 3.5. The scheme for projected surface area analysis.

Bulk density (g/cm ³)	15 μm Household foil	30 μm Al foil	100 μm AA 8006	200 μm AA 8006	300 μm AA 8006
0.86-0.90	x1	x1			
1.35-1.40	x1	x1	x1	x1	x1
2.06-2.12	x1	x1	x1	x1	x1

3.11.2. Porosity of briquettes determined by X-ray tomography

The porosity was of interest to quantify for briquettes with different bulk densities and foil thicknesses. The porosity was analyzed using X-ray tomography. The images had in all three dimensions a voxel size of 22.047 μm. Hundreds of 2D-images was produced along the vertical axis of the briquette and subsequently processed in ImageJ. To save time, a macro was created. The porosity inside a created rectangular area was measured for all images. Finally, the data was processed in Matlab in order to visualize the results. In Figure 3.15 below, the porosity of different briquettes can be seen. Because porosity analysis with x-ray tomography is a relatively time-consuming process, only the 8 most relevant briquettes were selected, as seen in Table 3.6.

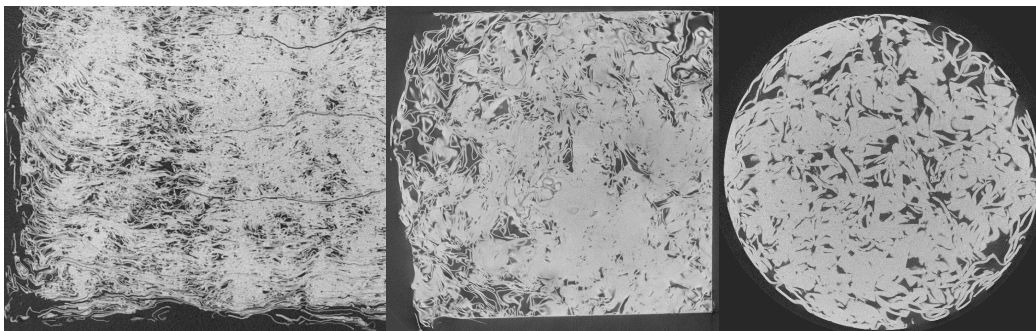


Figure 3.15. Examples of porosity images obtained from X-ray tomography. From left to right: 15, 30 and 300 μm all in the bulk density range 2.0-2.1 g/cm³.

Table 3.6. Scheme for briquettes analyzed in X-ray tomography.

Bulk density (g/cm ³)	15 μm Household foil	30 μm Household foil	100 μm AA 8006	200 μm AA 8006	300 μm AA 8006
0.86-0.90	x1	x1	-	-	-
1.35-1.40					
2.06-2.12	x1		x1		x1
2.41-2.54 (HPT)	x1		x1		x1

3.12. Metal recovery from melting briquettes in salt flux

In the final study, the chips and briquettes were melted and the recovery of these were measured. The recovery from the different foil thicknesses in the form of free chips and briquettes were evaluated. In this thesis, the foil material was recovered mainly by melting in salt flux.

Several melting studies were accomplished by melting briquettes covered in salt flux at high temperature in a small resistance muffle furnace. Because of the wide variety of possible melting procedures, a few parameters had to be investigated to produce a reliable method with errors reduced. This melting method was determined before the prepared briquettes in compaction scheme (Table 3.7 below) were melted. To determine final melting method, briquettes from the initial compaction study were utilized. Consequently, for the initial melting studies, briquettes consisting of non-sieved chips from different shred groups were used. From the results, potential errors could be identified and controlled and give indications on data to expect for the final melting of the well-prepared briquettes (consisting of sieved chips and group A). Specifically, the results from the initial studies would show the effect of heat treatment, which in turn can be traced back to the heat treatment study and determine a fixed heat treatment procedure for the final briquettes. The main parameters associated with melting experiments were charging method, salt flux content and holding time.

Table 3.7. Briquettes melted in final experiments.

Bulk density (g/cm ³)	15 μm Household foil	30 μm Household foil	100 μm AA 8006	200 μm AA 8006	300 μm AA 8006
Loose chips	x3	x3	x3	x3	x3
0.86-0.90	x2	x2	-	-	-
1.35-1.40	x2	x2	x2	x2	x2
2.06-2.12	x2	x2	x2	x2	x2
2.41-2.54 (HPT)	x2	x2	x2	x2	x2
2.62-2.67 (HPT+450°C)	x2	x1	-	-	-

On the basis of the real time results, several melting parameters were varied while some were held fixed. For productivity, two muffle furnaces were used initially until one was considered more reliable and therefore was used for the majority of melting trials. In the chosen Nabertherm muffle furnace, four Al₂O₃-SiO₂-crucibles, each containing one briquette and salt flux were heat treated at 800 °C. After the briquette was molten, it was hold in the furnace for a certain amount of time before removed from the furnace and cooled in room temperature.

Parameters investigated that were assumed important prior to melting was:

- The amount of salt to completely cover the briquette, both in solid and molten phase
- Solid or liquid phase of the surrounding salt flux
- Furnace temperature and the temperature drop due to charging briquette
- Holding time of briquette in furnace

Parameters held fixed were:

- Materials investigated had similar composition and not coated
- Salt composition: (NaCl:KCl:CaF₂) = (68.6:29.4:2) wt%
- Holding time was fixed after evaluating its impact
- Amount of salt was fixed after evaluating its impact
- The furnace atmosphere was air
- No stirring

- Crucibles dried in a furnace at 105 °C

Minimum amount of salt flux but enough to cover the Al was added in the crucible in accordance with suggestions in [98]. The salt flux composition was produced by weighing each component before it was well mixed. From initial melting trials, deviations in recovery were assumed to be caused by small deviations in CaF_2 content. To ensure that this factor would not contribute to errors, the 2 wt% CaF_2 was added separately in crucibles containing pre-mixed NaCl-KCl before they entered the furnace.



Figure 3.16. Crucible with solid and molten briquette, salt flux after operation and coalesced aluminum.

The melting trials in salt flux can be divided into two main studies. The first study investigated briquettes that were not heat treated before melting. The second study, and also more extensive study, were melting trials of heat-treated briquettes.

Two charging methods were used for melting of the non-oxidized briquettes. In one of the methods, a crucible was charged with a briquette covered by solid salt flux when the furnace temperature had reached 800 °C. In the other charging method, a crucible with only salt flux was charged at 800 °C and allowed to melt before the briquette was charged. To simplify, the former and latter is further denoted as solid- and liquid phase charging. In liquid phase charging, a larger amount of salt was required to ensure the briquette was completely covered. In fact, this method required 100 g salt flux (i.e. ratio of 5) compared to solid phase charging where only 40 g salt flux (i.e. ratio of 2) was needed.

For seven of the melting trials including both charging methods, a thermocouple was inserted to the salt flux to measure the temperature change during operation. Because the temperature was measured for both methods, data of the temperature per time unit was obtained for the salt flux-Al-mix in liquid- and solid phase. Important regarding temperature measurement, two different muffle furnaces were used for this first study of non-oxidized briquettes.

To understand the effect of heat treatment and oxidation on recovery, the first treated briquettes consisting of the material thicknesses 15, 30 and 300 μm were oxidized in 800 °C (well above solidus phase) for 1,5 hours or longer. In addition, a few briquettes of the same thicknesses were heat treated in 750 °C and 700 °C. After solid phase charging at 800 °C, they were hold in the furnace for 33-60 minutes. The salt-to-Al ratio was 2 and the two different muffle furnaces was used.

With regards to the results from previously described investigation, the final and only melting method was determined to be charging in liquid salt flux. For these trials, only 15 and 30 μm briquettes were at this stage most important and therefore melted. The results from these melting trials was used to identify any errors and establish the final and robust melting method. The muffle furnace was heated to 800 °C and the crucible with salt-to-Al ratio of 4-5 was charged. After 40-45 minutes as the salt flux had melted, the briquettes or chips were charged in each four crucible and potential floating was noted. If the briquette floated, it was gently pushed down into the salt to ensure it was covered by the molten salt flux. The briquettes and chips were heated and hold for 10 minutes before removed and cooled in room temperature.

A few parameters were changed for the final melting trials in salt flux. From the results of these experiments it was determined to reduce the salt-to-Al ratio to 4 for the final experiments. A ratio of 4 was enough to cover the briquettes. However, for melting of chips, 150 g was required for complete covering. Another error to control for before the final experiments was to add CaF_2 individually in all crucibles right before charging. In that way, the risk of varying CaF_2 content is eliminated.

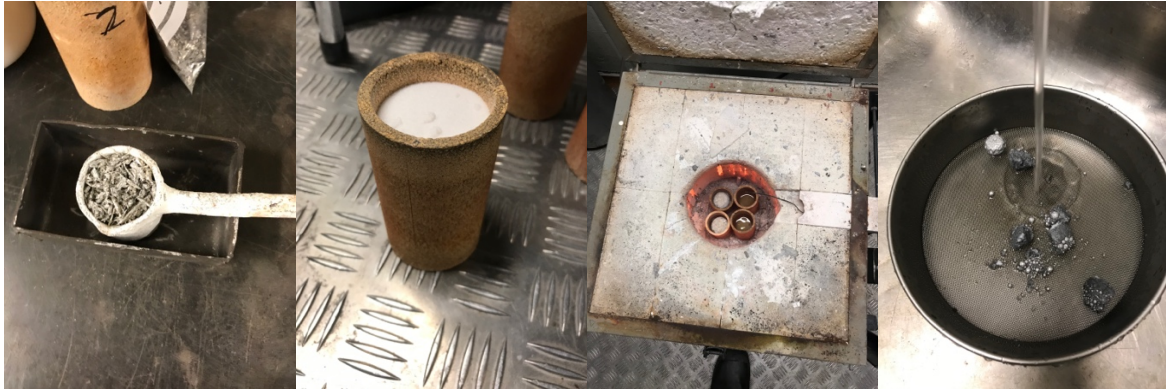


Figure 3.17. Chips, crucible with 150 g salt flux, 4 crucibles charged and recovered aluminum.

After the crucibles had cooled in room temperature for at least 2 hours, the coalesced aluminum was removed from the solid salt flux by gently poking it under warm water. The salt attached to the remaining aluminum particles (which had not coalesced) was removed by rubbing towards a 800 μm sieve. The clean coalesced aluminum and aluminum particles were then dried with a hair dryer and finally weighed.

3.13. Melting without salt flux

The melting behavior without salt flux was also investigated for differently compressed briquettes (Table 3.8). The furnace temperature was again 800 °C and four crucibles were charged at the same time. The crucibles were painted with boron nitride to avoid sticking to the crucible material. To ensure the boron nitride was dry, painted crucibles were heat treated in another muffle furnace for a short time. The crucibles with briquettes were heated for 30 minutes. A successful recovery was defined as a solid aluminum body which do not disintegrate and the compressed chips are not visible. This is illustrated in in Figure 3.19 below.



Figure 3.18. Dried crucible (left), charged crucible with briquettes inside (middle) and finished heated briquettes (right).



Figure 3.19. Successfully recovered Al (left), visible chips (middle) and fragile Al piece disintegrating (right).

To study the melting behavior, a thin steel stick covered in boron nitride as well, was used to poke the all briquettes after heating 15, 18 and 21 minutes. The state of the briquette was depending on result noted as “not melted, partially melted or melted”. At last the melted briquette was solidified in room temperature. Most of the boron nitride was removed with warm water. In addition to this, ultra-sonic bath treatment for 2,5 minutes was done. The density of the aluminum pieces was then measured in pycnometer AccuPyc II 1340. The density could give indications on porosity and the extent of oxidation.

Table 3.8. The briquettes melted without salt flux.

Bulk density (g/cm ³)	15 μm Household foil	30 μm Household foil	100 μm AA 8006	200 μm AA 8006	300 μm AA 8006
0.86-0.90		x1			
1.0-1.40	x1		x1	x1	x1
1.93-2.2	x2	x1	x1*	x1**	x3**
2.41-2.57 (HPT)	x1	x1	x2	x3	x2
2.58-2.67 (HPT+450°C)	x3		x2		x1

*Heat treated in 650 °C for 1 hour.

**One for each thickness was heat treated in 650 °C for 1 hour.

4. Results

4.1. Shredding behavior of different foil thicknesses

4.1.1. Initial study of different shred groups

The results of the initial study of size and shape of different shred groups of foil thickness 15 and 30 μm were analyzed by plotting the medians, median absolute deviation (MAD), and distributions. MAD is a robust measure of the variability of the data. It is more resilient to outliers in a data set than the standard deviation. The following graphs show area and aspect ratio (Major axis/Minor axis) for chips that were not sieved.

Size analysis of non-sieved chips

Size distributions of 15 μm chips of shred groups A-D are presented in Figure 4.1 below.

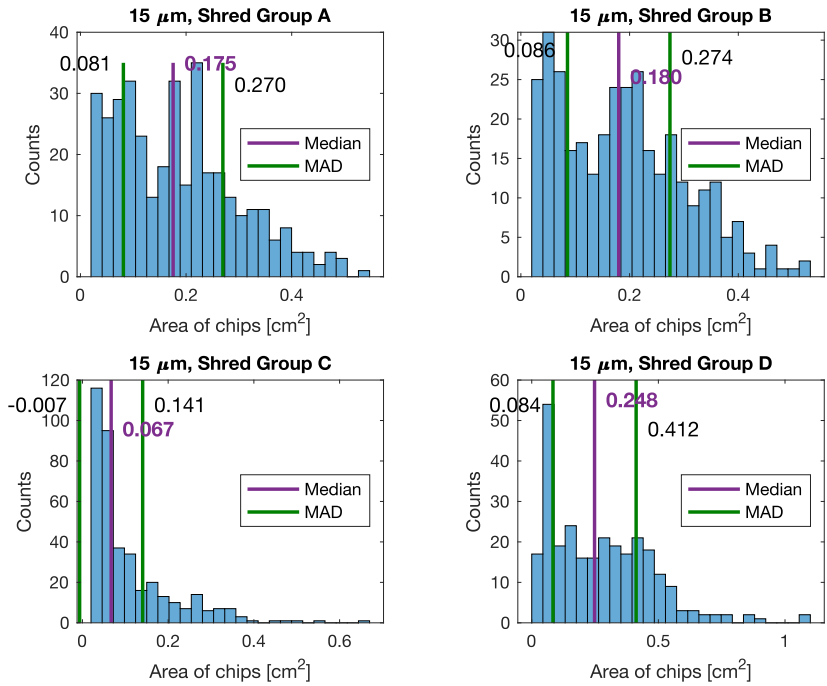


Figure 4.1. Size distribution of chip groups A-D of foil thickness 15 μm (non-sieved).

In general, the chip sizes are very different and mostly varies between 0-0.5 cm^2 , with the exception of group D. In addition, the distributions of the groups are dissimilar. Group A and B are most similar, both in median area and the distribution of areas. As expected, group D, which

could not pass the 8 mm holes at the bottom of the shredder, has the largest median area and the widest distribution.

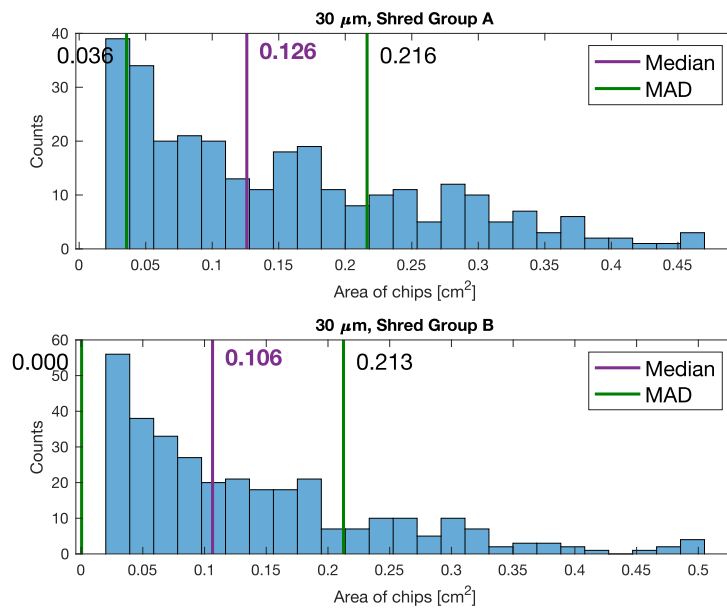


Figure 4.2. Size distribution of chip groups A-B of foil thickness 30 μm (non-sieved).

As for 15 μm, the median area of group A and B for the 30 μm were similar (Figure 4.2). However, both group A and group B differ between the thicknesses 15 and 30 μm chips. The median areas of 30 μm chips are smaller than median areas of 15 μm (comparing groups A and B) because chips of 30 μm with small area is much more frequent. On account of these results, the size of chips is considered diverse, which increases the risk of sampling error in photo analysis.

Shape analysis of non-sieved chips

Shape distributions of 15 μm chips of shred groups A-D are presented in Figure 4.3 below.

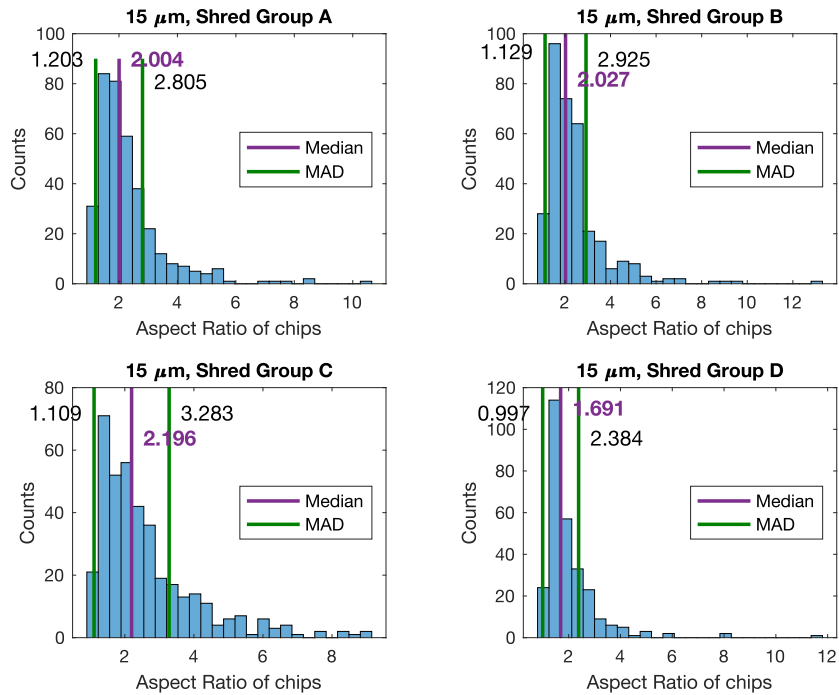


Figure 4.3. Shape distribution of 15 μm chips of shred groups A-D.

In Figure 4.3, the distributions of aspect ratio are more similar between groups than corresponding area previously explained. Again, group A and B are very similar in shape. The median aspect ratio is approximately 2 i.e. the chip is twice as long as it is wide for all shred groups. The distributions are more similar for shape than for size of chips. For all groups, the aspect ratio that occurs the most is below the median aspect ratio. In addition, the outliers are frequent for all groups i.e. chips that possess considerably higher aspect ratios. Chips of group D is most circular in shape. This means that the chance is higher for elongated chip to pass the 8 mm holes than it is for circular chips.

Shape distributions of 30 μm chips of shred groups A-B are presented in Figure 4.4 below.

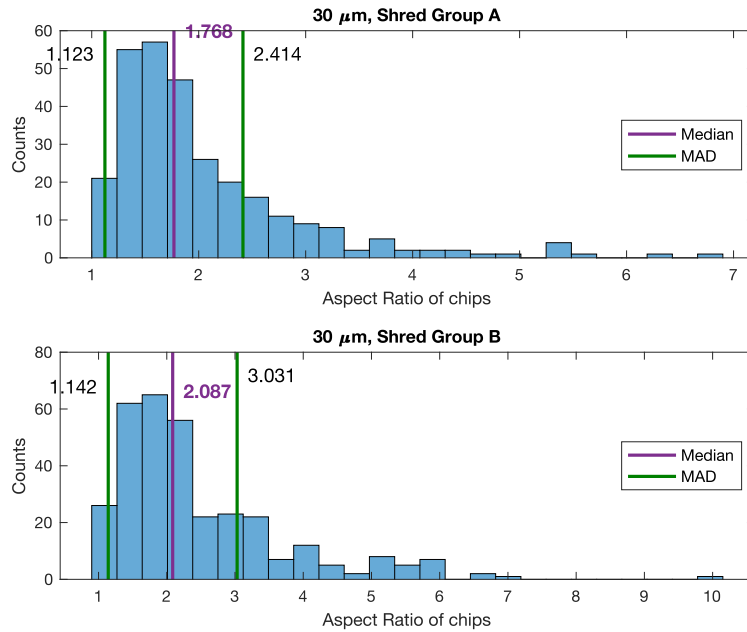


Figure 4.4. Shape distribution of 30 μm chips of shred groups A-B.

In Figure 4.4 above, the shape distributions of the 30 μm chips in the two groups are similar. In addition, the distributions are similar to the shape distributions of 15 μm chips, particularly chips of group B which have the same median aspect ratio. Also, the frequency of outliers is similar to 15 μm chips. However, a comparison between group A for the two thicknesses, the shape of 30 μm chips is more circular.

4.1.2. Study on sieved 15-300 μm chips

The chips resulting from the shed group A were sieved (using sieves of mesh size 2 and 5 mm) and analyzed by image processing. The size and shape of the different foil materials are plotted in graphs to facilitate understanding of how chip size and shape relate to subsequent compaction and recovery results.

In Figure 4.5 below, the size distributions of all foil thicknesses are presented. In contrast to non-sieved chips, the size distribution is similar between thicknesses. The chips' areas are relatively evenly distributed around the median i.e. they are approximately normally distributed. As for non-sieved, the distributions have a tail at higher values. In general, the median size of chips is similar between thicknesses.

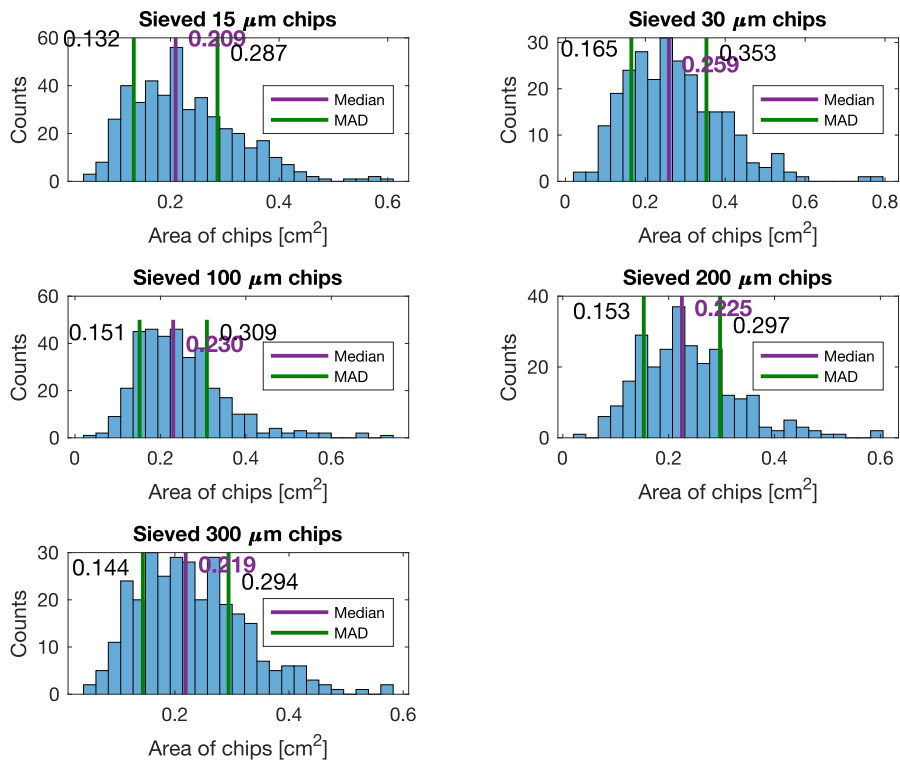


Figure 4.5. Size distribution of sieved chips of all foil thicknesses.

In Figure 4.6 below the aspect ratio distributions of all thicknesses are shown. The distributions of aspect ratio are dissimilar to the corresponding size distributions. The distributions are right-skewed (positive skewness) i.e. the most frequent aspect ratios are below the value of the median aspect ratio. Also, the shape distributions are skewed towards the higher aspect ratios to a greater extent than corresponding size distributions. Generally, it is observed that sieving has a greater impact on the size of chips than on the shape of the chips.

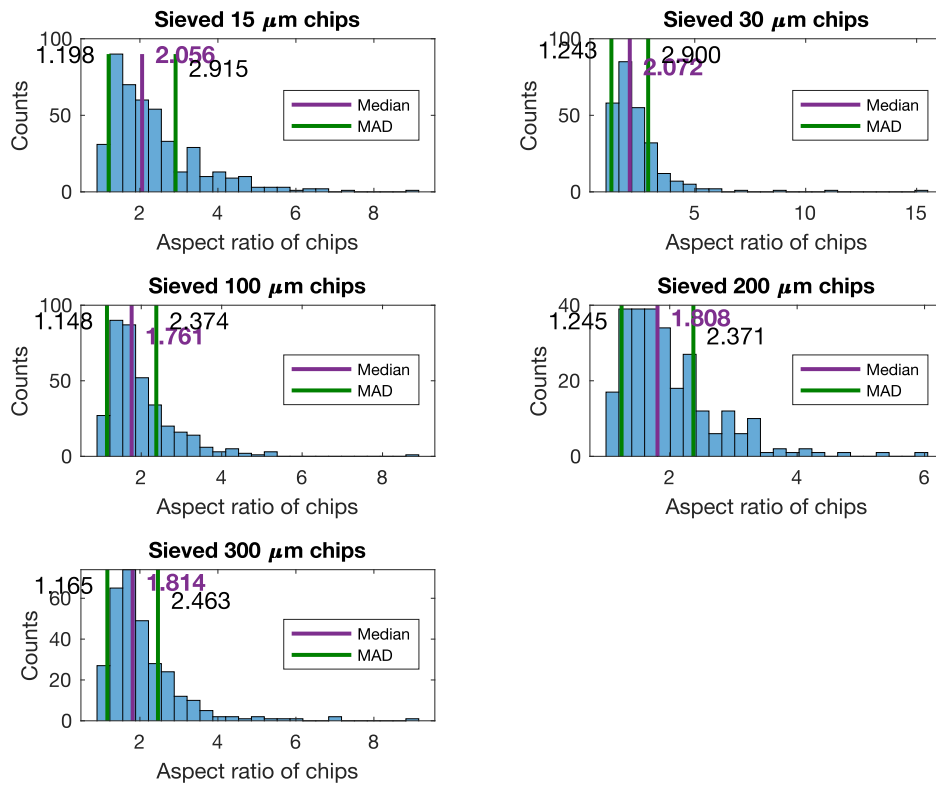


Figure 4.6. Shape distribution of sieved chips of all foil thicknesses.

The relationship between size and shape of sieved chips is shown in Figure 4.7 below. For all thicknesses, the median area was plotted against median aspect ratio. Chips of thickness 15 and 30 μm are similar in shape and 100, 200, 300 μm are similar in shape as well. Although the median aspect ratios of 15 and 30 μm are very similar, their median area differ the most. The median areas of thicknesses 100-300 μm are on the contrary similar. In general, the sieved chips of the given foil thicknesses have similar median area. In fact, the median areas of different thicknesses only deviated a few square millimeters and the size distributions are close to normal distribution. The quantification of size and shape of chips after sieving confirm that the chips about to be compacted are similar in size, shape and distribution of these. Errors due to varying chips properties is reduced. The probability that the randomly selected 20 g of chips (which is then compacted) is deviating from the median, is approximately the same for all foil thicknesses.

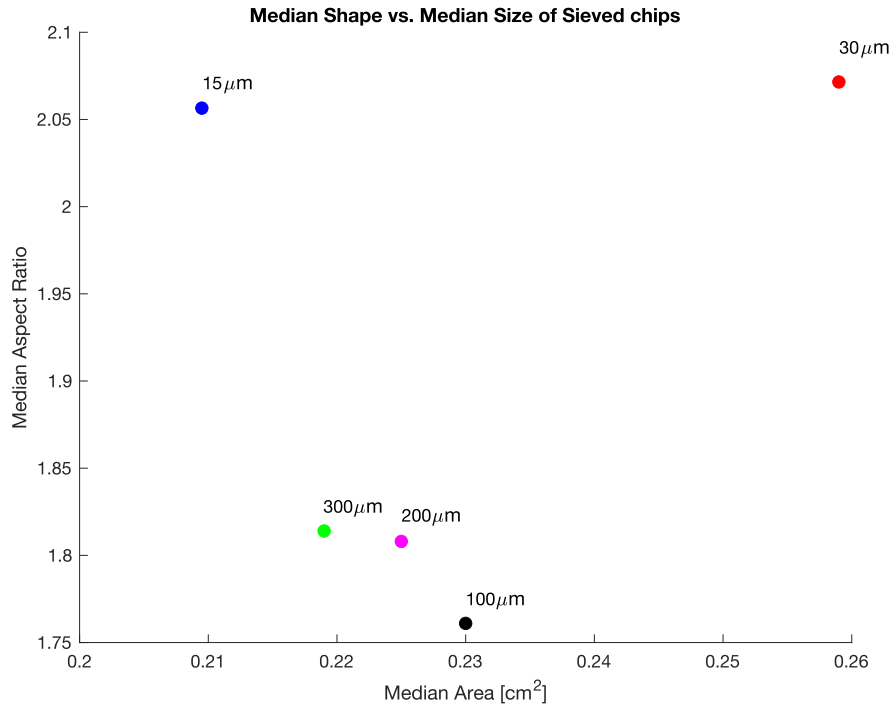


Figure 4.7. Median size of chips plotted against median shape of chips displaying all thicknesses.

4.1.3. The effect of sieving

In Figure 4.8 below, for the two thinnest foils, the median area is plotted against median aspect ratio for both non-sieved shred groups (filled circle) and chips that have been sieved (asterisk). For the 15 µm shred groups C and D differ most, opposite to group A and B which are very similar in size and shape. For 30 µm, the median size of chips is similar, while the shape differs significantly, compared to corresponding groups of 15 µm chips. In general, there is no significant trend between the same groups of different thicknesses.

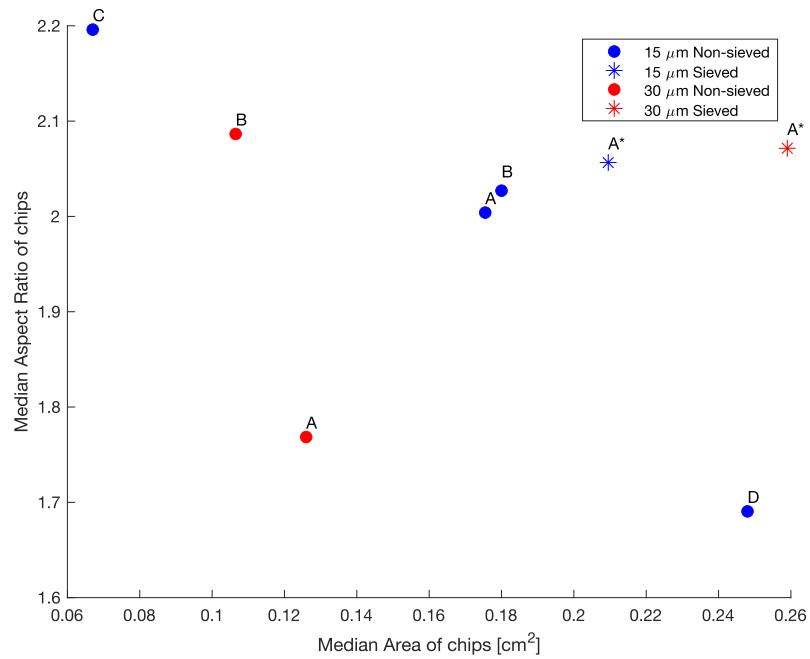


Figure 4.8. Size and shape characteristics of shred groups (non-sieved) and sieved chips.

The median size differs approximately the same between sieved chips (A* and A*) as it does for non-sieved chips (A and A) in Figure 4.8 above. However, as observed in Figure 4.9 below, the sieving lead to removal of particularly the smallest chips. Instead, as a result of sieving, the majority of chips are medium size (relatively).

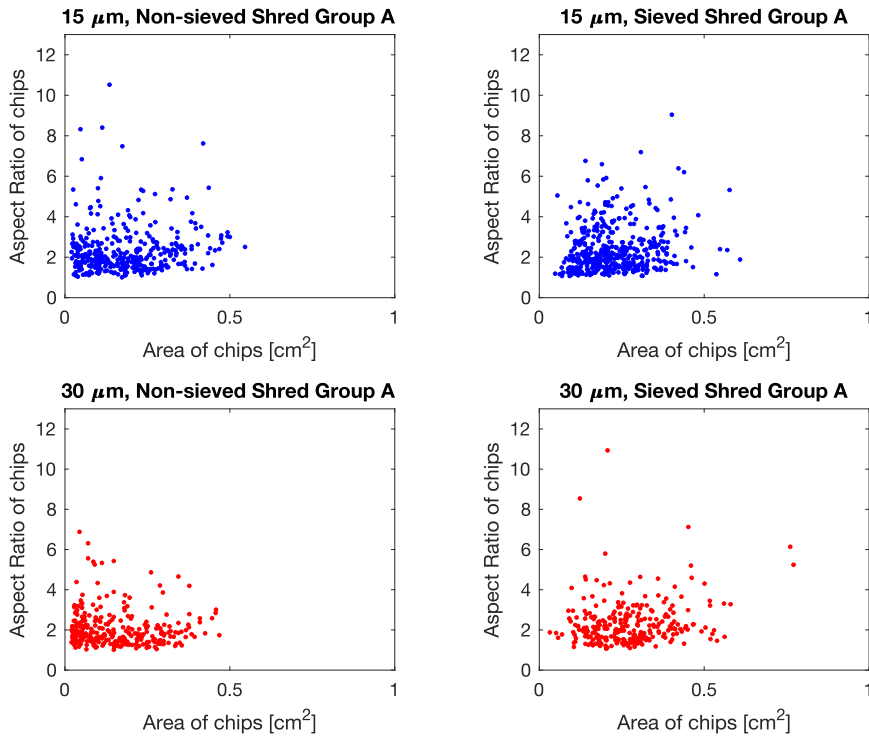


Figure 4.9. Comparison between size and shape of sieved and non-sieved chips for the two thinnest foil materials.

In Figure 4.10 below, size and size distribution between sieved and non-sieved chips is compared. As a result of sieving, mainly the smallest chips are removed. This leads to a more uniform size distribution near normal distribution, although slightly right-skewed with some very large chips that manage to pass the 5 mm sieve.

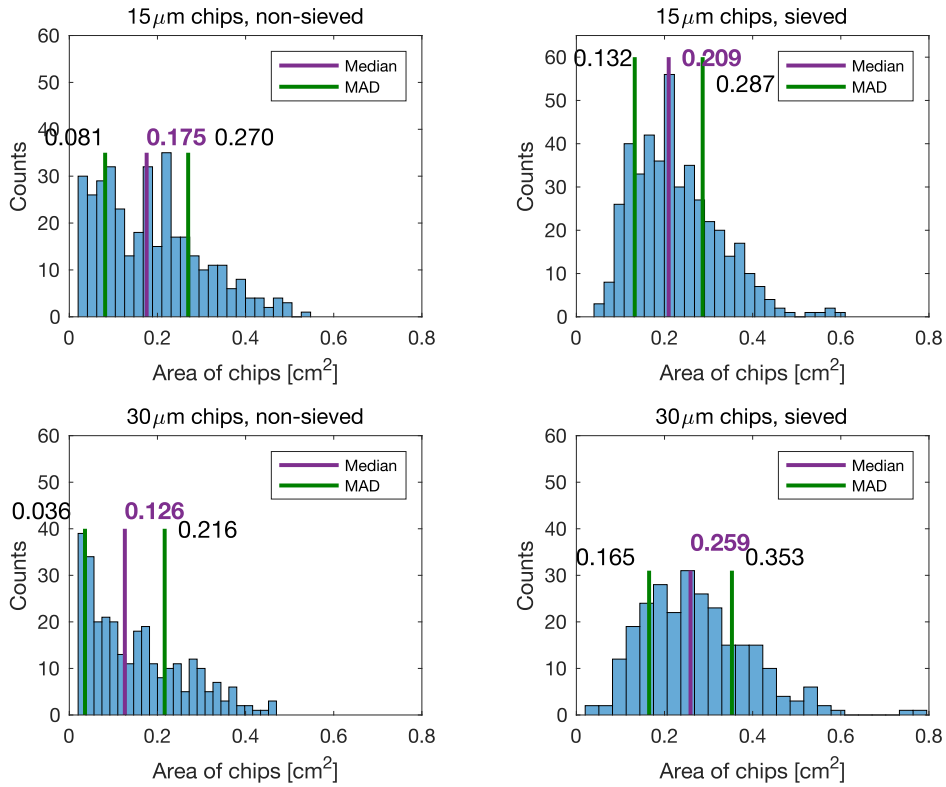


Figure 4.10. Comparison between distribution and median sieved and non-sieved chips of thickness 15 and 30 μm.

4.1.4. Settling volume and mass of chips

The difference between settling volume and mass per chip is shown in Figure 4.11 and Table 4.1 below. The settling volume of the chips was assumed to relate to the deformation degree of the chips. Thinner chips that are more deformed resulted in higher settling volume.

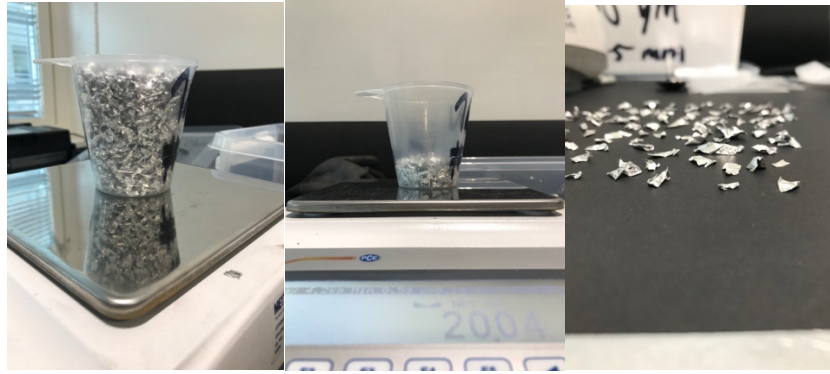


Figure 4.11. Estimation of settling volume of 20 g chips of 15 and 300 μm thickness. The right image exemplifies the effect of deformation degree on the surface exposed to the camera.

As seen in Table 4.1 and Figure 4.12 below, the mass of the chips is only proportional to the thickness for 15 and 30 μm foils. The mass of 30 and 100 μm chips are very similar, even though the mass is divided by area and shape, which are parameters that potentially could have impacted the results. The mass of the three thickest foils show that thickness is not proportional to mass due to different deformation degree.

Table 4.1. Settling volume of 20 g chips in a 175 ml cup and average mass per sieved chip for all foil thicknesses.

	15 μm	30 μm	100 μm	200 μm	300 μm
Settling volume (ml)	175-185	100-110	60-75	40-50	30-40
Avg. mass per chip (mg)	6.0	12.3	12.4	18.2	21.8
Avg. mass per chip per mean	26.5	45.0	50.1	76.9	95.0
Area (mg/cm^2)					
Avg. mass per chip per mean	2.5	5.1	6.1	9.1	10.5
Shape (AR)					

In Figure 4.12 below, the mean mass against mean area of chips including bars with deviations are shown for different foil thicknesses. These results may indicate that the measured mass of thicker chips, which are less deformed, is closer to the ideal mass as if they were completely flat. On the contrary for thinner chips, the higher deformation degree, result in a measured mass that can be significantly higher than if the chips were completely flat.

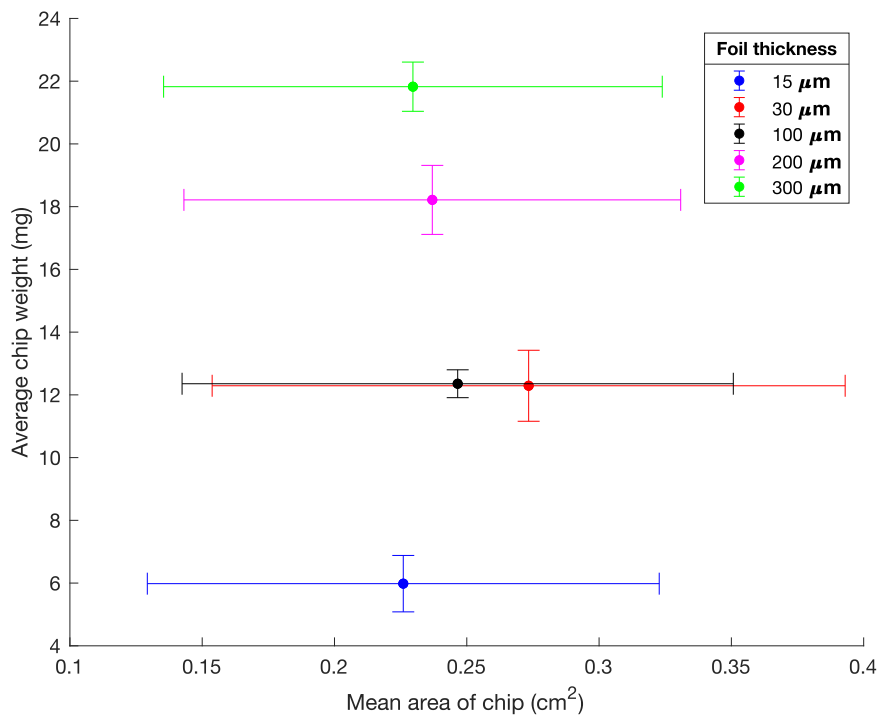


Figure 4.12. Average mass per chip with weighted STD (vertical) versus average area of chip with STD (horizontal) for sieved chips of all foil thicknesses.

In Figure 4.12 the weighted standard deviation of mass are shown as vertical bars and standard deviation of area are shown as horizontal bars. The deviation from area mean is 0.12 cm^2 for $30 \mu\text{m}$ while it is $0.09\text{-}0.10 \text{ cm}^2$ for the other thicknesses.

4.2. Compaction of chips to briquettes

Initially, chips from different shred groups of foil 15 and $30 \mu\text{m}$ were uniaxially compressed and the bulk densities were compared. Graphs were created to illustrate the bulk density achieved with varying compressive stress applied. The chips that were compressed at this initial stage were not sieved.

In the second compaction study, sieved chips were compressed by uniaxial pressing, HPT and HPT at $450 \text{ }^\circ\text{C}$. In this study, the objective was to achieve equal bulk densities for all foil

thicknesses. For a given thickness and range of bulk density, three parallel pressing were done, as seen in Table 3.3.

4.2.1. Shred group comparison and the relationship between bulk density and applied stress for manually compressed samples

First, bulk densities obtained from different shred group of foils 15 and 30 μm was investigated. One to three parallel pressings were done. The bulk densities obtained from different shred groups did not significantly differ neither for 15 nor 30 μm foils. Although the difference in bulk densities between thickness 15 and 30 μm were small, the results were large enough to indicate a potential difference, which was confirmed after further compaction of sieved chips with automatic compaction method.

In Figure 4.13 below, the bulk density obtained from different compressive stresses is shown. The compressive force that could be controlled during compaction was divided by the area (which was constant) to obtain compressive stress. As indicated in the box to the right, the different shred groups distinguished by colors. The maximum compressive force for A, B and D was 70 kN corresponding to 56 MPa. For shred group C, the maximum compressive force was 120 kN, corresponding to 96 MPa. The minimum compressive force that would result in a compressed briquette was 0.5 kN i.e. 0.4 MPa, however, the minimum plotted value was 2 kN (1.6 MPa).

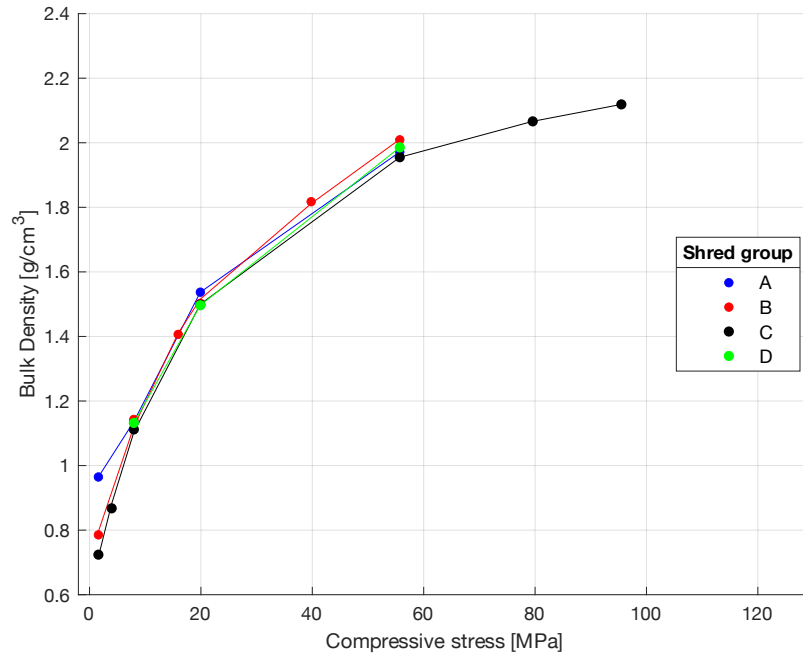


Figure 4.13. Average bulk density of compacted 15 μm foil chips from different shred groups.

In Figure 4.14 below, a similar plot for 30 μm is shown. For this thickness, chips from shred group A were compacted the most. The maximum force was 152 kN i.e. 121 MPa. The bulk density did not significantly differ between shred groups. An indication of error is the highest data point of group A. A compressive force of 130 kN resulted in higher bulk density than that achieved for 152 kN. Pressing at high force was less frequent and more compactations are required to confirm these results.

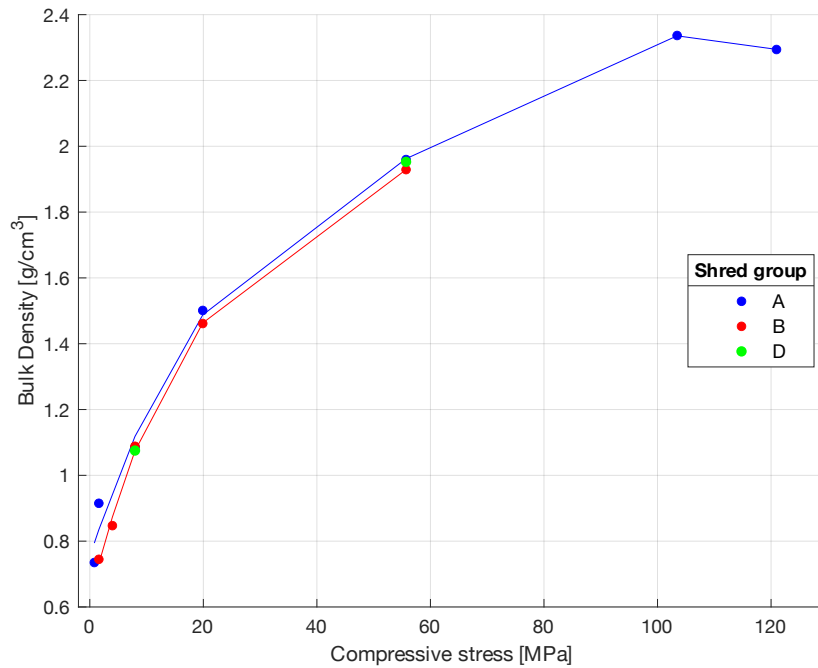


Figure 4.14. Average bulk density of compacted 30 μm foil chips from different shred groups.

The relationship between bulk density and compressive stress is similar for 15 and 30 μm foil chips. The bulk density is increasing as compressive stress increases, although the increase is diminishing as compressive stress increases. For both foil thicknesses, bulk density obtained from compressive force of 2 kN i.e. 1.6 MPa deviated significantly. In Figure 4.15 below, the difference in bulk density between thickness and shred groups was evaluated closer.

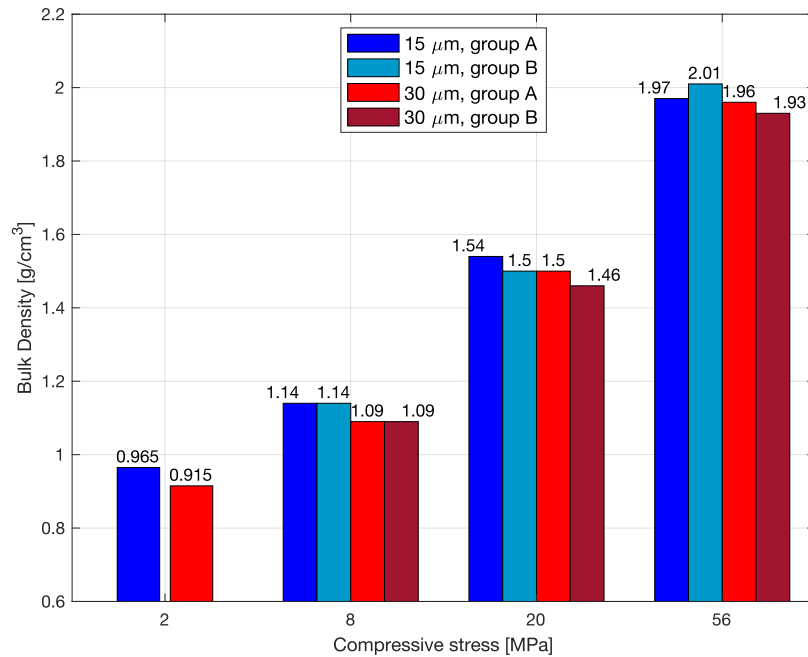


Figure 4.15. Bar graph showing average bulk density for 15 and 30 μm foil thickness and the shred groups.

As seen from Figure 4.15, the different shredding techniques resulting in group A-D did not lead to any significant difference in bulk density. This relates to the results from characterization of chips with ImageJ. The differences in size and shape between shred groups is small enough to not affect the outcome in bulk density.

In Figure 4.16 and Figure 4.17 below, the thicknesses 15 and 30 μm is compared, and the error bars are shown. With respect to these results, and in conjunction with results from chips size and shape, it was determined to average results from A and B before comparing 15 and 30 μm closer. By that, the effect of sampling is reduced i.e. the effect of size and shape on bulk density is reduced by averaging.

As observed in the Figure 4.17, the error bars are generally larger than the difference between thicknesses. In this graph, it is clear that the values deviate the most at the lowest compaction. Despite deviating results, for all compressive stresses, a slightly higher bulk density is reached for 15 μm . This indication lead to further investigation between the foil thicknesses, by

including 100, 200 and 300 μm . Also, the bulk densities achieved in this study were benchmarks for further, more precise compaction.

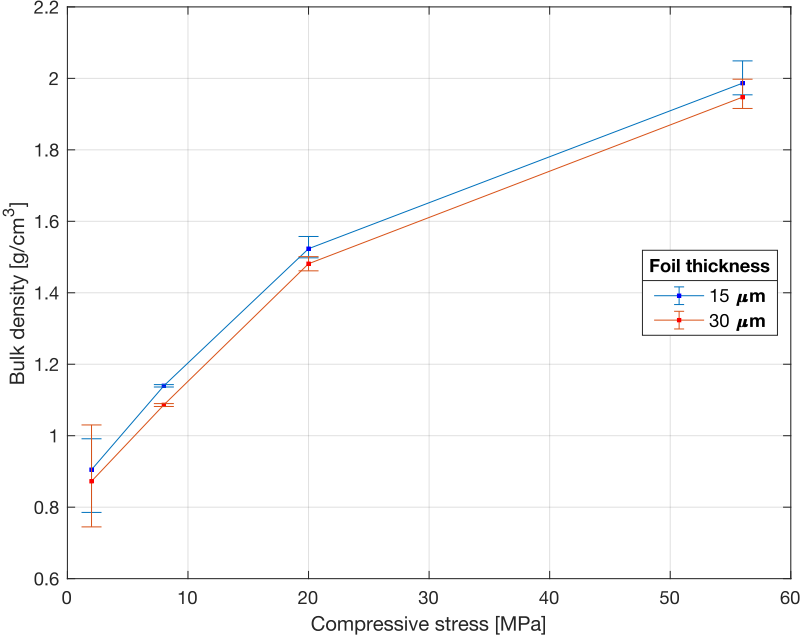


Figure 4.16. Bulk density from shred group A and B averaged for 15 and 30 μm with error bars with min-max. interval.

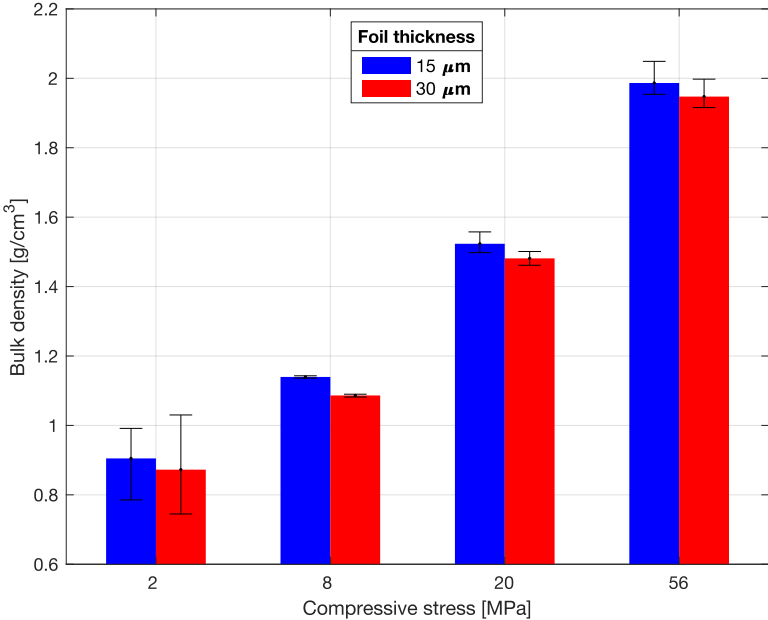


Figure 4.17. Bulk density from shred group A and B averaged for 15 and 30 μm with error bars with min-max. interval.

Potential errors leading to deviating results were not further quantified. However, potential errors were controlled by compressing chips from group A only and utilizing the automatic features of the pressing machine. By automatic pressing, the chips were compressed at a constant pressing rate and accurately up to the targeted compressive force. These results are treated in the next section.

4.2.2. Compaction results for automatically compacted sieved chips

To most accurately compare recovered Al melted in salt flux, the aim was to accomplish equal bulk density briquettes for the different foil thicknesses. This final compaction study also evaluated the impact of applied torque (HPT) and HPT at 450 °C.

As seen in Figure 4.18 below, to reach approximately the same bulk density, the applied force needed to compress the chips slightly varied slightly between foil thicknesses. In particular, the stress varied between thicknesses for bulk densities of approx. 2.1 g/cm³. The observed difference in bulk density between thicknesses was considered an acceptable range for later melting in salt flux.

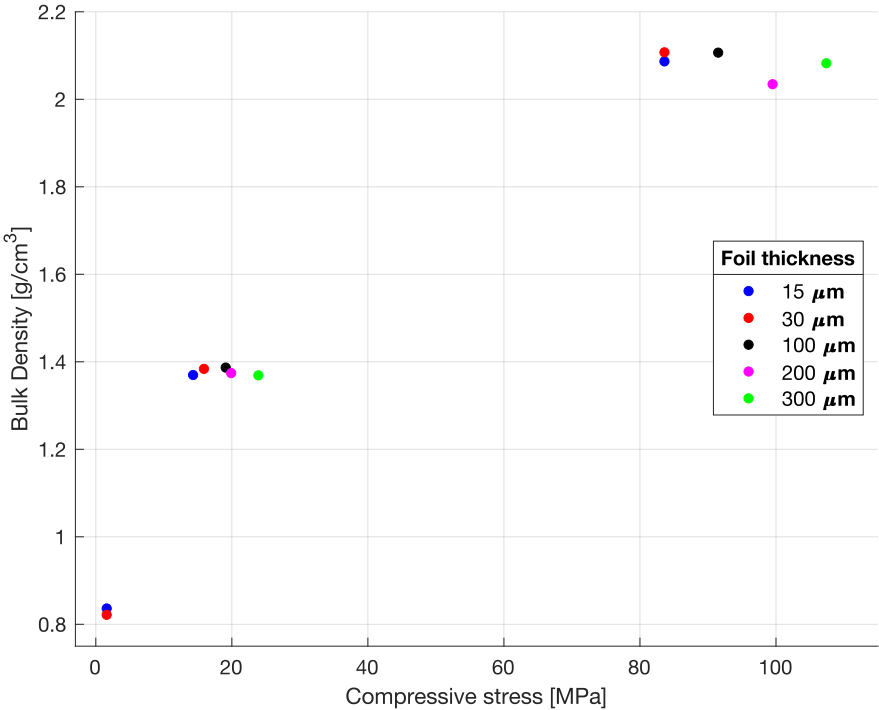


Figure 4.18. Bulk density of briquettes obtained by automatic compaction of sieved chips.

The effect of HPT was investigated by compaction of 300 μm foil. In Table 4.2 below, different HPT results is presented. The first two columns indicate a significant difference in bulk density between 200 and 500 kN of compressive force. Adding only half a turning after 200 kN of uniaxial pressing lead to significant higher bulk density than uniaxial pressing of 500 kN. Moreover, both 70 kN and 100 kN with applied torque lead to more compression than 200 kN of uniaxial pressing. The Table 4.2 indicate that HPT effectively increase compaction.

Table 4.2. The effect of torque (revolutions) in addition to uniaxial pressing of 300 μm foil.

Compressive force (kN) + Rev.:	500	200	200+1/2	100+4	70+4	25+4
Bulk Density (g/cm ³):	2.58	2.32	2.69	2.57	2.51	1.92

HPT at high temperature (450 °C) was performed to simulate screw extrusion. Figure 4.19 below indicate the effect of applied torque and at high temperature. Four turnings added to 56 MPa increased bulk density with 29, 24 and 37 % for 15, 30 and 300 μm , respectively, relative to 56 MPa compressive load only. The corresponding effect of HPT at 450 °C was 33, 32 and 47 % for 15, 30 and 300 μm , respectively. This indicate that bulk density of 300 μm is most increased by HPT at high temperature.

Torque (and hence torsion) is dependent on the angle of twist. Although four turnings were applied after targeted compressive force had been reached with uniaxial pressing, the angle of twist was not measured.

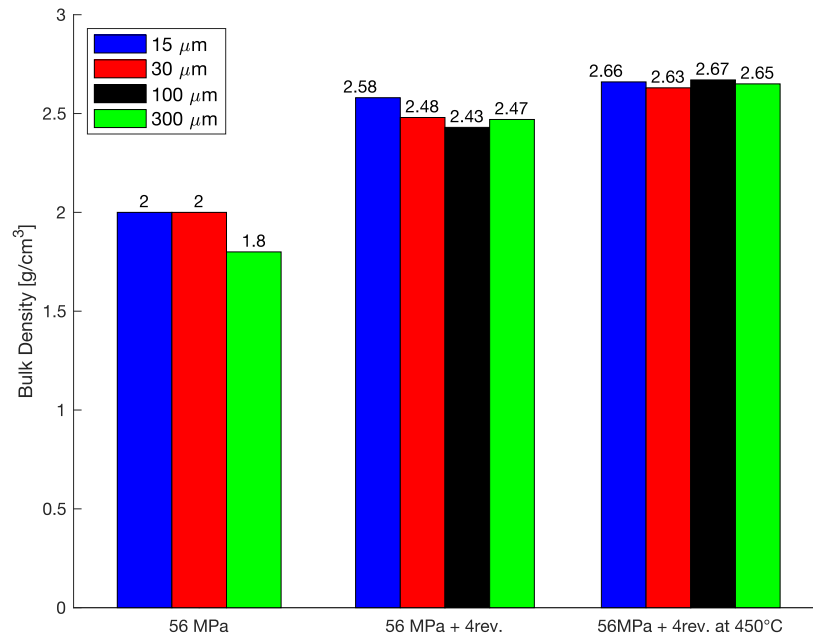


Figure 4.19. Mean bulk density comparison of the three compaction methods.

For a given foil thickness, the bulk density varied most for HPT (without heat). Presumably, this occurs due to manual pressing. For HPT at 450 °C, the pressings were automatic. HPT at 450 °C lead to bulk density 97-98 % of the real density of foil material. However, as seen in Table 4.2 above, a high bulk density can also be reached by HPT at room temperature.

4.3. Briquettes properties

4.3.1. Briquette surface area analysis

The surface of the briquettes compacted by uniaxial pressing were characterized using Alicona 3D-microscope. The parameters analyzed were true-to-projected area ratio, height profile for a given distance along the surface, root mean square gradient (Sdq) and developed interfacial area ratio (Sdr). In Figure 4.20 below, true-to-projected area ratio is plotted against bulk density. This parameter was suitable because of the difficulty to measure area of the cylindrical structure by image analysis. The higher the value is, the larger the surface area due to irregularities of compacted chips at the surface. A value of 1 correspond to a completely flat surface, hence small surface area.

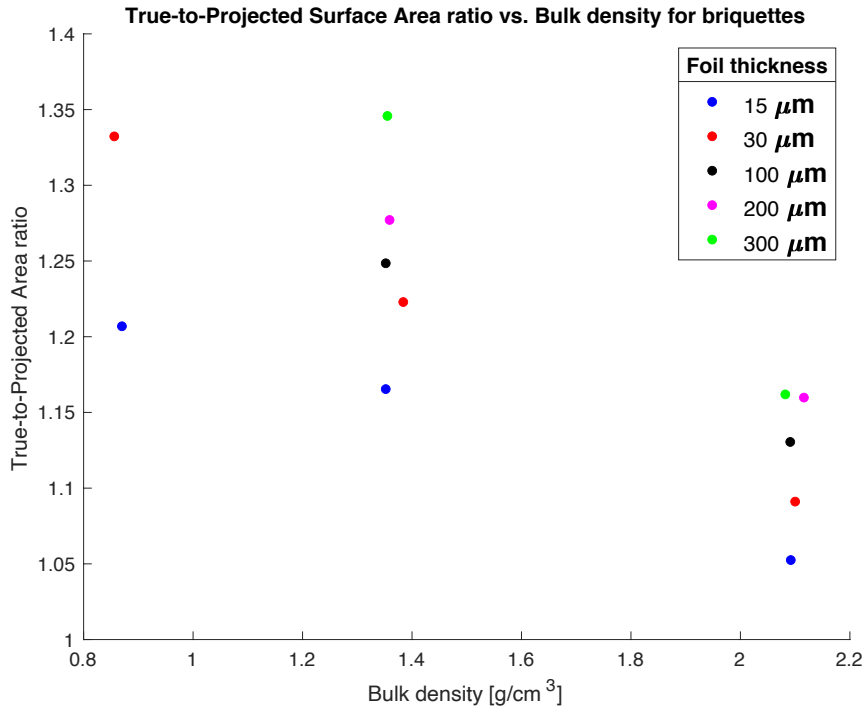


Figure 4.20. True-to-projected area ratio for different bulk density of briquette.

As seen in the Figure 4.20, the relationship is strong between surface area and thickness of foil. For a given bulk density, briquettes of thicker foil have larger surface area. The surface area decreases as the extent of compaction increases. For 15 and 30 μm the relationship is approximately linear. However, the difference between foil thicknesses at 2.1 g/cm^3 is relatively unchanged compared to lower density, with the exception of 200 and 300 μm .

The height profile was plotted as seen in Figure 4.21 below. In order to compare briquettes of different foil thicknesses and bulk densities, the data on height measurements had to be adjusted by subtracting the data points with the mean. As observed, a horizontal line (and the mean of adjusted data) is drawn to make observation clearer. Figure 4.22 shows the same height profile as Figure 4.21 but at a micro level in order to visualize the difference in micro roughness.

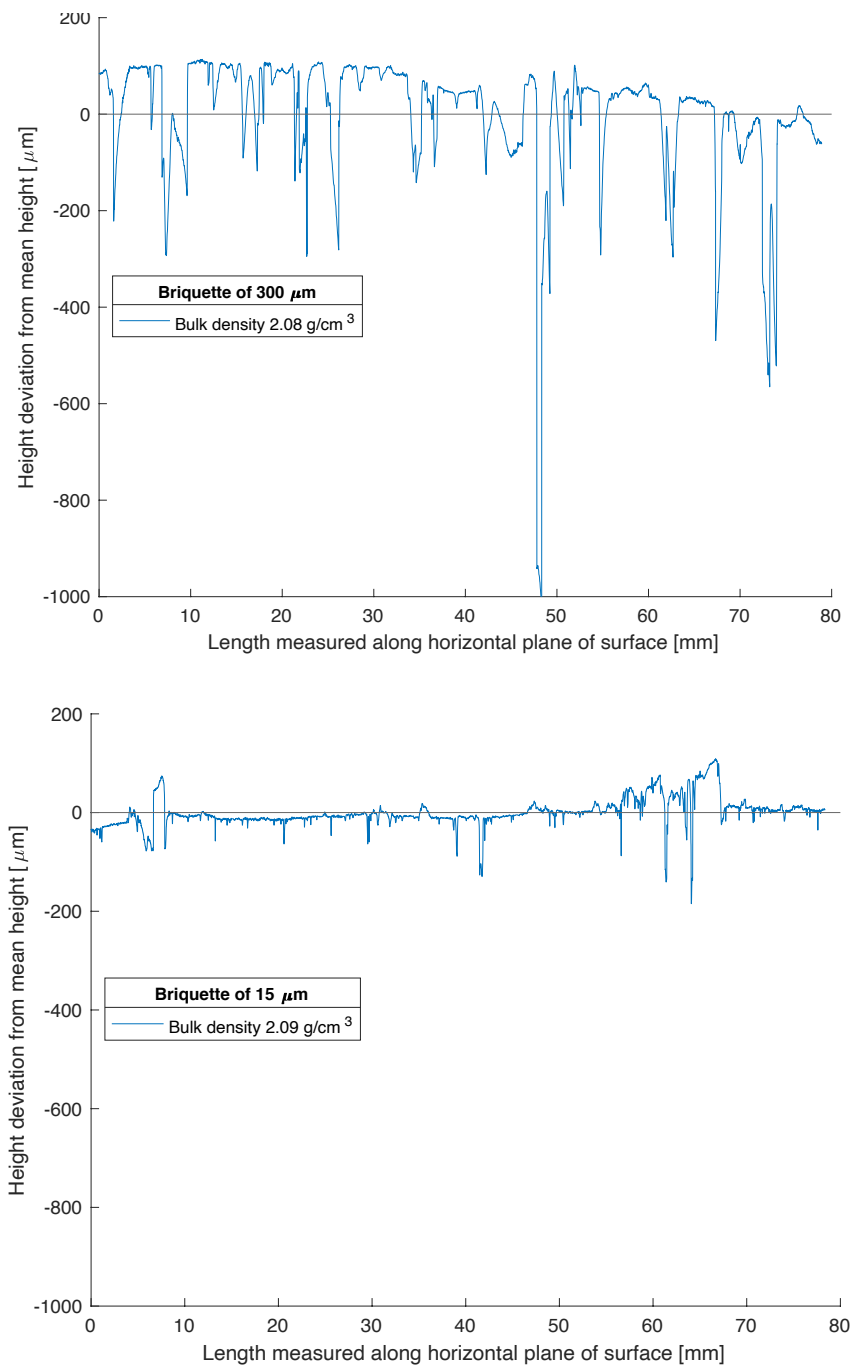


Figure 4.21. Surface height profiles of briquettes of 15 and 300 μm of similar bulk density with the mean height (zero) as reference.

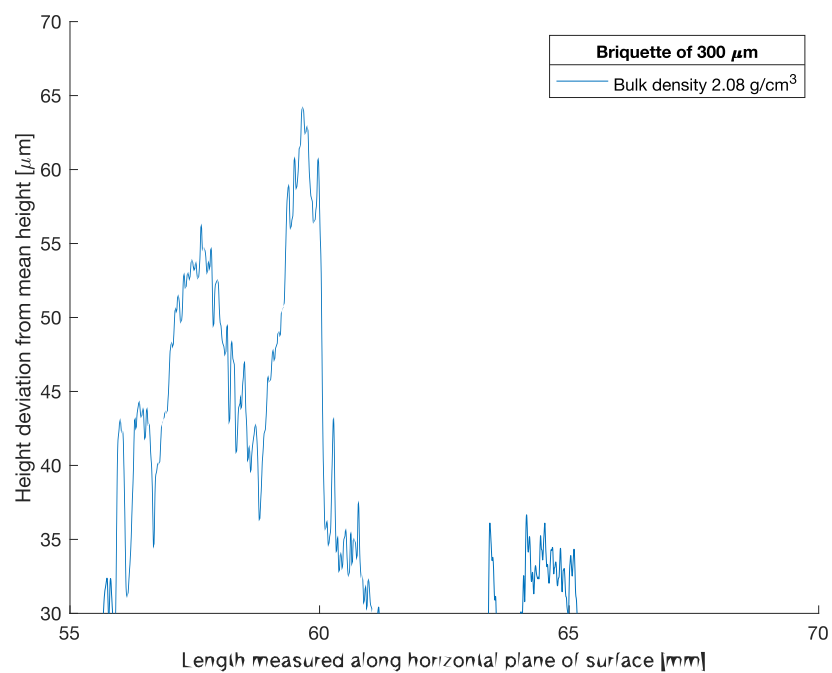
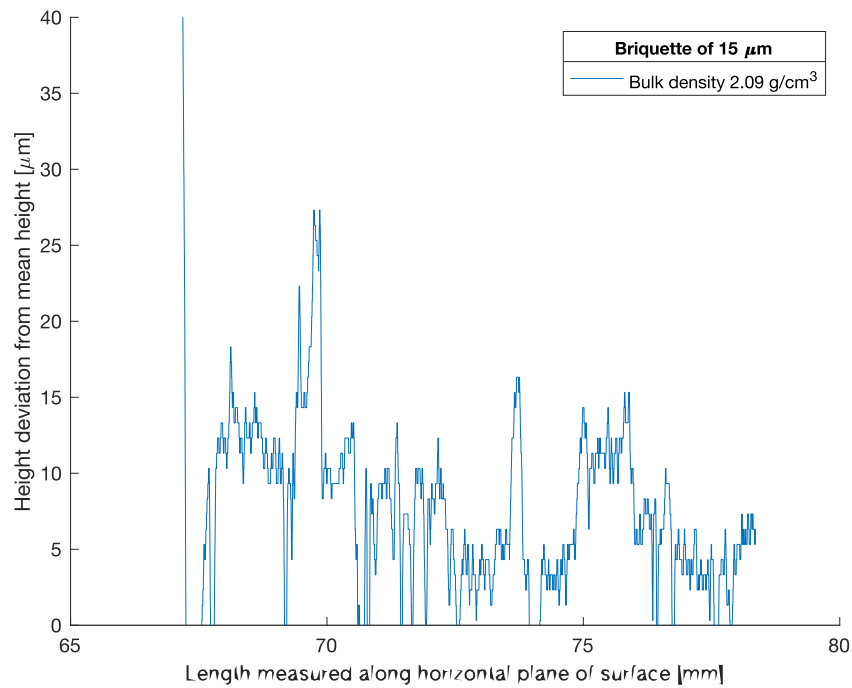


Figure 4.22. The surface height profiles of the same briquettes but at a micro level.

Comparing the graphs, peaks/spikes can be distinguished from hills/valleys i.e. micro and macro roughness. In other words, the surface can be affected by both spacing and texture amplitude. The thinner foils most significantly differ in texture.

Two additional roughness parameters were introduced and analyzed: Root mean square gradient (Sdq) and Developed interfacial area ratio (Sdr). The theory of these parameters is described in section Characterization of briquettes and the resulting values from the surface measurements are presented in Table 4.3 below.

Table 4.3. Sdq and Sdr values for briquettes of different bulk density and foil thickness.

Sdq	15 μm	30 μm	100 μm	200 μm	300 μm
0.86-0.90 g/cm ³	1.31	1.79	-	-	-
1.35-1.40 g/cm ³	1.07	1.36	1.50	1.85	1.61
2.06-2.12 g/cm ³	0.53	0.71	1.02	1.14	1.12
Sdr [%]					
0.86-0.90 g/cm ³	58.0	113.4	-	-	-
1.35-1.40 g/cm ³	39.7	63.8	80.5	124.8	98.2
2.06-2.12 g/cm ³	10.2	17.6	36.7	7.3	43.1

The Sdq is reduced with increased bulk density and thickness. The exception is the thickest foil, 300 μm , which has lower Sdq than 200 μm . The Sdq value is similar for low density 15 μm and medium density 30 μm . Likewise, medium density of 15 μm is similar to high density of 100-300 μm . The relationship is similar for Sdr. Sdr is significantly reduced with increased bulk density and decreased thickness of foil. The results indicate that macro roughness significantly influence the roughness measurement.

4.3.2. Porosity of briquettes determined by X-ray tomography

The mean porosity in percentage with standard deviation bars is shown in Figure 4.23. The asterisk with error bars represents data obtained from briquette that were cut before analysis in x-ray tomography. The circular markers represent data obtained from analysis of the whole briquette in x-ray tomography. In addition, these briquettes consist of sieved chips in contrast to the asterisk error bars, which were not sieved before compaction.

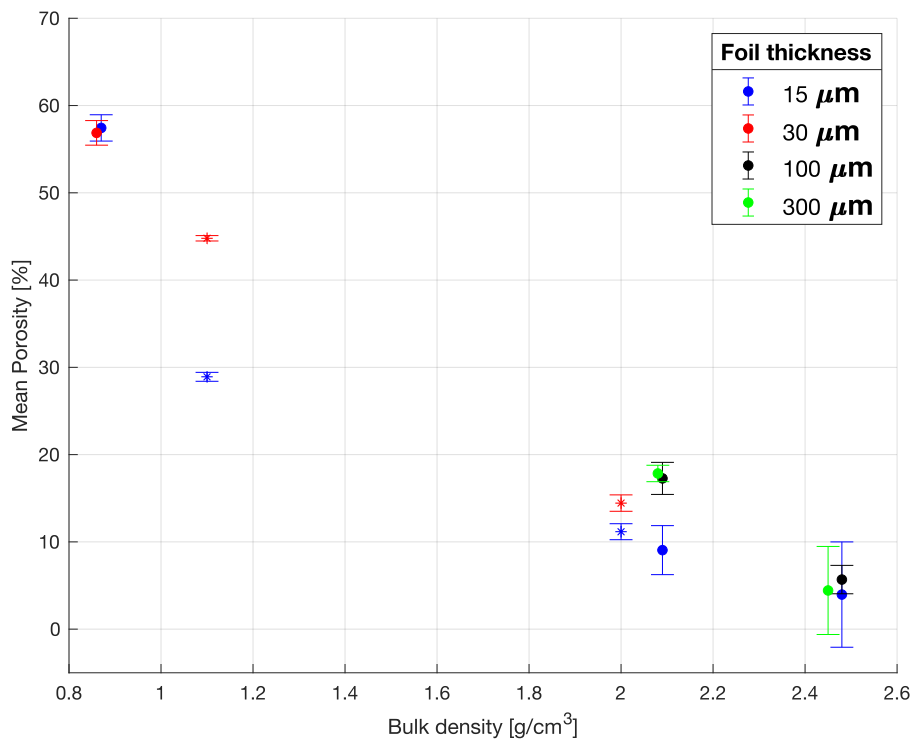


Figure 4.23. Mean porosity measured by x-ray tomography of briquettes with different bulk densities.

The difference between porosity of 15 μm and 30 μm at low bulk density is negligible. However, as the density of the briquette is increased to 1.1 g/cm^3 and 2.0 g/cm^3 , the thicker 30 μm briquette is more porous. The relationship of increased porosity with increased thickness also holds for bulk densities of approximately 2.1 g/cm^3 . In addition, the effect of thickness on porosity is weaker for the thicker foils, the difference in porosity between 100 and 300 μm is negligible.

For highest bulk densities, furthest to the right in the Figure 4.23 above, the difference in porosity between foil thicknesses is negligible. For these briquettes, torque was applied after initial uniaxial pressing. Corresponding uniaxial pressing without applied torque resulted in bulk density of approximately 2 g/cm^3 . Taking this into account, the result indicates that the torque contributes to reduced porosity. However, because of the large standard deviation, this effect is more uncertain for foil thickness 15 μm because the error bars exceed the porosity value of 15 μm at 2.1 g/cm^3 .

Images in Figure 4.24 below illustrate the large variety in porosity at different heights of the briquettes compressed with HPT. Therefore, the standard deviation of porosity is significantly higher than for briquettes compressed uniaxially, as shown in Figure 4.23 above.

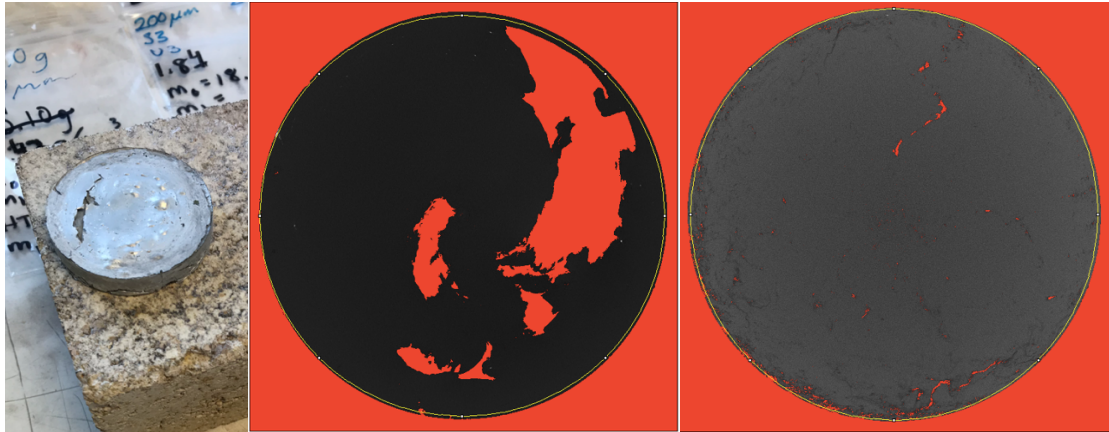


Figure 4.24. Varying porosity at different layers after HPT.

In Figure 4.23 , the data of 15 μm indicate that the relationship between porosity and bulk density is approximately linear above excluding the porosity at approx. 0.9 g/cm^3 i.e. between $1.1\text{-}2.5 \text{ g/cm}^3$. Although the data is less for 30 μm , with respect to the three porosity measurements, the relationship is approximately linear as well.

4.4. Oxidation due to heat treatment

4.4.1. Oxidation of briquettes

The mass of chips and briquettes were measured with an accuracy of 0.0001 g before and after heat treatment for 1 hour at $650 \text{ }^\circ\text{C}$. All of the chips and briquettes each weighed approximately 20 g . In Figure 4.25 below, the mean weight increase for the specified ranges of bulk density is plotted. Both the chips and briquettes were sieved as described in earlier sections. Heat treatments of chips were repeated 2-4 times, most often 3 times. Heat treatment of briquettes were repeated twice with regards to each bulk density. The furnace temperature could vary between $650\text{-}660 \text{ }^\circ\text{C}$ according to the thermocouple. In general, the mass increase measured after heat treatment was only a few tenths of a gram owing to the protective and stable aluminum oxide layer.

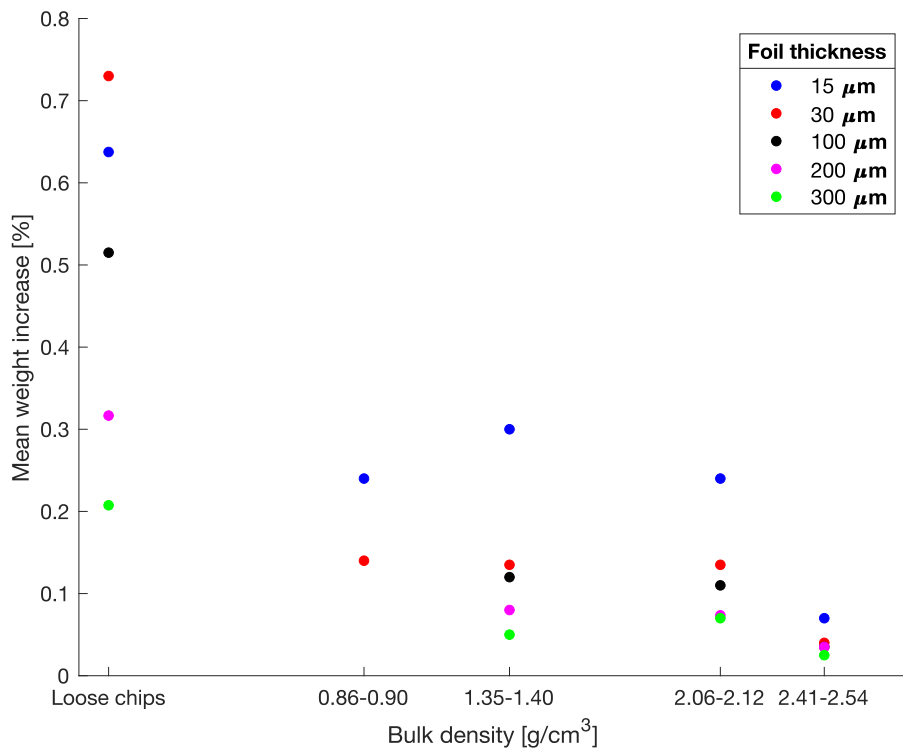


Figure 4.25. Mass increase of chips and briquettes with different bulk densities as a result of oxidation at 650 °C for 1 h.

The mass increase is most different between foil thicknesses for loose chips. Also, the measured mass increase of chips varied significantly more between repetitions compared to briquettes in general. Generally, thicker chips have a lower specific weight gain than thinner chips with the exception of 15 and 30 μm. This relationship is also observed for briquettes, although the difference in mass increase is much less compared to chips.

For the bulk density range 0.86-2.12 g/cm³, the oxidation for a given thickness is relatively unchanged with respect to bulk density. As the bulk density increased to 2.41-2.54 g/cm³, the resistant to oxidation was significantly increased for all foil thicknesses.

4.4.2. Oxidation of sheets

Sheets of thicknesses 100, 200 and 300 μm with the same “macro” surface area were heat treated at 650 °C 1 hour, 5 times. The mean mass increase per surface area (mg/cm²) is presented in Table 4.4 below.

Table 4.4. The mean mass increase per surface area of foil (mg/cm^2) for the three thickest foils.

Mean mass per area	100 μm	200 μm	300 μm
mg/cm^2	0.058	0.064	0.070
std	0.076	0.018	0.037

The standard deviation is high, particularly for 100 μm . Oxidized foil is fragile and small parts of the foil easily fell apart, which leads to a significant decrease in mass. For instance, instead of mass increase due to heat treatment, the mass decreased once for the 100 μm . This result contributes to the large standard deviation of this thickness.

4.4.3. Oxide thickness measurement with SEM

An attempt was made to identify and measure the oxide thickness of the different foil materials, including heat treated foils. EDS was used to investigate the difference in oxygen content between the surface and the core of the foil. However, it was not possible to identify the interface between aluminum, alumina and carbon (epoxy) in the images. In Figure 4.26 below, the oxide layer can be seen for foil of thickness 15 μm . For thicker foils, the oxide layer was less visible. The alumina thickness is expected to be nanometers thick and should tentatively be investigated in TEM.

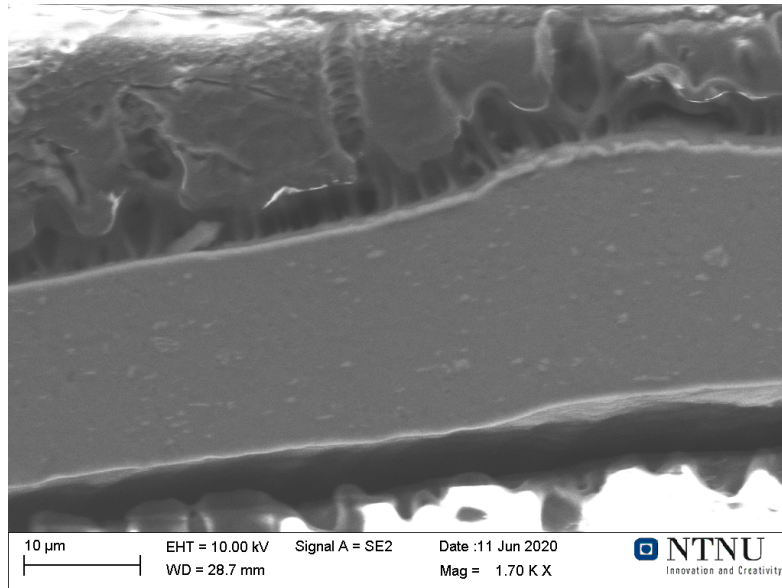


Figure 4.26. The household foil of thickness 15 μm observed in SEM.

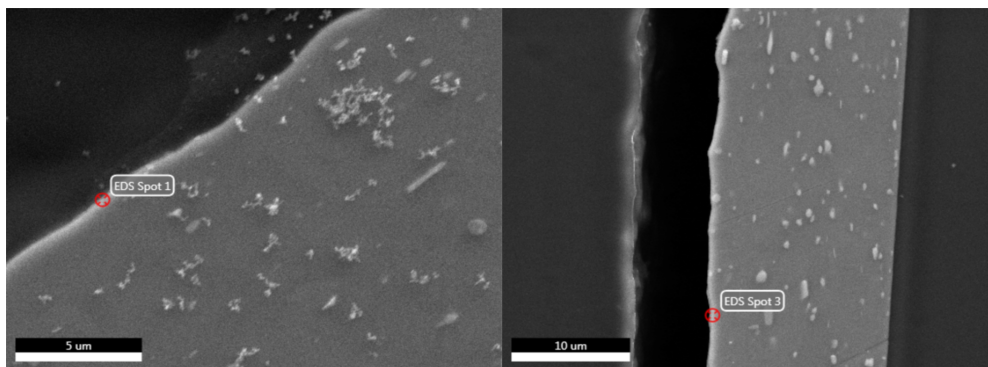


Figure 4.27. Attempt to identify the oxide layer by point-analysis in EDS.

4.5. Al recovery of melted chips and briquettes

The recovery studies are separated by non-heat treated and heat treated as well as melting experiments in salt flux and without salt flux. Initially, a small study was made on the recovery in salt flux of briquettes and chips that had not experienced any heat treatment. On the basis of the results, the largest study turned out to be on recovery of heat treated briquettes and chips. Finally, a smaller study was made on the melting behavior without salt flux involved.

4.5.1. Recovery of non-heat treated briquettes

In this study, mostly briquettes of 30 and 300 μm were melted in salt flux. These briquettes were completely recovered or very near 100 %. The percentage recovered of briquettes was independent on bulk density, salt amount (salt/Al ratio of 2 to 5) and melting time (10-60 minutes). Chips of 30 μm melted in 160 g salt resulted in 100 % recovery.

Interestingly, the briquettes covered in salt flux and charged at 800 °C melted after 25 minutes although the salt flux was still solid. In spite of solid salt flux, the briquettes coalesced, and the Al was completely recovered. This means that complete recovery is achieved regardless of solid or liquid salt flux.

For briquettes of 15 μm the recovery was slightly lower, 92-98 %. This was the first indication of lower recovery for 15 μm than for the thicker foil materials. Consequently, in the following study, investigation of the recovery of heat treated briquettes of 15 and 30 μm were prioritized.

4.5.2. Pre-study on recovery of heat-treated chips and briquettes

In this study, the effect of heat treatment was investigated. The salt/Al ratio was 5 (i.e. 100g salt: 20g briquette) for most melting experiments of briquettes. However, it was discovered that a ratio of 4 (i.e. 80 g salt) was enough to completely cover the briquette. The melted briquette melted consisted of chips that had not been sieved prior to compaction. Most of the briquettes melted were heat treated at 650 °C either one or two hours. However, initial heat treatments were done in 800 °C.

In Table 4.5 below, the recovery of 15 μm briquettes heat treated above the melting point of the material is shown. In these four experiments the crucibles containing briquette covered in 40 g salt were charged in the furnace at 800 °C. They were heated 38 to 60 minutes before removed and cooled in room temperature. As opposed to the recovery referred to in the subsequent studies, the percentage includes the mass recovered from the small non-coalesced particles. Specifically, it is the mass of the Al that is larger than 0.8 mm (that did not pass the holes of the sieve).

Table 4.5. Mass increase after heat treatment at 600 °C for 3.5 h plus 800 °C for 1.5 h, and subsequent recovery of 15 μm briquettes.

Bulk Density [g/cm ³]	0.7	0.8	2.0	2.0
Mass increase due to heat treatment [mass%]	1.22 %	1.32 %	1.13 %	0.77 %
Recovery [mass%]	20.7 %	52.7 %	70.3 %	70.9 %

The heat treatment led to significant oxidation as seen by the percentage mass increase. The relatively low recovery obtained indicate that growth of the protective alumina layer prevents coalescence and recovery. Insufficient recovery also occurred for the briquette of 30 μm. In Figure 4.28 below, the absence of coalescence of recovered Al is shown, corresponding to column 1, 2 and 4 in Table 4.5 above.



Figure 4.28. The recovered Al of briquettes corresponding to column 1, 2 and 4 in Table 4.5 above.

Briquettes of 300 μm heat treated above the melting point successfully coalesced and the recovery was near 100 %. However, it was observed that the ability to coalesce was weakened for this thick foil material. The melted Al piece appeared significantly different compared to briquettes that successfully coalesced. Specifically, complete spherical transformation did not take place, possibly as a consequence of thicker oxide layer that can withstand shape change. In Figure 4.29 below, the left image shows the recovered Al from a briquette of 1.35 g/cm³ heat treated 800 °C for 1.5 h. The right image shows the recovery of a briquette of 2.4 g/cm³ heat treated at 750° C for 1 h. The mass increase was 0.14 % and 0.04

%, respectively. Although the Al appeared differently than a usual coalesced briquette, the recovery was almost 100 % for both (Figure 4.29).

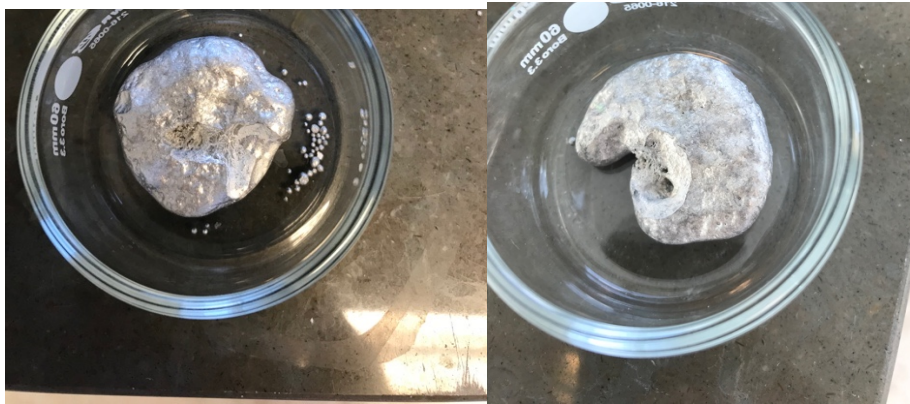


Figure 4.29. Recovered briquette of 300 μm , heat treated above melting point prior to melting.

In Figure 4.30 and Figure 4.31 below, the recovery of 15 and 30 μm briquettes heat treated at 650 °C for 1 and 2 hours are shown. The time of heat treatment had no significant effect on recovery. The briquettes consisted of chips that had not been sieved prior to compaction. In contrast to the recovery shown above, in the subsequent studies, recovery is defined differently. The definition along with an image is shown in Figure 4.32 below.

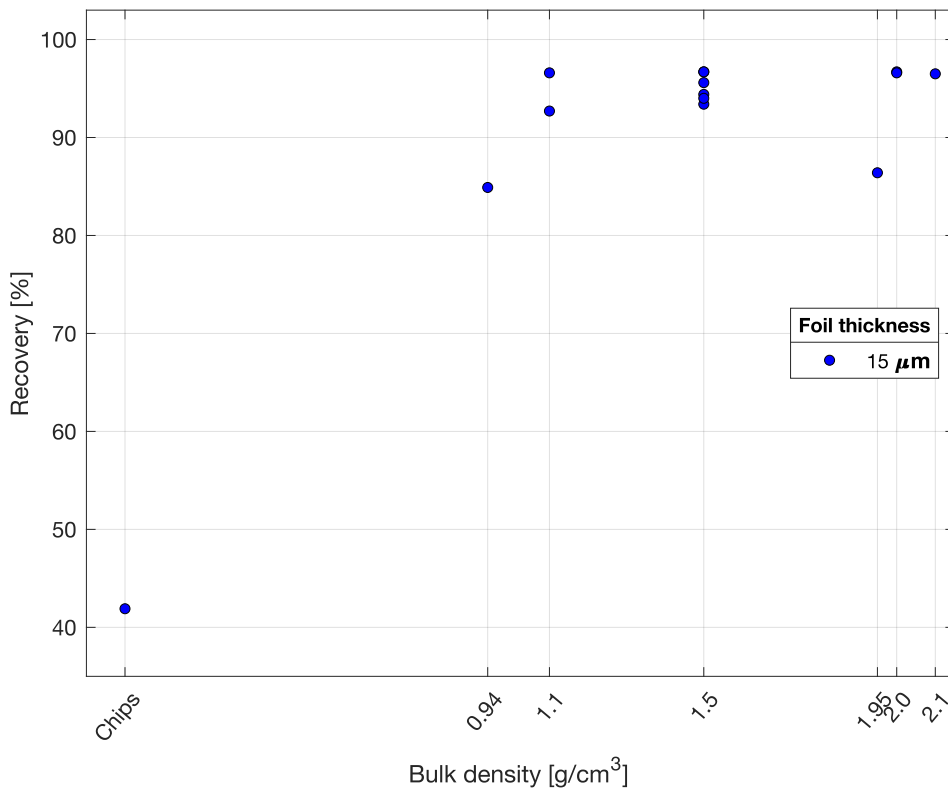


Figure 4.30. Recovery of chips and briquettes of 15 μm in salt flux with varying experimental setup.

Generally for the 15 μm foil, recovery increases with increased compaction i.e. bulk density. For both 15 and 30 μm the difference in recovery is most significant between chips and briquettes in general. However, for briquettes of 30 μm foil, the relationship between bulk density and recovery is absent. The recoveries are much lower from briquette of bulk density 1.95 and 1.92 g/cm^3 for 15 and 30 μm , respectively. Varying CaF_2 content could be the reason. As earlier described, a batch of four crucibles with briquettes are melted simultaneously. The recovery of all briquettes in this batch differed relative to other experiment with similar bulk density of briquette. The method of pre-mixing of CaF_2 was therefore rejected and in the final recovery study the CaF_2 was added individually to each crucible.

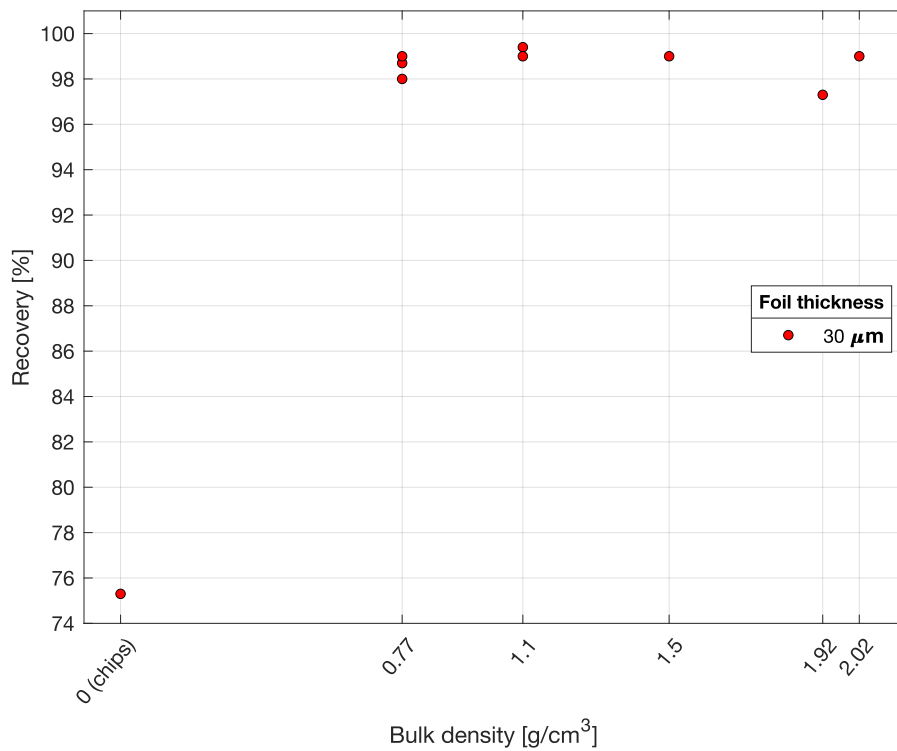


Figure 4.31. Recovery of chips and briquettes of 30 μm in salt flux with varying experimental setup.

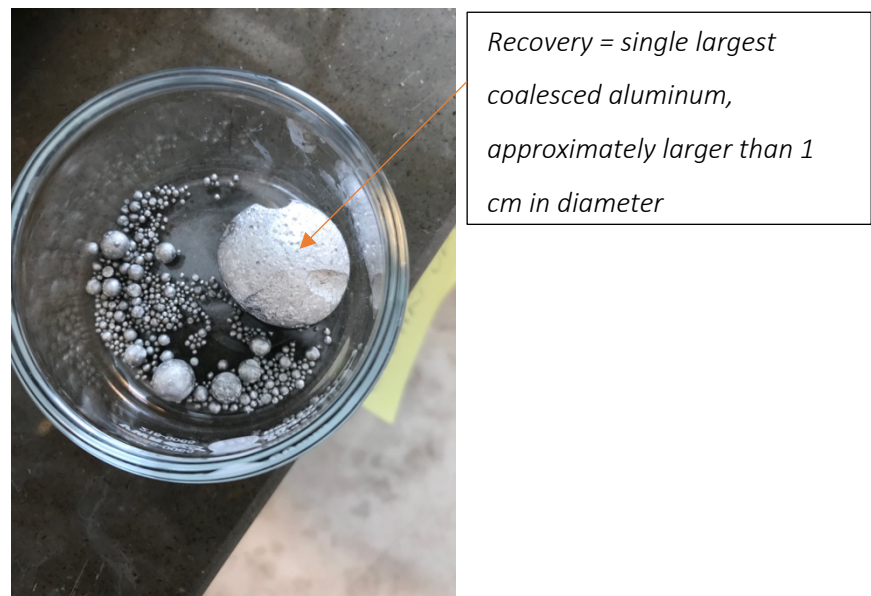


Figure 4.32. Example of coalesced aluminum and smaller aluminum particles obtained from melting a briquette in salt flux.

4.5.3. Recovery in salt flux with final experimental setup

Recovery percentage obtained was quite similar for foil thicknesses 30-300 μm in salt flux. Consequently, it was most suitable to plot recovery of 15 μm individually and all the thicker foils in a separate graph. In the final experiments, briquettes heat treated at 650 °C for 1 h were charged in 80 g of molten salt flux at 800 °C. Chips on the other hand required 150 g of salt to be completely covered. 2 mass% of CaF_2 was added in each crucible prior to melting to ensure the desired composition of salt flux. All the briquettes melted consisted of sieved chips to reduce risk of deviation in size. The melted briquettes were removed from the furnace after 10 minutes.

In Figure 4.33 below, the recovery chips and briquettes of 15 μm foil is shown. As indicated by the pre-study, the relationship between recovery and bulk density is confirmed. Generally, the deviation between repeated experiments deviate less with increased bulk density. The alignment of compacted chips risk deviating more with decreased compression. A few chips (weighing on average 6 mg) were missed during charging in molten salt.

The three asterisk markers, furthest to the right (in Figure 4.33), show recovery of 97, 99 and 100 %. These are special because they were achieved by HPT at 450 °C. In addition, the chips were heat treated at 650 °C 1 h prior to this compaction method. The recovery was high in spite of significant oxidation of chips with thickness of 15 μm .

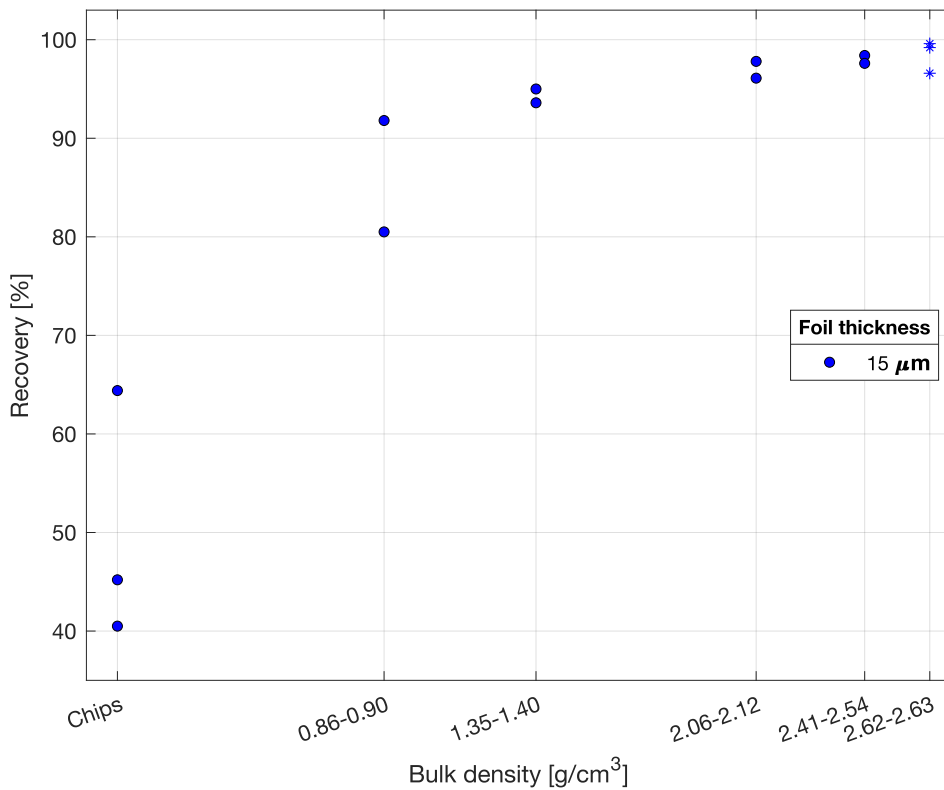


Figure 4.33. Recovery of heat treated (650°C 1 h) briquettes of 15 μm in the last experimental setup.

In Figure 4.34 below, the recovery of briquettes and chips of 15-300 μm is showed. Because the percentage recovery for briquettes were very similar regardless of bulk density, the data is compiled. The recovery of free chips is increased with increased thickness and recovery of briquettes is higher than that of chips. Although the difference is very small in terms of percentage recovered, the recovery of 30-300 μm foil briquettes increases with bulk density. For all these foils, briquette of bulk density 2.41-2.54 g/cm^3 led to maximum (100 %) recovery (including for all repetitions). The recovery of briquettes with bulk density 0.86-2.12 g/cm^3 were all slightly below 100 % and also significantly similar within all thicknesses (30-300 μm). This is related to oxidation results, i.e. the later density range differ (uniaxial pressing) from the former (HPT pressings). The results presented in Figure 4.33 and Figure 4.34 seems to be dependent on the specific surface area and the cohesive mass of chips. This further evaluated in the section Discussion.

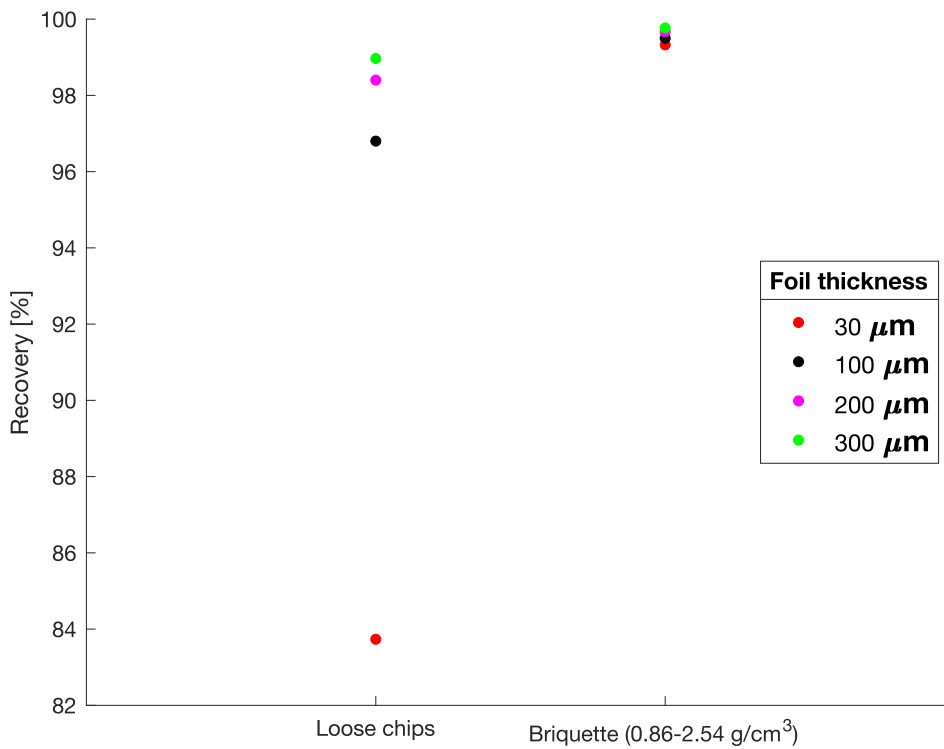
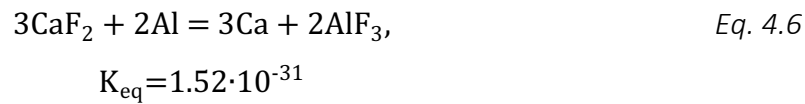
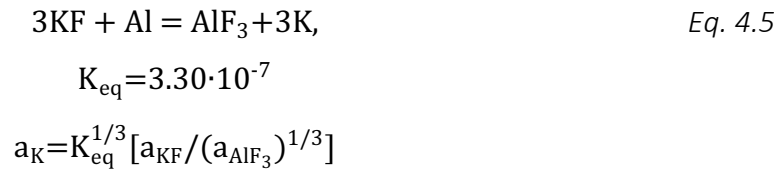
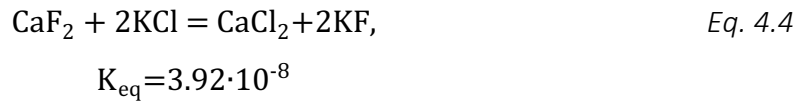
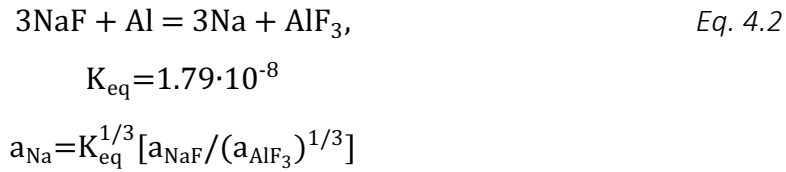
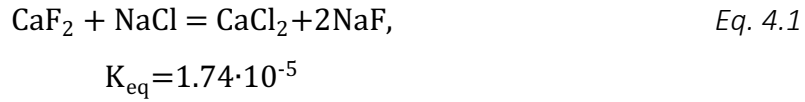


Figure 4.34. Recovery of heat-treated briquettes of 30-300 μm in the last experimental setup.

Displacement reactions

As described in [86], as the activity increases of the surface active elements Na and K, the fractional surface coverage and adsorption at the interface increase. This in turn decrease the interfacial tension between Al and salt and coalescence is favored. At 800 °C it expected that the following displacement reactions (Eq. 4.1-4.6) occur between the salt and Al (with equilibrium constants at 1100 K calculated from JANAF thermochemical tables) [103].



Similar to [86], the activity of Na and K is governed by Eq. 4.2 and Eq. 4.5. Similar to fluoride additive LiF, it is also possible that interfacial tension is reduced by interface adsorption of Ca. As a consequence, it is possible that Na, K and Ca is found in the Al metal phase and Al loss in the form of AlF_3 . As observed by the equilibrium constants in (Eq. 4.1, Eq. 4.4 and Eq. 4.6) the activity of fluoride and calcium is governed by the concentration of NaCl and KCl rather than Al.

Briquette floating behavior

The floating behavior of the briquette was observed as the briquette was charged in molten salt flux at 800 °C in a crucible slightly larger than 4 cm in diameter. Briquettes of bulk density

1.5 g/cm³ and below floated and those with higher bulk density sunk, as illustrated in Figure 4.35 below.

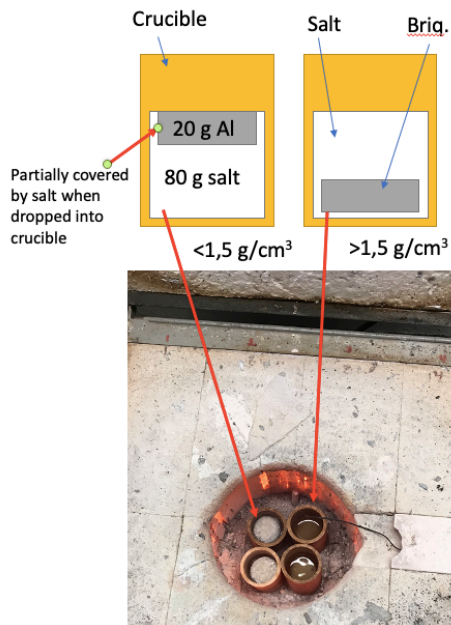


Figure 4.35. Illustration of briquette floating (left) and sinking (right).

4.5.4. Recovery of briquettes without the use of salt flux

Briquettes of all foil thicknesses with bulk density of 1.3-1.4, 2.1 and 2.4-2.6 g/cm³ were heated in the muffle furnace at 800 °C for 30 minutes. The crucibles were covered in boron nitride to avoid Al sticking to the crucible material. The temperature of the furnace atmosphere was measured with a thermocouple and fluctuated between 795-820 °C. Only briquettes with bulk densities in the range 2.4-2.6 g/cm³ melted and were transformed into a solid Al body upon cooling. Briquettes with lower bulk densities did not melt properly and i.e. oxidized and disintegrated during cleaning. For all melting trials, parts of the boron nitride were detached from the crucible walls and deposited on the Al piece. The melting time for these briquettes was 15-18 minutes.

After the Al had cooled, been washed and treated in ultra-sonic bath, the mass of the piece was measured. The mass after melting and washing increased with increased bulk density of the briquette. The main explanation for this is solid Al disintegrating upon washing in warm water.

Briquettes of bulk density 1.3-1.4 g/cm³ did not coalesce into a solid Al body. The compacted structure of chips was unchanged, clearly visible and oxidized. Briquettes of bulk density 2.1 g/cm³ melted completely or partly melted depending on foil thickness. The briquettes of the two thinnest foil materials melted into an Al body. However, the body was very fragile and disintegrated during washing, as seen in Figure 4.36 below.



*Figure 4.36. Unsuccessful coalescence of briquettes with approximate bulk density 2.1 g/cm³.
15 and 30 μm , from left to right.*

The briquettes of 100, 200 and 300 μm on the contrary did not melt into a full Al body. Instead, as seen Figure 4.37 below, the briquettes partially melted, where the original chips are still visible. However, these were not as fragile as the corresponding briquettes of 15 and 30 μm .



Figure 4.37. Unsuccessful coalescence of briquettes with approximate bulk density 2.1 g/cm^3 .
100, 200 and 300 μm , from left to right.

Briquettes of bulk density $2.4\text{-}2.6 \text{ g/cm}^3$ successfully melted into a solid Al body, as seen in Figure 4.38 below. The chips which the briquettes consisted of, coalesced.



Figure 4.38. Briquettes of 15, 100 and 200 μm , with bulk density 2.6, 2.5 and 2.5 g/cm^3 , respectively.

Density of briquette melted without salt

The pycnometer was used to measure the density of briquettes melted without salt flux. The density of briquettes melted without salt were measured to give indication on the porosity level and amount of oxide produced due to elevated temperatures. These densities are compared to the real density of the foil material. Higher porosity level is expected to have a reducing

effect on the measured density. Oxides, on the contrary, is expected to lead to higher measured density owing to higher inherent density of alumina.

The two household foils (of thickness 15 and 30 μm) are from the alloy series 1xxx. With respect to measured composition with XRF gun, the compositions are much similar to aluminum alloy 1100. The real density of this material is 2.710 g/cm^3 . The density of the three thickest foils (alloy 8006) is 2.74 g/cm^3 . In Figure 4.39 below, the measured density relative to the real density (%) is plotted against bulk density (achieved from compaction).

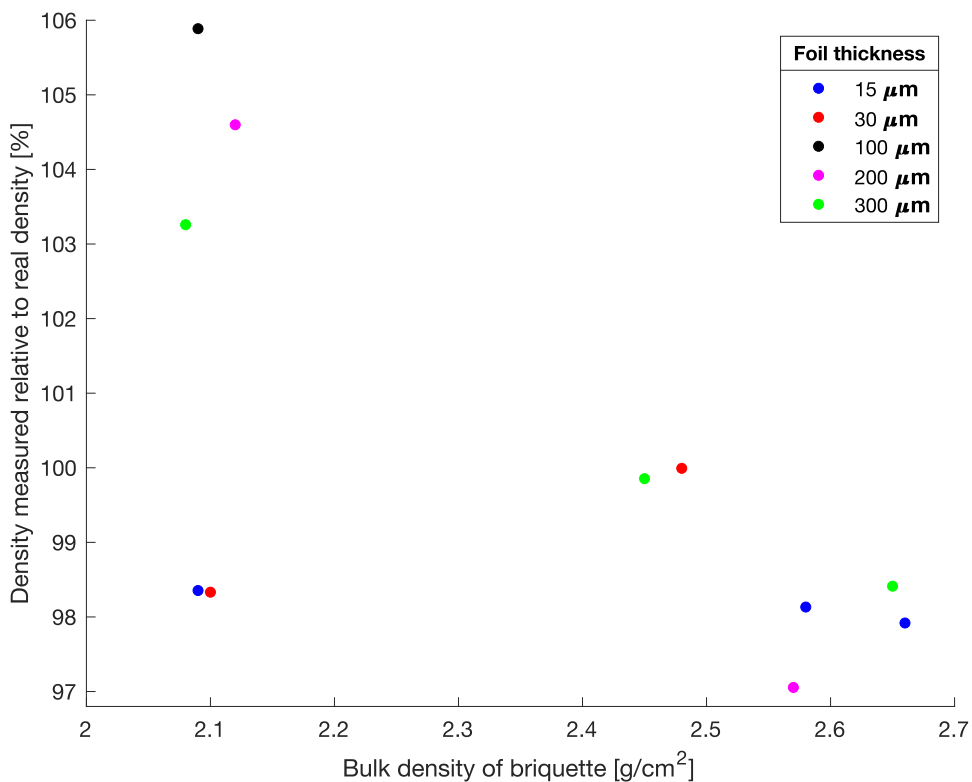


Figure 4.39. Density of melted briquette compared between briquettes of different thickness and compaction.

The melted briquettes of 15 μm is relatively constant with bulk density. Before melting, the measured porosity with x-ray tomography differed only approx. 5 % between approx. bulk density 2.1 and 2.5 g/cm^3 . Upon melting it can be assumed that this difference is reduced as

the chips inside the briquette coalesce. A similar porosity between these means that the results in the graph must also depend on the degree the briquettes are oxidized during melting. Referring to the oxidation results of these bulk densities, the mass increase differed significantly from heat treatment at 650 °C for 1 h. Therefore at 800 °C for 30 min, the 2.1 g/cm³ is expected to oxidize significantly more than 2.5 g/cm³. This led to an increased value of density for the briquette of bulk density 2.1 g/cm³ and should be lower if oxidation was avoided.

In general, the differences in percentage of real density is decreased between thicknesses as the bulk density is increased. The density difference between the two thinnest foil and the three thickest foil is relatively large at bulk density 2.1 g/cm³.

The five to ten volume measurements lead to density standard deviation of 0.002 to 0.01 g/cm³. Because the boron nitride attached to the Al could not be completely removed by water, the Al pieces were treatment in ultra-sonic bath. Despite treatment in ultra-sonic bath, some boron nitride was seen stuck on the Al. With boron nitride attached, which has lower density than Al, leads to a measured density that is lower than actual density.

5. Discussion

Overall, the results, as shown in section 4 (Results), indicate that mainly two properties of the chips and briquettes influence recovery, namely (i) specific surface area exposed to the environment and (ii) the mass allocation of chips. The results show that the recovery of thin uncoated foil in salt flux increases with increased compaction. It is therefore expected that by compaction, the specific surface area (including micro roughness) is reduced and that partial solid-state coalescence (due to compaction) increases the cohesive mass of the chips. The relationship between compaction, foil thickness and recovery may be different for other salt flux compositions than the one used in the current study (68.6NaCl:29.4KCl:2CaF₂). The results indicate that a recovery-model dependent on salt composition and surface area of scrap can be developed. This is thoroughly discussed in the following sections and linked to theories presented in other research.

5.1. Shredding behavior of different foil thicknesses

There are particularly two errors that may influence the size and size distribution of chips produced by shredding. Ideally, the chips photographed are flat, exposing their whole surface towards the camera and the height is equal to the thickness of the foil. Unfortunately, the size and shape obtained from image processing is affected by some degree of deformation of individual chips. Deformation degree is expected to relate to the settling volume of the chips and average mass per chip (Figure 4.12). Flat chips have less settling volume than well deformed chips. As a result, although the projected size of chips are the same for all foils, thinner chips that are more deformed have relatively larger surface area.

According to the theory of coalescence Kamp et al. [82] the approach that “contact” between droplets influence the probability of coalescence. This is considered an important factor regarding the melting results of free chips as the melt was not agitated. With decreased thickness of the chips, the settling volume i.e. contact between chips also decreases.

However, this error only concerns comparison between chips of different thickness and not comparison between briquettes. For briquettes, with respect to bulk density and porosity measurements it is assumed that the allocation of chips is very equal between briquettes of

different foil thickness, given that their bulk density is the same. In spite of this, recovery decreased with decreased thickness. This confirms that other factors than density and porosity influence the recovery in salt flux.

In Table 4.1, the influence of size and shape on mass per chip was investigated by dividing with area and aspect ratio (shape). By that, the influence of area and shape is eliminated. Yet, values in row three and four show that 30 μm foil is closer to 100 μm than 15 μm foil. The same relationship holds for settling volume. The relatively large mass per chip of 30 μm means that less volume is occupied. This is in accordance with the measured recovery as the percentage recovery for 30 μm foil despite its thickness was similar to 100 μm foil.

The thickness of chips does not have a linear relationship with mass of the chips due to deformation from shredding. The average mass of 15 μm chips are half the mass of 30 and 100 μm . The relative increase in thickness do not correspond the relative increase in mass of chips, with exception of 15 and 30 μm . Thinner chips relative to its mass deform much more than thicker chips. For instance, chips from 200 μm foil is not twice as heavy as 100 μm . 15 and 30 μm may be deformed similar, hence their mass difference corresponds to their thickness difference, which can be studied in row three and four in Table 4.1. Also, the mass difference between 100-300 μm is relative to their thicknesses small because deformation decreases with thickness. With increased compaction, the influence of mass and deformation degree of chips is diminishing for different thicknesses, hence the recovery is more equal.

5.2. Compaction of chips to briquettes

5.2.1. Uniaxial pressing

The bulk density of briquette increases with increased applied uniaxial compressive stress, however, the rate of the increase is diminishing as compressive stress increases. This relationship was also reported by Mashhadi et al. [44], Puga et al. [35] and Fogagnolo et al. [45] and in agreement with theory on plastic deformation from compression. However, the bulk density-stress relationship is very different between studies and the results in this thesis. A thorough comparison is not possible due to lack of detailed descriptions on their compaction techniques. To obtain the same bulk density as in other studies, the stress needed was relatively

low in experiments for this thesis. The main parameters that can influence the results are mechanical properties of the Al alloy, size of chips, crucible diameter and amount of lubricant used.

For compressions at the low force used in the current work, it was discovered that the pre-compaction of chips i.e. as the chips were carefully hammered into the crucible, was the main reason for deviating bulk density between repetitions. Because of the difficulty to be consistent, this error is reduced by increased number of repetitions. For higher compaction approximately $>1.1 \text{ g/cm}^3$, this error is avoided.

5.2.2. High Pressure Torsion (HPT) and with heat

The results indicate that bulk density similar to real density of the material can be achieved with the pressing technique HPT with relatively low axial applied stress. This is in agreement with theory presented by Wan et al. [39]. The torsion (or twisting) of the briquette due to applied torque was not measured. To calculate the torsion, the angle of twist must be measured. One method to measure the angle is by placing a vertical object of suitable length among the chips prior to compaction.

Applied torque as a supplement to uniaxial pressing (HPT) increases bulk density of the briquette by 29, 24 and 37 % for 15, 30 and 300 μm , respectively. Correspondingly, for HPT at 450 °C, the increase was 33, 32 and 47 %, respectively. The numbers show that torque effectively can reduce bulk density of aluminium chips. 97-98 % of the foil material's real density was achieved with HPT at 450 °C. In addition to increased bulk density, the surface roughness and surface area was significantly reduced (although not measured) by HPT, and with heat, which is beneficial for recovery, as is discussed in the section Al recovery of melted chips and briquettes.

5.2.3. Compaction of oxidized chips

To investigate the effect of oxidation on recovery, chips of 15 μm foil were oxidized prior to compaction. Subsequently, the chips were compressed with HPT at 450 °C to bulk density 2.62 g/cm^3 i.e. 97 % of real density. Although the weight gain was high (approx. 1 %), the mean

recovery was 98.5 %. This indicate that the oxide layer can be significantly ruptured and dispersed in the briquette and the chips can partially solid-state coalescence before melted in salt flux. In addition, the specific surface area is reduced.

5.3. Briquette properties

5.3.1. Porosity and surface area

Although porosity measurements with x-ray were few, the data indicate that “macro” porosity (here approx. >tenths of a micron) somewhat increases with thickness of foil, for a given bulk density. Analysis of whole briquettes showed a resolution insufficient for analysis of “micro” porosity (here approx. <tenths of a micron). In general, for a given bulk density, the difference in porosity between foil thicknesses is low. As “micro” roughness was found to be higher for thinner foils by measurements in optical 3D-microscope, the recovery difference between the foil thicknesses may be more related to micro specific surface area/roughness than macro specific surface area/roughness and porosity.

Although the measured (macro) porosity increased with thickness of foil, it is possible that thicker foils compressed have smaller specific surface area in the interior of the briquette. In Figure 5.1 below, this is illustrated.

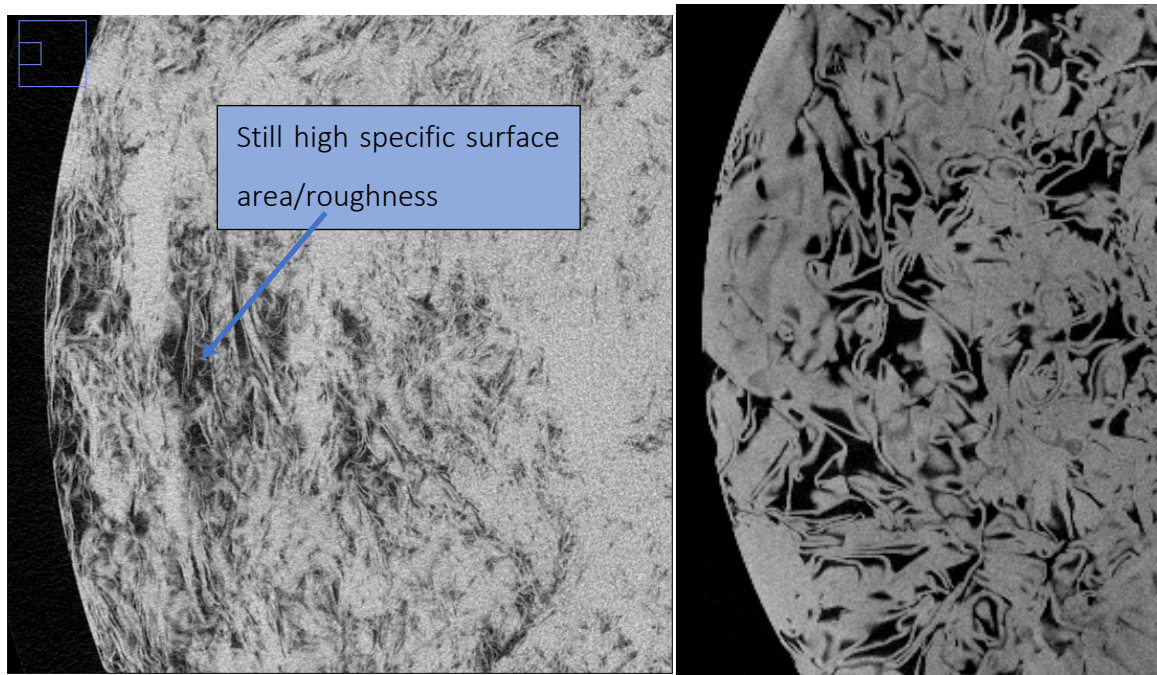


Figure 5.1. Briquettes of 15 μm foil (left) and 100 μm foil (right), both with bulk density 2.09 g/cm^3 .

The difference in porosity between 15 and 30 μm foil at 0.9 g/cm^3 is not significant. The porosity of briquettes with bulk density 1.1 g/cm^3 showed a larger difference between the two foils. The validity of this measurement is higher because the briquettes were cut prior to analysis, hence the resolution was higher. Unfortunately, briquettes of lower density were sensitive to cutting, which could not be performed without disintegrating the briquette.

For uniaxially compressed briquettes of density 2-2.1 g/cm^3 , the difference in mean porosity between 15 and 100/300 μm foil is 8 %, which somewhat can be visualized in Figure 5.1 above. Referring to the oxidation study, it is likely that the specific surface area/roughness of the interior is significantly larger for 15 μm foil than 100/300 μm foil. This is the most plausible reason for higher oxidation and lower recovery of the former foil.

The effect of foil thickness on porosity is diminished by increased compression and/or by HPT. It is possible that the shear stress generated by torque equalize porosity differences that would otherwise arise from uniaxial pressing.

Furthermore, by referring to the oxidation study, it is seen that porosity lower than 10 % is needed if oxidation should be significantly reduced. A critical porosity and density value is exceeded for oxygen to no longer meet the interior of the briquette during heat treatment, hence only the surface area that is visible to the atmosphere can oxidize. This critical value of abrupt decrease in oxidation can be determined by studying briquettes in the bulk density range 2.06-2.41 g/cm³.

The standard deviation was largest for briquettes compressed with torque. The relatively large standard deviation is caused by irregular and cracked surfaces as shown in Figure 4.24. The size of surface cracks varied significantly between briquettes compacted by HPT. The standard deviation bars are smaller for x-ray samples that were cut to a smaller piece before analysis. This is a consequence of higher resolution compared to analysis of whole briquettes.

In Figure 4.23 the data of 15 μm indicate that the relationship between porosity and bulk density is approximately linear above excluding the porosity at approx. 0.9 g/cm³ i.e. between 1.1-2.5 g/cm³. Although there is less data for 30 μm foils, with respect to the three porosity measurements, the relationship is approximately linear as well. Recovery can therefore be seen to be equally proportional to porosity as for bulk density. However, the “projected” porosity calculated from the measured bulk density is a factor larger than the porosity measured by x-ray tomography. The value of this coefficient can be determined by more measurements with x-ray tomography, including the thicker foils.

5.4. Oxidation due to heat treatment

For the bulk density range 0.86-2.12 g/cm³, the oxidation for a given thickness is relatively unchanged with respect to bulk density. The likely explanation is that oxygen in the air can pass through the interior of the briquette, hence react with the majority of the surface area that is related to the chip morphology. For briquettes of 2.41 g/cm³ and above, the briquette body is mostly closed i.e. the surface area in pores are so-called close pores, and reaction with oxygen is eliminated. This is illustrated in Figure 5.2 below for the 100 μm foil.

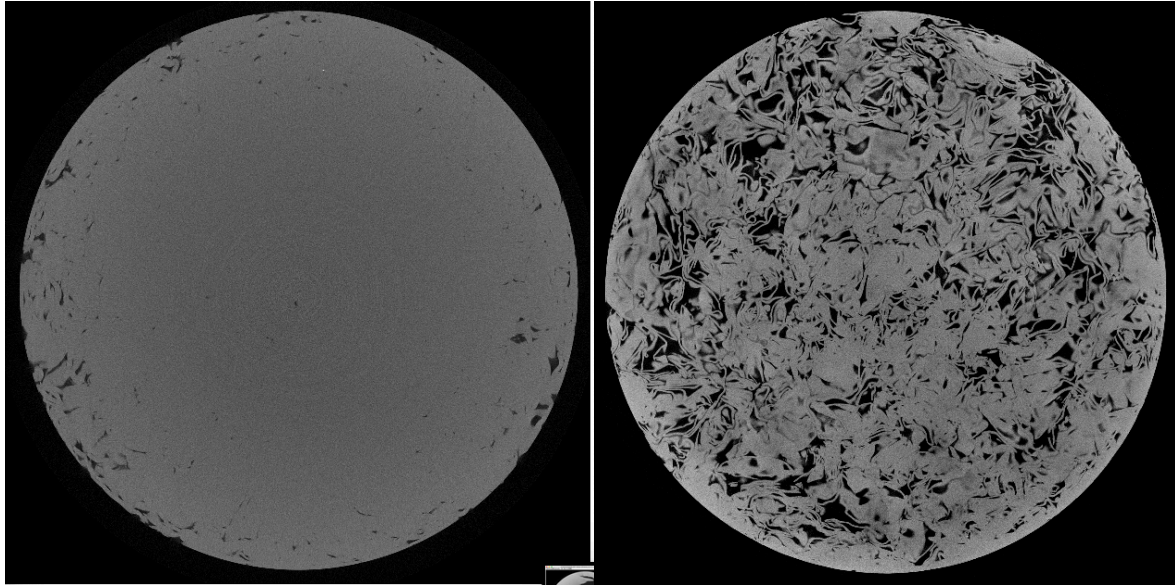


Figure 5.2. Briquettes of 100 μm foil with bulk density 2.48 (left) and 2.09 g/cm^3 (right).

As for chips, the briquettes of thinner foil material have a higher specific weight gain/oxidation than thicker foils. It is therefore expected that for decreased thickness of foil, the specific surface area and micro roughness increase. The effect of (micro) roughness on oxidation is in accordance with Impey [100] and earlier research. With respect to the average mass per chip measured (Figure 4.12), for a given mass the number of chips of 15 μm foil is approximately twice the number of chips of 30 and 100 μm foils. The difference in micro roughness of the foil may originate from rolling. Indications on this can be seen in Figure 4.22.

For bulk density 2.41-2.54 g/cm^3 of foil thicknesses 15, 100 and 300 μm , the porosities were 4 % and 4/6 % and the recovery were 98 % and 100/100 %, respectively. Between 2.1 and 2.41 g/cm^3 the briquette transforms from an open structure to a closed structure. This drastic decrease in specific surface area results in significant less oxidation compared to less dense briquettes. This is in agreement with other studies on the relationship between oxidation and surface area [46-53]. The difference between thicknesses is also reduced at this high level of compaction. The explanation of reduced surface area due to compaction is strengthened by the fact that the difference in weight gain between 2.1 to 2.5 g/cm^3 is most significant for 15 μm .

For heat treated chips oxidation decreases with increasing thickness of foil. Assuming that the size and size distributions presented (Figure 4.5) are valid, after sieving, the size of chips are the same for all foils. However, the average chip mass measured indicate that the mass increases with thickness (although not as much as the thickness increases). Consequently, the specific surface area must increase with decreasing thickness of foil. In other words, for a given mass (20 g in experiments), the number of chips required are higher as the thickness of foil decreases.

Another reason may be that thinner foils have higher micro roughness. For chips, the deformation degree may also influence the oxidation behavior. Deformation can lead to increased surface roughness. Thinner chips are more deformed and therefore the surface area is larger than for thicker chips.

The roughness of briquettes was analyzed by the roughness parameters sdq and sdr . The values of these presented in Table 4.3 indicate that briquettes of thicker foils are rougher. However, the height profiles in Figure 4.21 and Figure 4.22 show more frequent height changes for thinner foils i.e. micro roughness. Although this micro roughness is not quantified, increased micro roughness of thinner foil may be an influencing factor. The roughness quantified by [99] showed that ductility may relate to distortion and hence more roughness. This could be related to deformation degree, where thin foil which is more deformed after shredding also would result in rougher surface.

The macro roughness measured and presented in Table 4.3 clearly cannot relate to oxidation. The standard deviation can be reduced by utilizing a furnace of controlled atmosphere e.g. TGA analysis for sheet material of predetermined surface area.

5.5. Al recovery of melted chips and briquettes

The increased recovery by compaction increased the most for less thick foil. For all foil thicknesses, the largest difference in recovery was between free chips and briquettes in general. However, the recovery increased significantly with increased compaction for the 15 μm foil. The same effect, although to an almost negligible amount, was observed for foils of

thickness 30-300 μm . As the bulk density of the briquette increased, it was seen that the difference in recovery between foil thicknesses diminish. Put differently, regardless of foil thickness, near complete recovery can be achieved by extensive compaction of Al.

In general, previous theories describing oxide layer removal and coalescence of Al droplets can be projected on the results obtained for this thesis. The recovery in salt flux is increased by compaction owing to mainly (i) reduced specific surface area exposed to salt flux and (ii) increased partially “solid-state coalesced” chips. In (i), the concentration of surface-active elements (per area unit) is high, which lead to sufficient oxide rupture to promote coalescence. If the concentration is insufficient, Al “pearls” are dispersed in the salt. In (ii), partial coalescence means increased cluster of mass, hence the thermal expansion is more significant to promote oxide rupture and further coalescence of Al. Melting of compacted briquette without the use of salt flux strengthens the theory of (ii) and that (i) may be the most important factor for coalescence and recovery in salt containing fluoride.

In Figure 5.3 below the coalescence of thin and thick chips are illustrated. To illustrate that chips of thicker foils have less specific surface area and higher mass, the number of chips drawn are fewer. As illustrated, thinner chips coalesce less, hence lower recovery. For free chips, regardless of foil thickness, the process of coalescence can be described as:

- (1) Free chips are heated and the Al transforms to liquid phase and thermal expansion occur. Simultaneously, due to the high activity of surface-active elements (Na, K and C) they attack and weaken the oxide layer. As a result, displacement reactions occur.
- (2) The activity of surface-active elements cause change in interfacial tension between salt and Al. This result oxide rupture and thermal expansion can proceed which means that the initial chip shape change to spherical shape to reduce free energy. A sufficiently ruptured oxide layer promotes coalescence of drops that have collided, which reduce the free energy in the system even further. As a consequence, in the contact between Al and salt, Al is lost in the form of AlF_3 dispersed in the salt.
- (3) The oxide layer is more ruptured or completely stripped due to expansion and shape change. Reactions between salt and Al can proceed.

For decreased thickness of foil, the following occurs: Because a charge of thinner chips has larger specific surface area, the concentration of surface-active elements (Na, K and Ca) is lower per area unit of interface. As a consequence, the weakening in (2) of the oxide layer is less significant. Simultaneously, because thin individual chips have less mass to expand during phase change and heating, the induced stress on the oxide layer is less. The activity and expansion were, however, enough to cause oxide layer rupture to allow spherical transformation (regardless of thickness). The following relationships hold:

$$m_{tot,thin} = m_{tot,thick}$$

$$m_{chip,thin} < m_{chip,thick}$$

$$A_{free,thin} > A_{free,thick}$$

where A_{free} is the specific surface area of the chips melted (including micro roughness), m_{tot} is the total mass of the charge and m_{chip} represent the mass of an individual free chip.

Because the coalescence is relatively slow for free chips, maintained high specific surface area increases the probability of displacement reactions (Eq. 4.1-4.6) between fluoride and aluminum resulting in loss, particular in the form of AlF_3 . In general, results indicate that the largest contribution to Al loss is due to visible “pearls” that disperse in the salt. As illustrated, chips of thicker foils coalesce to a higher degree than chips of thinner foils.

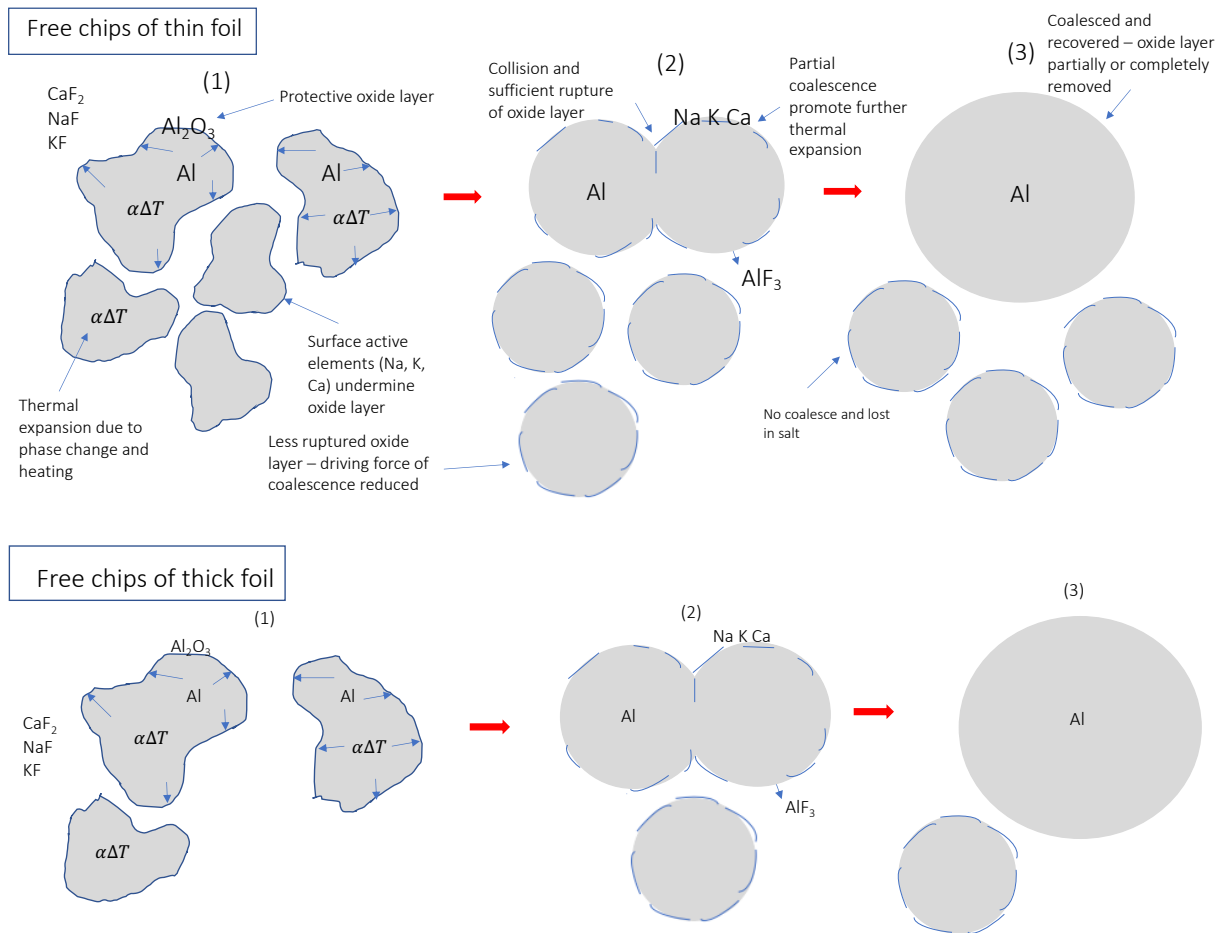


Figure 5.3. Coalescence mechanism of thin and thick chips illustrated.

In Figure 5.4 below, the coalescence of compacted chips (as in briquettes) is illustrated. In difference from chips, the partial coalescence and oxide rupture due to compaction is depicted. Also, the coalescence occurs in two steps instead of three i.e. spherical transformation before complete coalescence is avoided. The coalescence process can be described as:

- (1) Partial “solid-state coalesced” chips (due to compaction) are exposed to surface active elements that weaken the oxide layer and reduce interfacial tension between the salt and Al. Due to partial coalescence, thermal expansion is favored, which simultaneously with surface active elements cause rupture of the oxide layer. Spherical transformation can take place. Given a certain bulk density, the concentration of surface active elements per area unit to reduce interfacial tension is lower for thinner foils that have higher specific surface area and higher micro roughness.

- (2) The oxide layer is more ruptured or completely stripped due to expansion and shape change. Reactions between salt and Al can proceed.

The surface area of thin chips is exaggerated to illustrate the effect of high surface area and roughness. Furthermore, for the same mass, four thinner chips correspond to two thicker chips (which was the case for 15 μm foil vs. 30 and 100 μm foils). Because partial coalescence occurs by compaction, the mass of clustered Al is increased. This can also be expressed by the following relationships:

$$\begin{aligned}m_{tot,thin} &= m_{tot,thick} \\m_{compacted\ chips} &> m_{free\ chips} \\A_{compacted,thin} &> A_{compacted,thick}\end{aligned}$$

where $A_{compacted}$ is the specific surface area of the briquette melted (including micro roughness) for a given bulk density, and $m_{compacted}$ represent the mass partially coalesced chips (due to compaction). For the same material, larger mass corresponds to larger volume, hence the change in volume due to heating and melting is also higher for compacted chips than for free chips. This in turn means higher probability of coalescence.

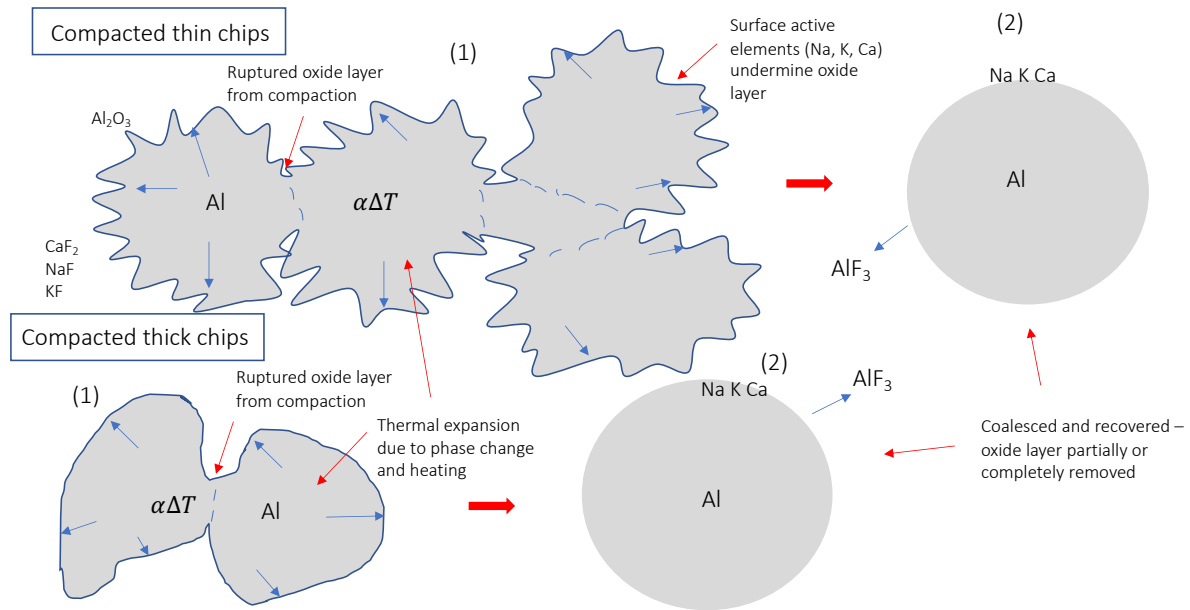


Figure 5.4. Coalescence mechanism of compacted thin and thick chips.

The oxidation study indicates that only after very high bulk density ($>2.12 \text{ g/cm}^3$) is obtained, the specific surface area (hence oxidation) is reduced. As bulk density of briquettes gets closer to the real density of the material, the difference in specific surface area and recovery between thick and thin foils diminish. As a result of very high compaction, the following relationship hold instead:

$$A_{\text{compacted,thin}} = A_{\text{compacted,thick}}$$

where $A_{\text{compacted,thin/thick}}$ are specific surface area of briquettes of thin and thick foils. In addition to more similar specific surface area, the extent of partial coalescence (equal porosity) between foil thicknesses also becomes more similar.

5.5.1. Effect of surface area on recovery

There are two suitable indications on an existing relationship between specific surface area exposed to salt flux and percentage recovery. Firstly, the chips of thinner foils led to less recovery than for thicker foils. The sizes of the chips are approximately the same for all foils. Interestingly, the recovery difference between foil chips is similar to the average mass difference between the foil thicknesses. Specifically, the extent of the increase of recovery/mass with respect to thickness diminish as the thickness increases.

Secondly, another indication is the difference in recovery between briquettes of same bulk density but consisting of different foil thicknesses. Similar to the explanation presented, the decrease in recovery is exponential with decreased thickness of foil. This is in agreement with results presented by Rossel [58], Stewart et al. [77] and Xiao and Reuter [80]. The size effect in their studies can be related to the thickness effect in this study.

Surface measurements of briquettes showed that surface area increased with thickness of foil. However, height profiles indicated more micro roughness of thinner foils (Figure 4.22). Therefore, it is expected that micro roughness is not taken into account in the optical 3D-microscopy measurements. Micro roughness may be related distortion and deformation [99], which is more likely for thinner foils as a result of shredding. Micro-roughness may also be a feature of the initial, un-shredded foil owing to different rolling techniques.

Although chips and briquettes of thinner foils oxidized more, the oxide layer seem to be ruptured enough for spherical transformation of small “pearls” also took place, as seen Figure 5.5 below:

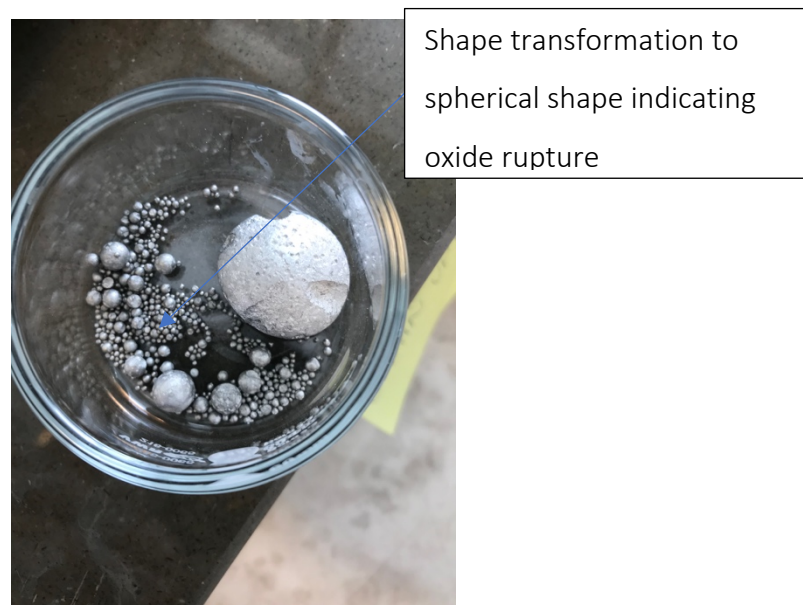


Figure 5.5. Coalesced Al and spherical “pearls” recovered.

In this discussion, there are two mechanisms presented in which recovery is reduced with increased specific surface area. Firstly, the activity of fluoride addition does not lead to significant change in interfacial tension between salt and Al. As a result, the oxide layer is still intact to protect from fusion of Al. The validity of this explanation increases as the fluoride addition is small or absent. The fluoride addition of 2 wt% is considered small in this study due to lack of coalescence for thinner foils, as seen in Figure 5.5 above.

In the first mechanism, the effect of surface area exposed to salt flux on recovery depend on the concentration of surface active elements per area unit. By that, larger specific surface area means that less concentration per unit area of Na and K is present at the interface, hence the change in interfacial tension between salt and Al is low. As a consequence, the demolition of the oxide layer (and coalescence) is less effective. However, it might be seen that the oxide is ruptured to a low extent and the large surface area due to lack of coalescence facilitate dispersion of Al in the molten salt. As seen in Figure 5.5 above, many spherical pearls did not coalesce. The transformation to spherical shape occurs due to the activity of surface active elements and thermal expansion weakening the protective oxide layer. However, the activity of the elements is insufficient to cause enough reduction in interfacial tension in order for Al to fuse.

The second mechanism is most likely to occur as the addition of fluoride (hence the activity) increases. In this case displacement reactions is much more significant and Al is dispersed in the molten salt flux. The effect of this mechanism is less compared to the former mechanism in this study. Indications on this mechanism is good coalescence but high metal loss. However, it is also possible that both mechanisms cooperate, i.e. oxide layer rupture is insufficient for coalescence but sufficient for displacement reaction to occur. This is discussed more thoroughly below.

The second mechanism is seen present in this study due to the following results. The total recovery (including "pearls") was proportional to coalesced recovery. The Al loss obtained from total recovery indicate loss of Al particles smaller than 0.8 mm (sieve), possibly by the formation of AlF_3 . The total recovery of 15 μm chips and briquettes decreased with decreased compaction

(as for coalesced recovery). For chips and briquettes of 30 μm foil, metal was lost also in terms of the total recovery. For foils of thickness 100-300 μm , although complete coalescence occurred (without any visible pearls) the metal loss was 1-2 wt% (decreasing with thickness) and zero, for chips and briquettes, respectively.

Roy and Sahai [85] reported metal loss of 0.45 % and 3.55 % for addition of 5 wt% CaF_2 and NaF , respectively. The higher metal loss is explained by higher activity of surface active elements due to displacement reactions. The higher activity results in better coalescence due to more decreased interfacial tension between salt and Al, but also metal loss due to formation of AlF_3 dispersed in the molten salt.

In their experiments, the surface area exposed to the molten salt has less of an influence on metal loss. Droplets were held in the molten salt flux for 6 hours. However, for addition of the fluoride compounds (CaF_2 , NF , KF , Na_3AlF_6 , LiF and MgF_2) with exception of AlF_3 , the Al coalesced in the matter of minutes. Because all Al droplets coalesced long before 6 hours, the surface area exposed to the molten salt is expected to be similar for all fluoride additions. The metal loss measured by Roy and Sahai was not considered to be influenced by surface area but only by the activity of the surface active elements. This is in contrast to experiments for this thesis, where the surface area exposed to salt varied significantly depending on degree of compaction. Neither the size, thickness, nor the surface area of the Al chips was reported by the authors, making a metal loss comparison difficult.

It is likely that 5 wt% CaF_2 is much higher addition than necessary to achieve coalescence. Milke et al. [98] stated that addition of 0.5 wt% fluoride is enough for coalescence and that higher additions resulted in higher metal loss. This information supports the explanation that Roy and Sahai observed metal loss possibly due to relatively high activity of surface active elements. However, results in this thesis indicate that the specific surface area must be included in the model when determining the addition of fluoride content for maximum recovery.

Although specific surface area is not always discussed in available research, size, thickness, thermal expansion and compaction is mentioned, which can all be related to surface area. The diameter and size (hence the surface area) of the chip or particle melted according to Kamp et

al. and Xiao and Reuter. In addition, Paulitsch et al. [78] also reported increased recovery by compaction (hence surface area) before melting. Unfortunately, in the latter reference, more detailed information cannot be obtained due to lack of translation. Thermal expansion which is related to mass and volume (and therefore also surface area) influence oxide removal and coalescence according to Roy and Sahai. Compaction, hence reduced specific surface area generally led to increased recovery reported by Mashhadi et al. [44]. In general, it is misleading to compare individual numbers between the references mainly because of different process parameters. In experiments where Al is recovered in salt flux, it also seen that fluoride content influence the recovery according to Milke et al. It is proposed that recovery of scrap in salt flux should be discussed in terms of surface area and fluoride content rather than size and thickness in order to facilitate further research in this area.

In Figure 5.6 the increased recovery of thin scrap due to melting in salt flux can be seen. The Al loss is proposed to be higher melted in liquid Al because of surface oxidation and formation of dross, in contrast to protective salt flux.

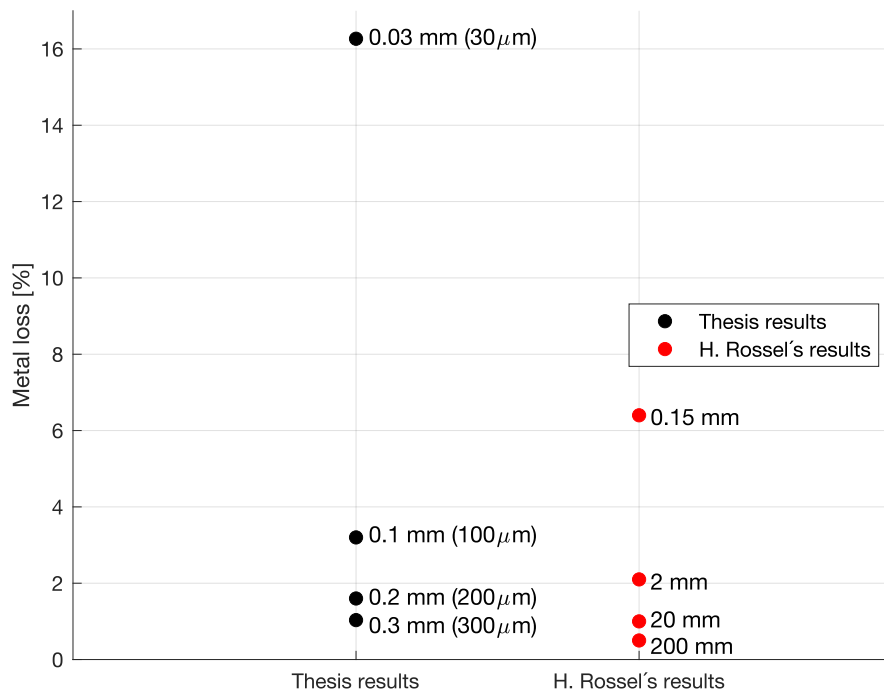


Figure 5.6. Metal loss compared to Rossel's metal loss showing the thickness of low-alloy scrap/foil melted at 800 °C adapted from [58].

5.5.2. Partial solid-state coalescence and the condition of oxide layer

The mass of individual Al chips is related to volume and thermal expansion. Thinner chips have less mass to expand, hence the induced stress on the surrounding oxide may not exceed the strength of the oxide to cause rupture. Due to partial coalescence of chips from compaction, this can be described as individual chips increasing their mass and volume. As a consequence, during melting the thermal expansion is larger for cluster of chips (inside briquettes) than that of chips. In addition, according to the oxidation study, the weight gain in terms of oxides is also increased with decreased thickness of foil. This in agreement with explanation proposed by Roy and Sahai [85, 86] and Ye and Sahai [90], as the mass, thermal expansion and the thickness of the oxide were found to have an impact on coalescence. Rossel [58] also reported that the oxide can withstand expanding liquid 20 times the weight of the oxide.

Oxidation affects recovery, especially for the 15 μm foil. Chips both oxidized the most and resulted in lowest recovery in salt flux. For briquettes the oxidation is same for medium-

compacted and decreased for high-compacted briquettes, which is different from recovery data as recovery steadily increased with compaction (for 15 μm foil). An explanation is that briquettes of medium-high density have chips that are more partially coalesced than medium-low density, although the surface area is the same (in terms of oxidation). This increases the validity of the conclusion that thermal expansion also plays a role in increased coalescence.

The theory presented by Roy and Sahai that is also based on earlier research on coalescence can be related to the research presented by Kahl and Fromm [61]. Kahl and Fromm reported that evaporation and incorporation of the elements Li, Na and Ca effects the strength of the oxide layer. This can be related to the description presented by Roy and Sahai where these elements act as surface-active elements reducing the interfacial tension and weakening the oxide layer.

The chips and briquettes were oxidized to simulate thicker oxide layer of coated scrap. According to Capuzzi et al. [28], the oxide thickness of coated scrap can be 10 times the thickness of uncoated scrap due to anodization process applied before coating. As seen in Figure 5.7, the shape of the recovered Al differs between briquettes of 300 μm foils heat treated at 800 °C 3.5 hours (left) and heat treated at 650 °C 1 hour (right). This occur although the weight gain for the briquette of 300 μm foil was relatively low i.e. 0.14 %. This indicate that the Al_2O_3 -phase could be a factor that impacts the coalescence of Al. This can be related to studies by Bartlett [51], Cochran and Sleppy [53] and Smeltzer [57] as the rate of phase transformation from amorphous to crystalline γ -phase is increased above the melting point of Al. This information may be relevant for melting multiple briquettes i.e. in semi-industrial or industrial scale.



Figure 5.7. Recovered briquette of 300 μm heat treated at 800 $^{\circ}\text{C}$ 3.5 hours (left) and arbitrary briquette recovered after heat treatment at 650 $^{\circ}\text{C}$ 1 hour (right).

Roy and Sahai also reported that the thicker oxide layer due to the formation of MgO prevent coalescence. The oxide growth owing to significant Mg alloying content is in agreement with many other oxidation studies. In this thesis it is uncertain if the oxide thickness between foils differed. The main reason for higher weight gain of thinner foils is possibly owing to larger surface area. It is possible that the explanation proposed by Roy and Sahai i.e. a thicker oxide layer prevents adsorption of Na and K and in turn the interfacial tension cannot be reduced must be considered in conjunction with specific surface area.

5.5.3. Fluoride addition and oxide rupture

As stated by Roy and Sahai [86], the more the interfacial tension between molten salt and aluminum is decreased, the better the ability to coalescence. The change in interfacial tension is related to displacement reactions at the surface of the Al droplet. More displacement reactions taking place also mean that the interfacial tension is more reduced. The displacement reactions shown in Eq. 4.2 and Eq. 4.5 (same as for Roy and Sahai) are expected to have occurred. Higher activity of Na and K lead to more formation of AlF_3 which is dispersed in the molten salt and therefore the Al loss is also higher.

The metal loss increases with decreased interfacial tension between metal and molten salt. Although, in this thesis, coalescence meant less metal loss/higher yield, the explanation of metal loss by Ye and Sahai [90] and Tenorio and Delgado [88] may be applied to the results in

this thesis. In these works, metal loss was most significant for fluoride compounds such as NaF that resulted in the most change in interfacial tension between salt and Al. For CaF₂ the metal loss reported was 0.45 %. The metal loss of samples that completely coalesced (without and small spherical Al particles), was similar to their reported metal loss for CaF₂ additions. This indicate that adsorption of surface active elements took place and Al likely dispersed in molten salt. As the displacement reactions show (Eq. 4.1-4.6), the metal loss is also dependent on the amount of fluoride compound, which is very low relative to other salt elements. To maximize recovery of Al, it is therefore expected that an optimum between good coalescence and low metal loss can be achieved by taking into account the surface area, fluoride compound and the amount of it.

According to Milke et al. [98], the solubility of CaF₂ in 70:30 NaCl-KCl at 800 °C is 4-6 wt%. This means that the 2 wt% additions used in experiments in this thesis is well below the solubility level. Theory indicate an optimum level of CaF₂ in order to maximize recovery. The content should be enough to promote oxide rupture (hence coalescence) and limited to avoid drastic decrease in interfacial tension, which lead to dispersion of Al in the salt. The viscosity may also be related to coalescence and recovery. Increased dispersion of removed oxide layer increase viscosity, which negatively affect further coalescence. Therefore, the negative effect of increased viscosity can be seen to increase with surface area (i.e. more oxide layers). Therefore, increased viscosity due to large specific surface area e.g. for chips (relative to briquettes) may also be a contributing factor to lower percentage recovery.

Unnecessarily high salt/Al ratio could increase metal loss according to Milke et al. (Figure 2.29). A salt-Al ratio of 1.5, which is small relative to the ratio in this thesis, showed a significant but small Al loss. Chips and briquettes required a salt-Al ratio of 7.5 and 4 (molten salt) to ensure the salt completely covered the salt. Although the ratio was much higher for chips than for briquettes, the recovery for chips was significantly lower. This indicate that specific surface area (which is much higher than for briquettes) can be a factor that has to be taken into account. Although the CaF₂ content increases with more salt, it is probable that the concentration and activity of surface active elements per unit of surface area Al is too low to promote sufficient

oxide rupture and coalescence. For briquettes that generally coalesced, it is possible that the CaF_2 -content can be reduced without reducing the Al recovery.

5.5.4. Coalescence dependency on state of the salt flux

According to Roy and Sahai [85] the oxide was stripped only when the salt (containing NaF) was molten. Given that coalescence can only occur subsequently to stripping of the oxide layer, the results in this thesis differed in the sense that coalescence was seen to occur although the salt flux was solid. The activity of surface active elements is high enough to result in displacement reactions although the salt flux is in solid phase. The difference in thermal expansion of Al chips in their study and briquette in this study may also be a factor.

In the pre-study of recovery in salt flux, the crucibles containing salt and Al were charged in 800 °C (i.e. salt had not been pre-melted). Although the salt flux was solid, coalescence of Al briquettes occurred after approximately 25 minutes. Because salt that is solid consist of coarser salt particles than in liquid state, it is expected that the interface area between salt and Al is less. This may influence the reaction rate between fluoride and aluminum i.e. affect the metal loss. With respect to this, the interface area between Al and salt may not only be reduced by compaction but also by recovering Al in solid salt flux.

5.5.5. Recovery and coalescence – the pre-study

The errors that mainly influence the percentage recovery are CaF_2 content and chip size variety. The CaF_2 consisted of much smaller powder particles than NaCl and KCl and could result in a heterogenous mix. In the pre-study of compaction, the slightly higher recovery obtained for briquette of bulk density 1.1 and 1.5 g/cm^3 and lower for 1.95 g/cm^3 may be attributed to different CaF_2 contents. The unusually low or high recovery concerned melting batches i.e. similar recoveries for all four crucibles in that batch. Another explanation could be the size of chips compressed. For compression of non-sieved chips, the probability is higher that the sample of chips compressed are much lower/higher than the mean size.

5.5.6. Other parameters that may influence recovery

The provided relationship between recovery and compaction may change by changing other parameters. As reported by many other researchers, the recovery will depend on time, temperature, composition of the alloy and salt flux, and agitation of the melt. These variables were held fixed in this thesis, hence the recovery may vary as these are different.

The kinetics were found important for coalescence according to Racunas [91]. They described three process steps: time for melting the chip, time for weakening the strength of the oxide and time for stripping significant fraction of the oxide layer. As the process time in experiments for this thesis was kept constant, the effect of time on recovery was not studied. Referring to the study by Ye and Sahai [90], the metal loss of pure Al was almost null with time. In addition, the effect of stirring is expected to increase the energy in the system, hence promote coalescence.

According to Gibbs free energy, increased temperature mean that the energy input is increased. Higher temperature in these experiments may therefore mean that more energy is provided to allow oxide removal, hence coalescence. The activity of surface active elements increases with increased temperature according to the relationship of Gibbs free energy and equilibrium constant. Increased activity of surface active elements Na and K leads to reduced interfacial tension between salt and Al, which promote oxide removal and coalescence. However, the increased activity of Na and K may have led to increased loss in the form of AlF_3 as seen by the results of total recovery of Al earlier described.

5.5.7. Melting without salt

The measured density of melted briquette without salt flux was plotted against bulk density. The measured density is expected to be influenced by oxidation (increases the density) and/or porosity (reduce the density). Not enough measurements were made to determine if the results are significant, but the measurements facilitate understanding of important properties of the recovered material, which can be of use for further studies.

The oxidation during melting can be related to the density of the thinner foils. Evidently, the 15 μm is in general more prone to oxidize than 30 μm and briquettes compressed with HPT to approx. 2.5 g/cm^3 oxidized significantly less than uniaxially compressed briquettes. At lower bulk density (2.1 g/cm^3), due to the large specific surface area (including micro roughness) the oxidation is more of a determining factor for increased measured density (with pycnometer) than the porosity that emerge from melting. On the contrary, at higher bulk density (2.5 g/cm^3), the porosity generated from melting decrease the measured density more than the oxidation increase it.

The density of 100-300 μm is high relative to other density measurements. An explanation for this could be that the coalescence of the chips was insufficient in these briquettes. The partial melting led to incomplete coalescence of the chips, as seen in Figure 3.19. Consequently, the melted briquette is more porous, and the helium is capable of passing through the briquette, hence density appears high. Differently for the 15 and 30 μm , the coalescence upon melting is much more evident, hence the helium cannot pass through. Instead, pores entrapped lead to a measured density that is lower than the real density.

Sufficient coalescence, hence proper melting occurs only for the briquettes with highest bulk density i.e. above 2.41 g/cm^3 . This concerns all foil thicknesses. However, the two thinnest foils compacted transformed into a piece with significantly smoother surface. Without salt flux, the previously described displacement reactions and change in interfacial tension are omitted. Instead, the partial solid-state coalescence and the condition of the oxide layer play a more important role.

Better coalescence of compacted chips than free chips are a possible consequence of increased partial solid-state coalescence (i.e. larger thermal expansion) and more ruptured and dispersed oxides, similar to the coalescence illustration (Figure 5.4). Unsuccessful melting of chips and low compacted briquettes indicate that the oxide layer in salt flux cannot by itself rupture as consequence of thermal expansion for these given thicknesses and sizes of chips. It is also likely that for a critical surface area of the Al, the oxide thickness growth is thick enough to resist

rupture from expanding liquid Al. By observation, applied torque effectively equalize surface irregularities, in particular the “macro” roughness.

Melting without salt flux, the aluminum oxide layer is allowed grow at the elevated temperature, which can prevent rupture of aluminum oxide and fusion of liquid aluminum. The growth of the oxide layer for the investigated material (almost pure Al) is relatively low for high-density briquettes and without any stirring of the melted Al to avoid increased oxygen exposure. Bulk density above 2.41 g/cm^3 i.e. 88-89 % of real density is enough for good melting behavior (coalescence).

5.5.8. Implication of the thesis results for the recovery of thin foil in the recycling industry

The implications of the discussed results for the recycling of aluminum foil are important. Assuming that the thickness of the foils used in packaging will continue to decrease, it is proposed that the recovery of uncoated foil can effectively be increased by extensive compaction in conjunction with suitable fluoride content added to the salt. A model of recovery dependent on specific surface area and fluoride content with respect to temperature and agitation can be developed.

6. Conclusion

In order to recycle thin Al scrap such as foil, material properties associated with recovery, in particular compaction, were investigated to facilitate further research aimed at more efficient industrial scrap processing.

Al foils from two different alloys (1100 and 8006) and five thicknesses (15, 30, 100, 200 and 300 μm) were shredded into chips, sieved and compacted to briquettes weighing 20 g by three methods (uniaxial, high pressure torsion (HPT) and HPT at 450 °C) obtaining a wide range of bulk densities. The briquette properties (bulk density, projected surface area and porosity) were determined. The impact of briquette properties and heat treatment on the recovery in salt flux was determined. The results of the different parts of the study can be summarized as:

6.1. Shredding behavior of different foil thicknesses

- Sieving was a suitable method to narrow the size distribution of shredded chips. Also, sieving led to a similar size distribution for different foil thicknesses and appeared near normal distribution.
- As a result of sieving, the maximum difference of mean chip size between foil thicknesses was 0.05 cm^2 . Sieving had little or no effect on the shape of chips.
- Although the apparent size of chips was similar for all foils, the mean mass of chips was not proportional to its thickness due to deformation of thinner chips.

6.2. Compaction of chips to briquettes

- Applied compressive stress and bulk density of briquette have a positive relationship and the rate of increase in bulk density is diminishing with increased stress.
- The maximum axial compressive stress of 398 MPa resulted in bulk density near the maximum density for all foil thicknesses.
- The maximum deviation of bulk density between foil thicknesses was 0.06 g/cm^3 by automatic compaction of sieved chips.
- The influence of foil thickness on bulk density is greater the more the chips are compressed.

- Torsion (HPT) as a supplement to uniaxial pressing alone increases bulk density of briquettes by 29, 24 and 37 % for 15, 30 and 300 μm foils, respectively. Correspondingly, HPT at 450 °C applied, the density increased by 33, 32 and 47 %, respectively.
- Applied torque combined with relatively low uniaxial compressive stress led to bulk density near the real density of the aluminum alloy. This compressive technique at 450 °C increased the bulk density even more, reaching a bulk density of 97-98 % of real density. Other pressing trials indicate that near real density can be achieved if uniaxial pressing higher than 100 MPa is applied.
- The highest bulk densities reached are similar to those needed for solid state recycling.

6.3. Briquette properties

- For briquettes compacted to 2.1 g/cm^3 and below, briquettes of thinner foils have in general less macro surface area and less porosity than corresponding thicker foils.
- HPT resulted in a porosity level of 4-6 % for 15, 100 and 300 μm foils.
- Indications of a linear relationship between porosity and bulk density was found. The values of projected porosity (relative to its real density) derived from bulk density measurements were systematically a factor higher than the porosity measured by x-ray tomography. The factor was lower for high-density briquettes due to less surface pores.

6.4. Oxidation of chips and briquettes due to heat treatment

Larger specific surface area and more porosity resulted in more oxidation owing to heat treatment in 650 °C for one hour. This is based on the following findings:

- Heat treatment of briquettes of 15 μm foil resulted in decreased recovery, compared untreated briquettes.
- For all thicknesses, chips oxidized more than the same chips compacted to a briquette due to larger specific surface area.
- For a given thickness of foil, the amount of oxidation was constant for briquettes with bulk densities 0.86 to 2.12 g/cm^3 . However, briquettes with bulk densities in the range 2.41 to 2.54 g/cm^3 with porosity 4-6 % oxidized significantly less than the former specified range. This correlate to the drastically reduced specific surface area and porosity.

- Chips or briquettes of thinner foil oxidized more due to higher specific surface area and micro roughness.

6.5. Al recovery of melted chips and briquettes

6.5.1. The effect of thickness on recovery of heat-treated briquettes and chips in salt flux

In general, previous theories describing oxide layer removal and coalescence can be projected on the results obtained for this thesis. Compaction led to near complete recovery of the input Al. The recovery in salt flux was increased by compaction owing to a combination of (i) reduced surface area exposed to salt flux and (ii) increased partial coalescence chips. In (i), the concentration of surface-active elements (per area unit) was high, which led to sufficient oxide rupture to promote coalescence. If the concentration is insufficient, Al “pearls” are dispersed in the salt. In (ii), partial coalescence means increased cluster of mass, hence the thermal expansion is more significant to promote oxide rupture and further coalescence of Al. Because coalescence behavior was different as briquettes were melted without salt flux, it was concluded that (i) is a crucial factor for coalescence and recovery. The conclusions for each foil thickness were:

- For 15 μm foil, high specific surface areas were, compared to thicker foils, most drastically reduced with compaction. Therefore, recovery increased with compaction.
- For 30 μm foil, only a small increase in partial coalescence (achieved by compaction) were necessary for sufficient thermal expansion (hence oxide rupture) so that maximum recovery could be achieved.
- The same phenomenon as for 30 μm occurred for foil thicknesses 100, 200 and 300 μm , although this effect was smaller and was seen to decrease with thickness. Lower specific surface area and greater thermal expansion promoted oxide rupture and coalescence of Al.
- Although good coalescence could be achieved for all foil thicknesses, it is expected that small amount of Al was lost in the form of AlF_3 due to displacement reactions at the Al-salt interface.

6.5.2. Melting behavior without salt flux

Without salt flux, good coalescence and recovery is only achieved for very high compaction (2.41 g/cm^3 and above) regardless of foil thickness. It was observed that the macro roughness (higher for thicker foils) negatively influence the coalescence. However, the porosity of the melted briquette and oxide growth must be further studied.

6.6. Additional conclusions

- Independent on thickness, briquettes with bulk density of 1.5 g/cm^3 and below floated in liquid salt flux
- The briquettes coalesced at $800 \text{ }^\circ\text{C}$ although the salt flux was not molten

7. Bibliography

1. Circular Aluminium Action Plan. 2020 [cited 2020 May]; Available from: <https://www.european-aluminium.eu/>
2. Global Aluminium Cycle [cited 2020 May]; Available from: <http://www.world-aluminium.org/statistics/massflow/>.
3. Future Protects with Aluminium [cited 2020 May]; Available from: <http://packaging.world-aluminium.org/home/>.
4. The Aluminium Agenda 2019-2020, E. Aluminium, Editor., European Aluminium.
5. EU Export Destinations of Aluminium Scrap. 2020; Available from: <https://www.european-aluminium.eu/data/recycling-data/eu-exports-destination-of-aluminium-scrap/>.
6. Daly, T. China to tighten restrictions on scrap metal imports from Monday. 2019 June 28, 2019; Available from: <https://uk.reuters.com/article/uk-china-metals-scrap/china-to-tighten-restrictions-on-scrap-metal-imports-from-monday-idUKKCN1TT07N>.
7. Market Overview. Activity Report 2019-2020; Available from: <https://www.european-aluminium.eu/activity-report-2019-2020/market-overview/>.
8. Tabereaux, A.T. and R.D. Peterson. Chapter 2.5@ Aluminum Production. 2014.
9. Aluminium life cycle. 2019 March 11 [cited 2020 May]; Available from: <https://www.hydro.com/en/about-aluminium/aluminium-life-cycle/>.
10. Schlesinger, M.E., Aluminum recycling. First Edition ed. 2007, Boca Raton, FL: CRC Press/Taylor & Francis Group.
11. Sjökvist, T. and M. Andersson, Processmetallurgins grunder 1st ed. 2002, Stockholm: KTH
12. Martchek, K.J., Life cycle benefits, challenges, and the potential of recycled aluminum. 1997, Proc. Air & Waste Manage. Assoc. 90th Ann. Meet. Exhib. .
13. Xiao, Y., M.A. Reuter, and U. Boin, Aluminium recycling and environmental issues of salt slag treatment. J Environ Sci Health A Tox Hazard Subst Environ Eng, 2005. 40(10): p. 1861-75.
14. Ayres, R.U., Metals recycling: economic and environmental implications. Resources, Conservation and Recycling, 1997. 21(3): p. 145-173.
15. Big Power in a Small Package GETECHA Beside-the-Press Granulators. GETECHA GmbH/Inc.
16. Hamers, C. and A. Jessberger. Aluminum Cycle: Machining, Briquetting, Melting. 2018 [cited 2020 May]; Available from: <https://global-recycling.info/archives/2354>.
17. Bell, S., et al., Final Report on Scrap Management, Sorting and Classification of Aluminum. 2003.
18. Sanders, R.E.J., A.B. Trageser, and C.S. Rollings. Recycling of lightweight aluminum containers: present and future perspectives in TMS–AIME. 1990. Warrendale, PA: in 2nd Int. Symp. Recycl. Met. Eng. Mater.
19. Gesing, A. and R. Wolanski, Recycling light metals from end-of-life vehicle. JOM, 2001. 53(11): p. 21-23.
20. Rombach, G., Future Availability of Aluminum Scrap. Light Metals, 2002: p. 1011-1017.
21. Glenn, J., Innovations in processing and sorting recyclables. Biocycle, 1991. 32: p. 35.

22. Arimoto, M., et al., Pre-sorting technologies in a waste recycling system. 1998: p. 39-43.
23. Bauer, A.J.R. and C. Laska, Libs For Automated aluminum scrap sorting 2018, Hydro Aluminum Products, GmbH: TSI Incorporated
24. ; Available from: <https://www.secopta.com/applications/recycling>.
25. Cui, J., A. Kvithyld, and H. Roven, Degreasing aluminium turnings and implications for solid state recycling. TMS Light Metals, 2010: p. 675-678.
26. McAvoy, B., J. McNeish, and W. Stevens. The Alcan decoater process for UBC decoating. in 2nd Int. Symp. Recycl. Met. Eng. Mater. 1990. Warrendale, PA: TMS-AIME.
27. Kvithyld, A., et al. DECOATING OF ALUMINUM SCRAP IN VARIOUS ATMOSPHERES. in Annual meeting; 131st, The Minerals, Metals & Materials Society; Light metals 2002, proceedings of the technical sessions presented by the TMS Aluminum Committee at the 131st TMA Annual Meeting. 2002. Warrendale, Pa.: TMS;.
28. Capuzzi, S., et al. Influence of Coating and De-Coating on the Coalescence of Aluminium Drops in Salt. 2017. Cham: Springer International Publishing.
29. Recyclable Tetra Pak Cartons. [cited 2020 April]; Available from: <https://www.tetrapak.com/in/sustainability/good-for-you-good-for-the-earth/tetra-pak-cartons-fully-recyclable>.
30. Charlier, P. and G. Sjöberg. Recycling of aluminum foil from post-consumer beverage cartons. in in 3rd Int. Symp. Recycl. Met. Eng. Mater. 1995. TMS-AIME.
31. Pawlek, R.P., Recycling of composite aluminum materials: the Aluminium Rheinfelden process. Light Metal Age, 2001. 63: p. 62.
32. Evans, C., Treatment of used cutting fluids and swarf: Techniques and typical equipment for separation, reclamation and recycling. Tribology International, 1977. 10(1): p. 33-37.
33. Pietsch, W., Briquetting of aluminum swarf for recycling. Light Metals 1993: p. 1045-1051.
34. Puga, H., J. Barbosa, and C.S. Ribeiro, Factors Affecting the Metal Recovery Yield during Induction Melting of Aluminium Swarf. Materials Science Forum, 2013. 730-732: p. 781-786.
35. Puga, H., et al., Recycling of aluminium swarf by direct incorporation in aluminium melts. Journal of Materials Processing Technology, 2009. 209(11): p. 5195-5203.
36. Shamsudin, S., M. Lajis, and Z. Zhong, Solid-state recycling of light metals: A review. Advances in Mechanical Engineering, 2016. 8(8): p. 1687814016661921.
37. Valiev, R., R. Islamgaliev, and I.V. Alexandrov, Bulk Nanostructured Materials from Severe Plastic Deformation. Progress in materials science, 2000. 45: p. 103-189.
38. Gould, J.E., Mechanisms of solid-state bonding. Microjoining and Nanojoining, 2008: p. 5-24.
39. Wan, B., et al., Review of solid state recycling of aluminum chips. Resources, Conservation and Recycling, 2017. 125: p. 37-47.
40. Kanetake, N., et al., Upgrading in Mechanical Properties of High Performance Aluminum Alloys by Compressive Torsion Process. Procedia CIRP, 2014. 18: p. 57-61.
41. Kanetake, N., E. Maeda, and T. Choh, Fabrication of Metal Matrix Composite with New Powder Forming Process. Proc. PTM'93, 1993: p. 491-496.
42. Güley, V., et al., Effect of die design on the welding quality during solid state recycling of AA6060 chips by hot extrusion. Materials Science and Engineering: A, 2013. 574: p. 163-175.

43. Ying, T., et al., Recycling of AZ91 Mg alloy through consolidation of machined chips by extrusion and ECAP. Transactions of Nonferrous Metals Society of China, 2010. 20: p. s604-s607.
44. Mashhadi, H., et al., Recycling of aluminium alloy turning scrap via cold pressing and melting with salt flux. Journal of Materials Processing Technology - J MATER PROCESS TECHNOL, 2009. 209: p. 3138-3142.
45. Fogagnolo, J.B., et al., Recycling of aluminium alloy and aluminium matrix composite chips by pressing and hot extrusion. Journal of Materials Processing Technology, 2003. 143-144: p. 792-795.
46. Drouzy, M. and C. Mascré, The oxidation of liquid non-ferrous metals in air or oxygen. Metallurgical Reviews, 1969. 14(1): p. 25-46.
47. Hinton, E.M., W.D. Griffiths, and N.R. Green, Comparison of Oxide Thickness of Aluminium and the Effects of Selected Alloying Additions. Materials Science Forum, 2013. 765: p. 180-184.
48. Haginoya, I. and T. Fukusako, Oxidation of Molten Al-Mg Alloys. Transactions of the Japan Institute of Metals, 1983. 24(9): p. 613-619.
49. Thiele, W., Die Oxydation von Aluminium- und Aluminiumlegierungs-Schmelzen. . Aluminium, 1962. 38: p. 707-715, 780-786.
50. Wightman, G. and D.J. Fray, The dynamic oxidation of aluminum and its alloys. Metallurgical Transactions B, 1983. 14(4): p. 625-631.
51. Bartlett, R.W., Growth Kinetics of Discontinuous Thermal Oxide Films; Aluminum. Journal of the Electrochemical Society, 1964. 111: p. 903.
52. Gulbransen, E.A. and W.S. Wyson, Thin Oxide Films on Aluminum. The Journal of Physical and Colloid Chemistry, 1947. 51(5): p. 1087-1103.
53. Cochran, C.N. and W.C. Sleppy, Oxidation of High-Purity Aluminum and 5052 Aluminum-Magnesium Alloy at Elevated Temperatures. Journal of The Electrochemical Society, 1961. 108(4): p. 322.
54. The Ellingham Diagram. [cited 2020 March]; Available from: https://www.doitpoms.ac.uk/tlplib/ellingham_diagrams/ellingham.php.
55. Peterson, R.D., Metal Contamination Associated with Dross Processing, in Light Metals 2013, B.A. Sadler, Editor. 2016, Springer International Publishing: Cham. p. 941-946.
56. Trunov, M.A., M. Schoenitz, and E.L. Dreizin, Effect of polymorphic phase transformations in alumina layer on ignition of aluminium particles. Combustion Theory and Modelling, 2006. 10(4): p. 603-623.
57. Smeltzer, W.W., OXIDATION OF ALUMINUM IN THE TEMPERATURE RANGE 400 -600 C. Journal of the Electrochemical Society (U.S.) Absorbed Electrochem. Technol., 1956: p. Medium: X; Size: Pages: 209-14.
58. Rossel, H., Fundamental Investigation about Metal Loss During Remelting of Extrusion and Rolling Fabrication Scrap. Light Metals 1990: p. 721.
59. Bahk, S., et al. Protecting aluminum alloy from particle-impact ignition with an Al₂O₃ film. 1993.
60. Smith, N. Methods of Oxidation Inhibition for Al-Mg Alloys. 2019.
61. Kahl, W. and E. Fromm, Examination of the Strength of Oxide Skins on Aluminum Alloy Melts. Metallurgical Transactions B, 1985. 16: p. 47.
62. Balicki, S., Prace Inst. Hutn., 1958. 10: p. 208.

63. ALCHALABI, R., F. MENG, and A. PEEL. Furnace operation optimization via enhanced bath circulation: Technologies for production increase and dross reduction. in *Light Metals*. 2002. Warrendale: TMS.
64. Groot, J. and J. Migchielsen, Multi Chamber Melting Furnaces for Recycling of Aluminium Scrap. 2013. p. 57-70.
65. Tilting Rotary Furnaces Available from: <http://www.meltingsolutions.com/tilting-rotary-furnace>.
66. Paitoni, C. and L. Benedini, Rotary smelting furnace Diecasting Technology, 2004. 31: p. 52.
67. Hall, C., Turn and tilt to melt mixed aluminium scrap. *MBM*, 2004. 400: p. 24.
68. Linden, J.H.L.V. and D.L. Stewart, Molten Salt Flux Composition Effects in Aluminum Scrap Remelting. 2016. p. 173.
69. Sydykov, A., B. Friedrich, and A. Arnold, Impact of parameter changes on the aluminum recovery in a rotary kiln. 2002. 1045-1052.
70. Akbari, S. and B. Friedrich, Salt-Metal Interaction in Magnesium Recycling. 2010.
71. Peterson, R.D., Effect of salt flux additives on aluminium droplet coalescence. *The Minerals, Metals & Materials Society*, 1990: p. 69-84.
72. Keller, F. and J.D. Edwards, Composition and Properties of the Natural Oxide Film on Aluminum. *Metal Progress*, 1948. 54: p. 195-200.
73. Freti, S., J.-D. Bornand, and K. Buxmann, Metallurgy of Dross Formation on Aluminum Melts *Light Metals*, 1982. Vol 2: p. 1003-1016.
74. Smeltzer, W.W., Oxidation of Aluminum in the Temperature Range 400-600 °C. *J. Electrochem Soc.*, 1956. 103: p. 209-214.
75. Sleppy, W.C. and C.N. Cochran, Oxidation of High Purity Aluminum. *J. Electrochem Soc.*, 1961. 108: p. 322-327.
76. Yang, Y., et al., Aluminium Recycling: Scrap Melting and Process Simulation. 2005.
77. Stewart, A., J. McCubbin, and J. Sulzer, Melting Aluminum and Aluminum Alloys. *Light Metal Age*, 1977. 35(11): p. 13-15.
78. Paulitsch, H., H. Antrekowitsch, and A. Schmid, Vergleich des Abbrandverhaltens beim Rezyklieren von Aluminiumspänen und -briketts. *BHM Berg- und Hüttenmännische Monatshefte*, 2011. 156(1): p. 6-13.
79. Kvithyld, A. Compact & Loose Turnings AA6063 - from machining of billets 2015. Orlando, Florida, USA: TMS.
80. Xiao, Y. and M.A. Reuter, Recycling of distributed aluminium turning scrap. *Minerals Engineering*, 2002. 15(11, Supplement 1): p. 963-970.
81. Berry, M.V., The molecular mechanism of surface tension. *Physics Education*, 1971. 6(2): p. 79-84.
82. Kamp, J., J. Villwock, and M. Kraume, Drop coalescence in technical liquid/liquid applications: A review on experimental techniques and modeling approaches. *Reviews in Chemical Engineering*, 2017. 33: p. 1.
83. Vijayan, S. and A.B. Ponter, Drop/drop and drop/interface coalescence in primary liquid/liquid dispersion separators. *Chemie Ingenieur Technik*, 1975. 47(18): p. 748-755.
84. Jeffreys, G.V. and G.A. Davies, *Recent Advances in Liquid-Liquid Extraction*. Oxford, 1971.
85. Roy, R.R. and Y. Sahai, Coalescence Behavior of Aluminum Alloy Drops in Molten Salts. *Materials Transactions, JIM*, 1997. 38(11): p. 995-1003.

86. Roy, R.R. and Y. Sahai, Interfacial Tension between Aluminum Alloy and Molten Salt Flux. *Materials Transactions, JIM*, 1997. 38(6): p. 546-552.
87. Tenorio, J.A.S., M.C. Carboni, and D.C.R. Espinosa, Recycling of aluminum – effect of fluoride additions on the salt viscosity and on the alumina dissolution. *Journal of Light Metals*, 2001. 1(3): p. 195-198.
88. Tenório, J.A.S. and F. Delgado, Optimization of salt composition in the recycling of aluminum cans. *Light Metals* 1997, 1997.
89. Tenorio, J.A.S. and D.C.R. Espinosa, Effect of salt/oxide interaction on the process of aluminum recycling. *Journal of Light Metals*, 2002. 2(2): p. 89-93.
90. Ye, J. and Y. Sahai, Interaction and Interfacial Tension between Aluminum Alloys and Molten Salts. *Materials Transactions, JIM*, 1996. 37: p. 1479-1485.
91. Racunas, B.J., Recovery of Aluminum from Secondary Sources by Means of Agitated Molten Salt. *ECS Proceedings Volumes*, 1976. 1976-6(1): p. 365-374.
92. Martin-Garin, L., A. Dinet, and J.M. Hicter, Liquid-liquid interfacial tension measurements applied to molten Al-halide systems. *Journal of Materials Science*, 1979. 14(10): p. 2366-2372.
93. Utigard, T.A., The properties and uses of fluxes in molten aluminum processing. *JOM*, 1998. 50(11): p. 38-43.
94. Sully, A.H., H.K. Hardy, and T.J. Heals, *Journal of the Institute of Metals*, 1953-54. 82: p. 49.
95. Johnson, T.J. and R.D. Peterson, *Recycle and Secondary Recovery of Metals*. The Metallurgical Society Warrendale, PA,, 1985: p. 417.
96. Roy, R. and Y. Sahai, Wetting Behavior in Aluminum-Alumina-Salt Systems. *Materials Transactions, JIM*, 1997. 38: p. 571-574.
97. Girifalco, L.A. and R.J. Good, A Theory for the Estimation of Surface and Interfacial Energies. I. Derivation and Application to Interfacial Tension. *The Journal of Physical Chemistry*, 1957. 61(7): p. 904-909.
98. Milke, E., et al., Solubility of CaF₂ in NaCl-KCl salt flux for Al-recycling and its effect on Al-loss. Vol. 4. 2005.
99. Larsson, F. Surface topography measurements of thin aluminium foil transferred to FE-simulations. 2016.
100. Impey, S.A. and S.o.I. Science, *The Mechanism of Dross Formation on Aluminium and Aluminium-magnesium Alloys*. 1989: Cranfield Institute of Technology.
101. IF-Laboratory Measurement-Module. Vol. Version 5.6. 2016: Alicona Imaging
102. Michigan Metrology Glossary of Texture Parameters. [cited 2020 May]; Available from: https://www.michmet.com/Texture_parameters.htm.
103. NIST-JANAF Thermochemical Tables 1998.

8. Appendices

In this section, additional data on size and shape of chips and data on compaction of the chips are presented graphically.

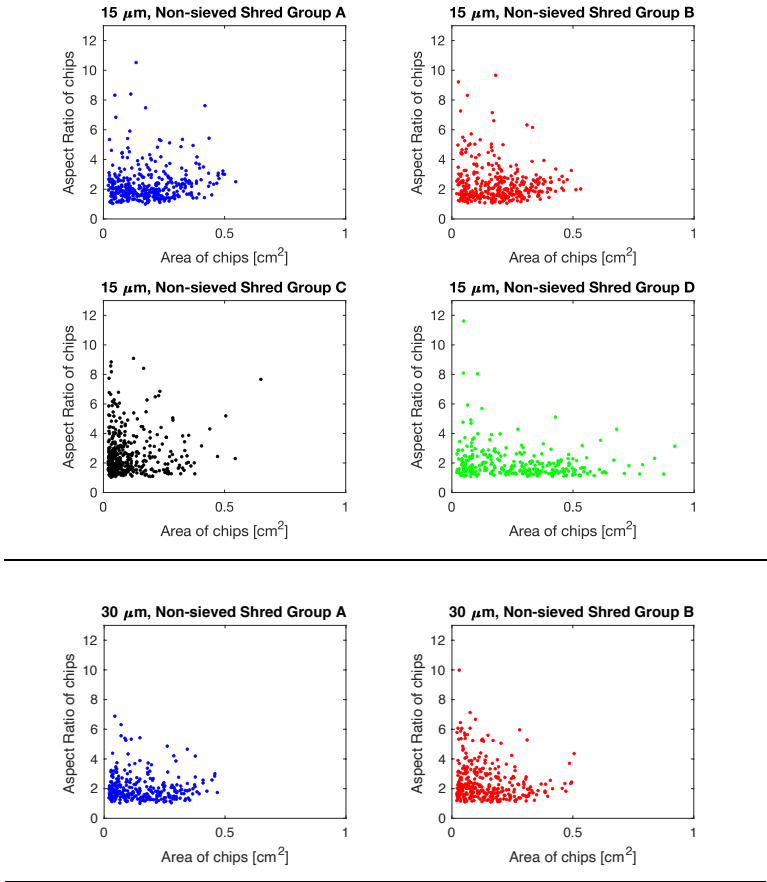


Figure 8.1. Plotted data on size and shape of chips of 15 and 30 μm for shred groups A-D.

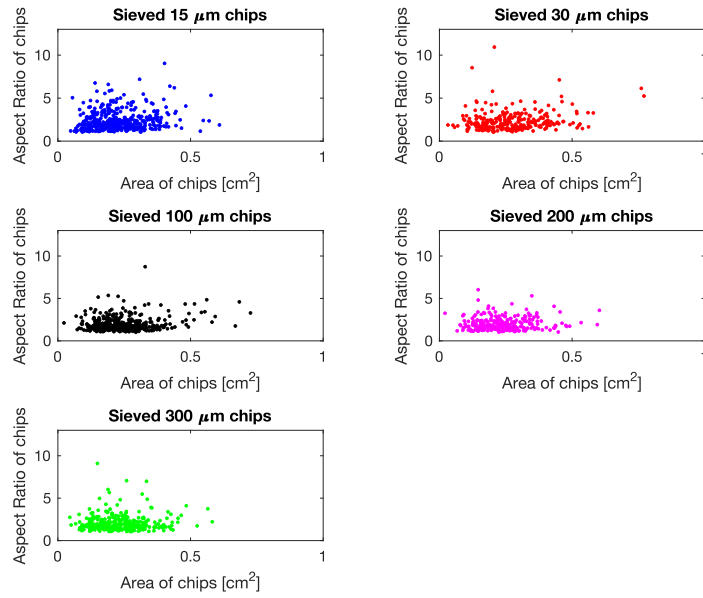


Figure 8.2. Plotted data on size and shape of sieved chips of 15-300 μm (only chips from shred group A).

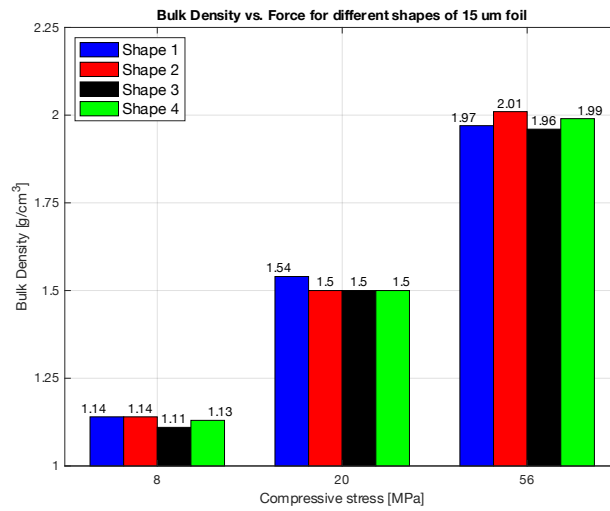


Figure 8.3. Bulk density comparison between chips of different shred groups of the 15 μm foil.

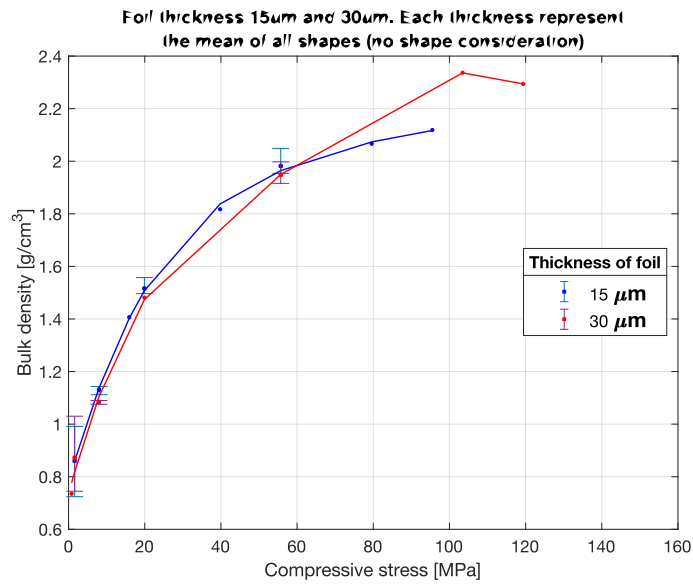


Figure 8.4. Average bulk density vs. Compressive force, all shred groups averaged for the two thinnest foil thicknesses.

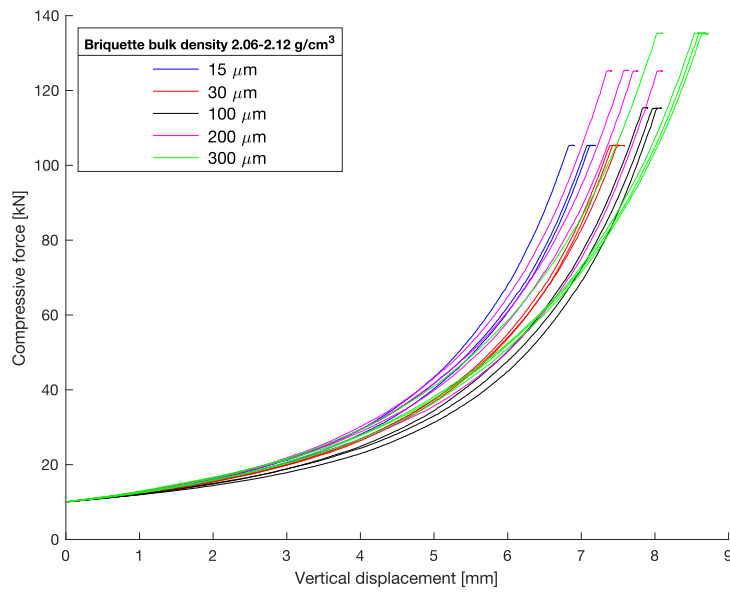


Figure 8.5. Vertical displacement due to applied compressive force on Al chips resulting in briquettes of bulk density 2.06-2.12 g/cm³.

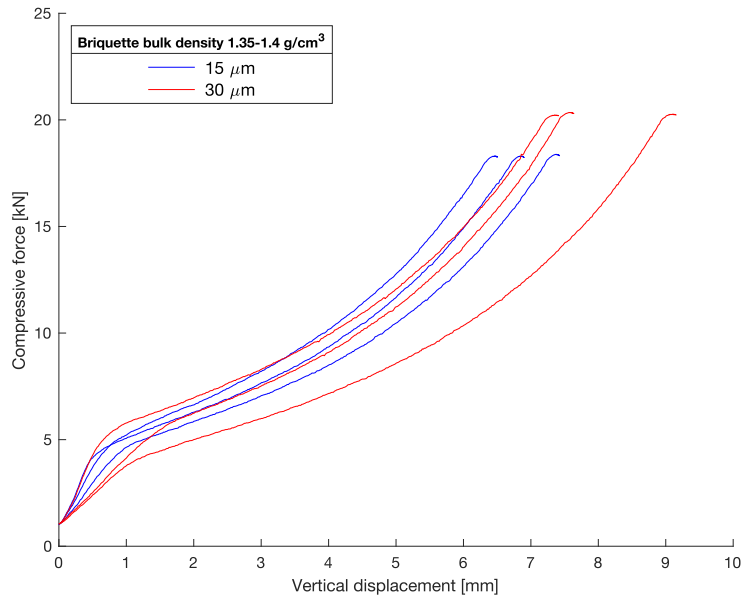


Figure 8.6. Vertical displacement due to applied compressive force on Al chips resulting in briquettes of bulk density 1.35-1.4 g/cm³.

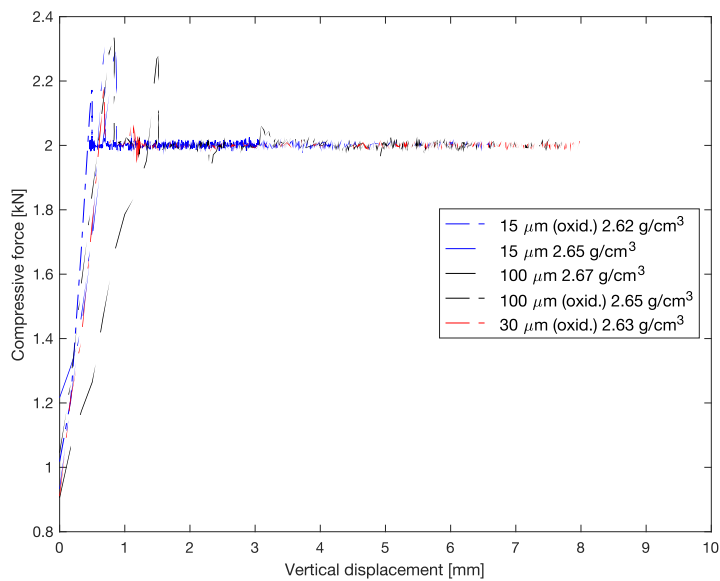


Figure 8.7. Vertical displacement due to 2 kN applied compressive force during heating from room temp. to 450 °C on non-oxidized and oxidized Al chips, displaying the briquettes of bulk densities.

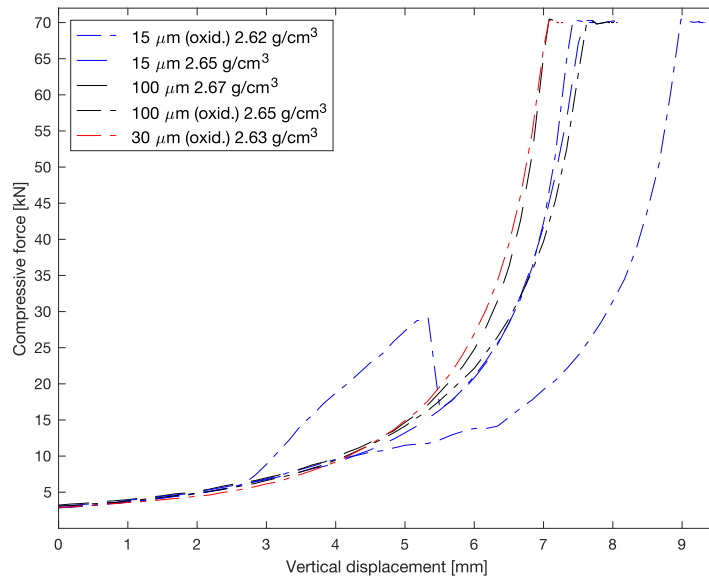




Figure 8.8. Vertical displacement due to applied compressive force from 2 to 70 kN at 450 °C on non-oxidized and oxidized Al chips, displaying the briquettes of bulk densities.

Risk assessment

		<h3>Hazardous activity identification process</h3>			Prepared by HSE section Approved by The Rector	Number HMR1/2020 Page 1	Date 2011-03-22 Replaces 2006-12-01	
Unit: (Institute)		IMA		Date: 06.05.2020				
Line manager:		Tor Grande						
Participants in the identification process (incl. function): <small>(supervisor, student, co-supervisor, others)</small>		Harald Philipson (me, master thesis student), Alicia Vallejo Olivares (PhD-student), Gabriella Tranell (supervisor), Pål Christian Skaret (room/equipment responsible)						
Short description of the main activity/main process:		Comminution and compaction using screw extrusion and uniaxial pressing for aluminium recycling						
Is the project work purely theoretical? (YES/NO)		NO						
<small>Answer "YES" implies that supervisor is assured that no activities requiring risk assessment are involved in the work. If YES, skip rest of the form.</small>								
Will you receive industry samples? (YES/NO)		NO						
<small>"YES" means that a separate risk assessment of the samples is required</small>								
Is the project work safe to perform outside normal work hours (8-17)? (YES/NO)		NO						
Responsible supervisor: Gabriella Tranell		Student: Harald Philipson						
ID nr.	Activity/process	Responsible person	Existing documentation	Existing safety measures	Laws, regulations etc.	Comment		
1	Shredding	HP						
2	Sieving	HP						
3	Compaction	HP						
4	Screw Extrusion	HP						
5	Sample Preparation: Dicing, polishing, cutting	HP						
6	Waste handling	HP						
7	Microscopy analysis (SEM)	HP						
8	Muffle Furnace	HP						
9	COVID-19	HP						

NTNU	Risk assessment	Prepared by	Number	Date	
		HSE section	HSESRV200	2011-02-04	
HMS AG		Approved by	Page	Replaces	
		The Rector		2010-02-09	

Unit: *(Institute)* **Material Science and Engineering** Date: 06.05.2020
Line manager: **Tor Grande**
Participants in the identification process (incl. function): *(supervisor, student, co-supervisor, others)* **Alicia V. Olivares, Gabriella Tranell, Pål Christian Skavet**
Risk assessment of: **Comminution and compaction using screw extrusion and uniaxial pressing for aluminium recycling**
Signatures: Responsible supervisor: Gabriella Tranell Student: Harald Philipson

ID nr.	Activity from the identification process form	Potential undesirable incident/strain	Likelihood: (1-5)	Consequence:			Risk value (human)	Comments/status Suggested measures
				Human (A-E)	Environment (A-E)	Economy/material (A-E)		
1	Shredding	Cuts, exposure to fragment, damage instrument	1	C	A	B	B3	Safety distance from the shredder, lab coat, gloves, goggles, ear protection, precaution
2	Sieving	Exposure chemicals: eyeskin/finger damage	2	B	A	A	B2	Gloves, lab coat, goggles, correct waste handling and cleaning
3	Compaction	Squeezing, exposure to fragments, damage instrument	1	C	A	A	C1	Goggles, safety distance, precaution, routine, steady compaction
4	Screw Extrusion	Burns, gas evolution, high noise, falling objects, damage instrument	3	C	B	C	C3	Heat resistant gloves, face protection, goggles, protective footwear, gas mask, precaution
5	Sample Preparation: Dicing, polishing, cutting	Exposure chemicals, eyeskin/finger damage, explosive chemicals	3	B	B	C	B3	Gloves, lab coat, goggles, correct waste handling and cleaning
6	Waste handling	Chemicals	2	C	C	A	C2	Gloves, lab coat, goggles, correct waste handling and cleaning
7	Microscopy analysis (SEM)	Damage instrument	1	A	A	E	A1	Precaution, training
8	Muffle Furnace	Splashing of hot metal, inhalation of gas/smoke	4	D	C	C	D4	Protective wear: lab coat, gaiter helmet with transparent visor, heat protective gloves and shoes, gas mask, clean pants, keep 2 m distance, max. 1-3 people in lab, washing hands, wipe surfaces (70-80% ethanol)
9	COVID-19	Disease	3	B	A	A	B3	

